A NUMERICAL INVESTIGATION OF THERMAL COMFORT WITH DIFFERENT AIR DIFFUSERS AT ENCLOSED OFFICE SPACE

A Thesis

by

Tolga Arda Eraslan

Submitted to the
Graduate School of Sciences and Engineering
In Partial Fulfillment of the Requirements for
the Degree of

Master of Science

in the
Department of Mechanical Engineering

Özyeğin University
September 2023

Copyright © 2023 by Tolga Arda Eraslan

A NUMERICAL INVESTIGATION OF THERMAL COMFORT WITH DIFFERENT AIR DIFFUSERS AT ENCLOSED OFFICE SPACE

Advisor: Prof. M. Pınar Mengüç, Özyeğin University
Coadvisor: Asst. Prof. Altuğ Melik Başol, Özyeğin University

Approved by:

Prof. M. Pınar Mengüç, Advisor
Department of Mechanical Engineering
Özyeğin University

Assoc. Prof. Özgür Ertunç
Department of Mechanical Engineering
Özyeğin University

Prof. Hakan Ertürk
Department of Mechanical Engineering
Boğaziçi University

Date Approved: 08 August 2023

To my beloved family, my dearest friends, and my wife,

Thank you for your endless love, trust, and support.

ABSTRACT

People spend most of their time in indoor environments, which highlights the significance of heating, ventilation, and air conditioning (HVAC) systems in these spaces. While ensuring the comfort of occupants in indoor spaces, it is also essential to maintain the efficient operation of these systems. Studies related to this topic are ongoing in the present day. HVAC should not only be seen as individual devices within it, but rather as a whole system. By doing so, the efficiency of each component can be enhanced. HVAC systems consist of various components, including heating and cooling units, ventilation units, dampers, air terminals, louvers, ducts, and pipes, among others. One of the most crucial elements that interact with the indoor environment is the air terminal.

In this thesis, the interaction of air terminals with occupants in indoor spaces was observed and visualized using Computational Fluid Dynamics (CFD). Three types of diffusers were used in the study: square diffuser, four-way swirl diffuser, and a hexagonal diffuser designed by Cem Keskin. The interaction of these diffusers with the air inside the room, their airflow characteristics, and their impact on thermal comfort were investigated. The Fanger method's six variables were discussed in this context.

Based on the findings, it was observed that the airflow characteristics of the hexagonal diffuser varied based on the openings, while the four-way swirl diffuser was found unsuitable for providing thermal comfort in an office environment. Additionally, when aiming for even air distribution, there is no energy difference among the diffusers. However, if only a specific area require conditioning, it's noticeable that the hexagonal diffuser consumes less energy compared to the other types of diffusers.

ÖZETÇE

İnsanlar çoğu zamanını kapalı ortamlarda geçirdiğinden dolayı bu alanların ısıtma, soğutma ve havalandırması (HVAC) büyük önem arz etmektedir. Kapalı alanda bulunun sakinlerin konforu sağlanırken aynı zamanda bu sistemlerin verimli çalışabilmesi sağlanmalıdır. Bu konuyla ilgili çalışmalar günümüzde devam etmektedir. HVAC sadece içerisindeki ana cihazlarla alınmamalı aksine bir bütün olarak gözler önüne serilmelidir. Böylelikle, içerisindeki her bir yapı taşının verimi arttırılabilir. HVAC sistemleri birçok komponentten oluşmaktadır. Bunlar içerisinde ısıtma soğutma üniteleri, havalandırma üniteleri, damperler, hava terminalleri, panjurlar, kanallar, borular gibi birçok element sıralanabilir. Kapalı alan içerisinde onunla etkileşime geçen en önemli unsur ise hava terminalleridir.

Bu tez çalışmasında hava terminallerinin kapalı alandaki sakinler ile nasıl bir etkileşim içerisinde oldukları Hesaplamalı Akışkanlar Dinamiği (CFD) kullanılarak gözlemlenip görselleştirilmiştir. Tezde kara difüzör, dört yön üflemeli swirl difüzör ve Cem Keskin tarafından tasarımı yapılan altıgen bir difüzör kullanılmıştır. Bu difüzörlerin oda içerisindeki hava ile etkileşimi, hava karakteristikleri ve ısıl konfora etkisi gözlemlenmiştir. Fanger tarafından bulunan methodun 6 değişkeni hakkında bahsedilmiştir.

Bunlar ışığında, altıgen difüzörün hava karakteristiği açıklıklarına göre değiştiği sonucuna varılmış, dört yön üflemeli swirl difüzörün ise ofis ortamında ısıl konforu sağlamak için uygun olmadığı sonucuna varılmıştır. Ayrıca eşit hava dağılımı hedeflendiğinde difüzörler arasında enerji farkı oluşmamamıştır. Ancak yalnızca belirli bir alanın şartlandırılması gerekiyorsa, altıgen difüzörün diğer difüzör türlerine göre daha az enerji tükettiği fark edilmiştir.

ACKNOWLEDGEMENTS

I would first like to express my sincere appreciation to my advisor Prof. Dr. M. Pınar Mengüç, for giving me the opportunity to carry out my master's study under his supervision. His dedicated involvement, guidance, and continuous support, even during the COVID-19, helped me a lot for the completion of this work.

I also would like to thank my thesis committee members - and - for sharing their valuable insights.

I would like to extend my sincere thanks to the EÇEM/CEEE family for all their help during my thesis work. Being a part of this family has been a privilege that I will carry throughout my life. Special thanks to Dr. Cem Keskin for their unwavering support and guidance throughout the entire thesis process, their invaluable contributions have been instrumental in shaping the quality and success of this work.

I would like to express my deepest gratitude to Onur Şen. I feel very fortunate to be your friend.

Most importantly, none of this could have happened without my family and my wife. I am eternally grateful for their love, trust, and support.

TABLE OF CONTENTS

DEDICATION . . . . . **iii**

ABSTRACT . . . . . **iv**

ÖZETÇE . . . . . **v**

ACKNOWLEDGEMENTS . . . . . **vi**

LIST OF TABLES . . . . . **ix**

LIST OF FIGURES . . . . . **x**

NOMENCLATURE **1**

ABBREVIATIONS **2**

I INTRODUCTION **3**

1.1 General Background 3

1.2 Research Objectives of Thesis 6

1.3 Outline of the Thesis 6

II LITERATURE REVIEW **8**

2.1 Ventilation Systems 8

2.2 Indoor Airflow 10

2.3 Thermal Comfort 14

III THEORETICAL ANALYSIS **18**

3.1 Conservation Equations 18

3.2 k-Epsilon Turbulence Model 19

3.3 Indoor Air Flow 21

3.4 Air Jets 23

3.5 Air Terminal Units 25

3.6 Thermal Comfort 27

IV METHODOLOGY **39**

4.1 Layout of the Experiment Office 39

4.2 Simulation Setup 52
4.2.1 Geometry of model 53
4.2.2 Initial and boundary conditions 55
4.2.3 Model physics 56
4.2.4 Mesh Selection 57
4.2.5 Validation of results 60

V RESULTS AND DISCUSSION 63

VI CONCLUSION AND FUTURE WORK 87

APPENDIX A — JAVASCRIPT CODE FOR PMV 89

APPENDIX B — SQUARE DIFFUSER DIMENSIONS 93

APPENDIX C — FOURWAY DIFFUSER DIMENSIONS 94

APPENDIX D — EXPERIMENT MEASUREMENTS FOR INLET AIR VELOCITY 95

REFERENCES 96

VITA 102

LIST OF TABLES

1 Fanger thermal sensation range [10] 16

2 Metabolic rate at different typical activities [60] 28

3 Testo 440 accuracy within specific ranges 48

4 The experimental air temperature result of experiment 1 50

5 The experimental air temperature result of experiment 1 50

6 The experimental turbulence intensity of experiment 1 50

7 The experimental draft rate of experiment 1 51

8 MAPE results of the cases at 0.98 m 62

9 Diffuser flap configuration 64

LIST OF FIGURES

1	Indoor Environmental Quality categories and their subcategories [9] .	4
2	Ventilation types of passive design	8
3	Inlet and Outlet visualization of different ventilation types [22]	9
4	Heat transfer between surroundings and human [45]	15
5	Schematic of airflow within displacement ventilation space [56] . . .	21
6	Flow patterns in room with horizontal supply in mixing ventilation (a) primary airflow in short room (b) primary airflow (c) primary and seconday airflows.	22
7	Free Jet zone characteristics [57]	24
8	Types of diffusers with their air jet characterizations (a) compact; (b) linear; (c) radial; (d) incomplete radial (e) conical [57]	26
9	Predicted percentage dissatisfied based on PMV [10]	36
10	Top view of the office model	40
11	Side view of the office model	40
12	3D model of the office space	41
13	HVAC system schematic of the office space	42
14	Inside of the square diffuser	44
15	Four-way Swirl Diffuser	45
16	Hexagonal air diffuser with operable flaps	46
17	Measurement tools, Testo 440, and its probes	47
18	The probe placement in the simulation model	48
19	Flowchart of simulation process	52
20	The utilized manikin geometry in the model	54
21	Manikin polyhedral and prism layer meshes	58
22	Mesh visualization of diffusers	59
23	Comparisons for different mesh selections	60
24	Residual of an experiment	61
25	Case 6: Velocity and temperature distribution	66

26 Case 9: Velocity and temperature distribution 68
27 Case 1: Velocity and temperature distribution 70
28 Velocity lines of Case 1 72
29 Velocity lines of Case 9 72
30 Case 1: Heat flux and cell relative velocity 73
31 Case 9: Heat flux and cell relative velocity 74
32 Case 9: Heat flux and cell relative velocity 74
33 Velocity and temperature distribution of Case 4 76
34 PMV, Turbulence intensity, velocity and temperature visual at 100 cm from floor of case 4 77
35 Case 7 velocity and temperature distribution 79
36 Heat flux and cell relative velocity of case 7 80
37 Case 8 velocity and temperature distribution 81
38 Case 3 with reduced airflow 83
39 Hexagonal diffuser with reduced airflow 84
40 Square diffuser with reduced airflow 85

NOMENCLATURE

A	Area (m^2)
AR	Archimedes number (-)
Tu	Turbulent intensity
u	Magnitude of air velocity (m/s)
cp	Heat capacity (J/kg-K)
Q	Volumetric flow rate (m^3/s)
Re	Reynolds number (-)
S	Source term
T	Temperature (°C or °K)
t	Time (s)
v	Velocity (m/s)
V	Volume (m^3)
μ	Viscosity (Pa.s)
ρ	Density (kg/m^3)
τ	Air change time (s)

ABBREVIATIONS

HVAC	Heating, Ventilation, Air Conditioning
CFD	Computational Fluid Dynamics
PMV	Percentage Mean Vote
PDD	Percentage Dissatisfied
RANS	Reynolds-Averaged Navier Stokes
ASHRAE	American Society of Heating, Refrigerating, and Air-Conditioning Engineers
SIMPLE	Semi Implicit Method for Pressure-Linked Equations
IEQ	Indoor Environmental Quality
IAQ	Indoor Air Quality
GHG	Greenhouse Gas

CHAPTER I

INTRODUCTION

1.1 General Background

The building industry is responsible for nearly 40% of total global energy use and 33% of total greenhouse gas (GHG) emissions in 2016 [1]. In addition, as per energy conservation report, more than 66% of the total energy consumed by the buildings is used due to Heating, Ventilation, Cooling (HVAC) and lighting equipment [2]. These findings show that the more we can minimize the energy need of the buildings, the less the energy need from the total consumption will tend to decrease. Therefore, while paying attention to the Indoor Environment Quality (IEQ) in buildings, we must also use energy efficiently.

IEQ is a comprehensive term that includes many factors including thermal comfort; indoor air quality (IAQ); lighting; and acoustics [3,4] inside the building that affects the health and well-being of the occupants. Indoor air quality can be calculated by percentage of pollutants within the air such as carbon monoxide or volatile organic compounds and smoke [5], lighting can be observed by measuring illuminance level, direct sunlight, and glare [6]. Acoustic can be measured with noise levels [7]. Study shows that the weighted average of these 4 categories on the IEQ is Thermal comfort: 36.5%, visual comfort: 8.4%, acoustic comfort: 30.7% and air quality: 24.4% [8]. Based on this percentage, thermal comfort can be assumed to be of greater importance for occupants.

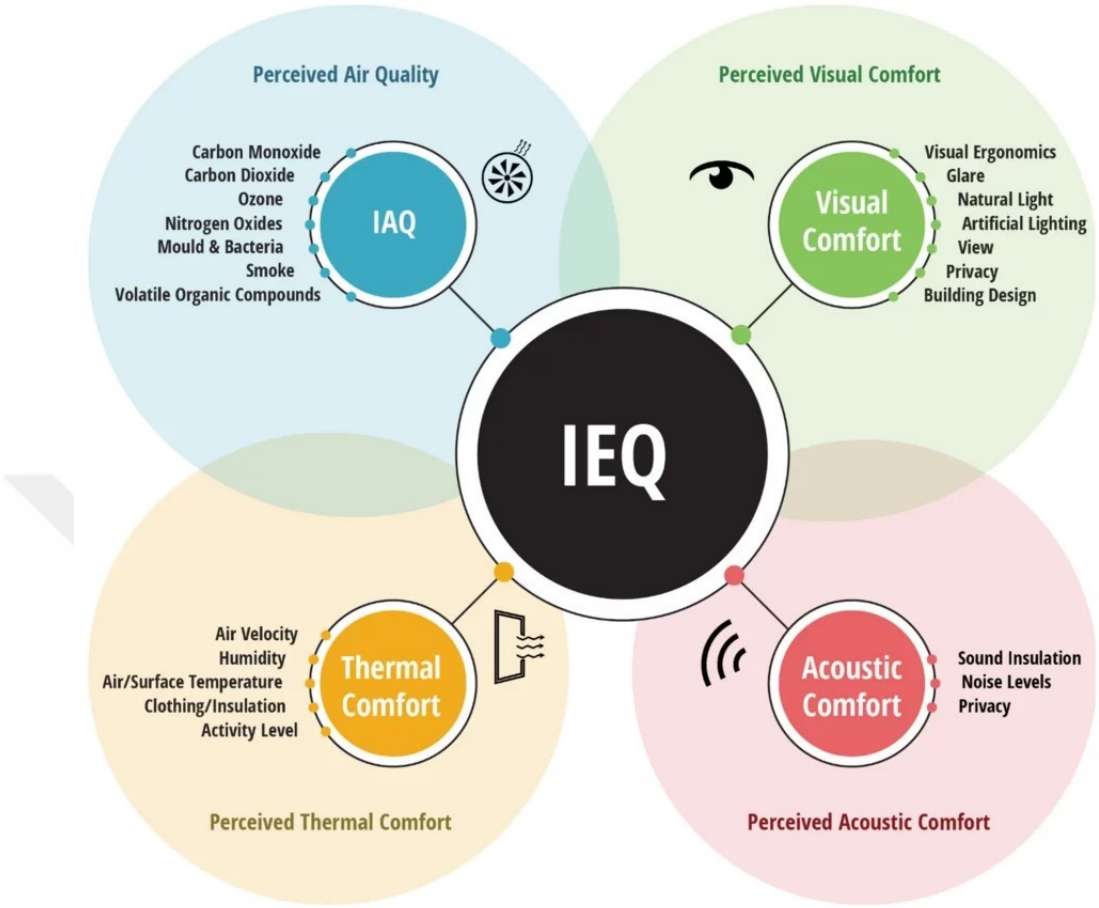

Figure 1: Indoor Environmental Quality categories and their subcategories [9]

According to ASHRAE (American Society of Heating, Refrigerating and Air-Conditioning Engineers) Standard-55, thermal comfort can be defined as condition of mind that expresses satisfaction with the thermal environment [10]. Thermal comfort is mainly related to thermal balance of the body as a whole. This thermal balance is influenced by the metabolic rate and clothing and also environmental parameters [11]. Thermal comfort can be achieved by using active or passive systems. Passive cooling/heating are systems that aim to cool/heat the space or building without requiring any energy source. These systems are models that aim to reduce energy consumption with architectural details such as canopies, natural vents, green façades. However, passive systems may not always give the best results as they are used by

directing the forces of nature. At such times, active systems can be preferred as they are controllable.

Active systems are defined as energy-consuming systems during operation. These systems require an input of energy to perform their functions. Unlike passive systems, active systems are more manageable due to their reliance on mechanical devices. Additionally, they can enhance air quality through the utilization of built-in filters. However, heating, ventilation, and air-conditioning (HVAC) systems are responsible for nearly half (45%) of the building energy demand [12]. Consequently, apart from ensuring thermal comfort, it becomes imperative to curtail the energy demand associated with these systems. Customizing HVAC systems for individual buildings might be necessary to achieve energy reduction. However, mere system modifications are insufficient to achieve this goal. The system encompasses various mechanical equipment and accessories like dampers and air terminals. Taking their impact into consideration contributes to further enhancing energy efficiency.

The air dampers installed within the ventilation ducts play a crucial role in regulating the airflow and ensuring an adequate supply of fresh air. However, these dampers introduce resistance to the HVAC system as the air passes through them. Reducing this resistance becomes beneficial in terms of energy consumption, making a positive impact [13]. Nevertheless, it is important to note that the efficiency of dampers does not directly influence comfort levels. While air diffusers can have a noticeable impact on the distribution of air, the performance of dampers may not make a significant difference in poorly planned spaces. The internal geometry of air diffusers can be adjusted to generate either a vertical pattern (during heating mode) or a horizontal pattern (during cooling mode). This design allows the air jet to attach to the ceiling and then spread outwards in a radial manner along its surface [14]. This can direct us to use single diffuser for both modes with different angles that can create patterns vertically and horizontally. By doing so, we don't need to warm/cool

the unoccupied spaces.

To understand the relationship between air diffusers and the patterns that it's created, analytical, numerical or/and experimental techniques can be used. Analytical methods can give 100% true results, but they cannot be used for complicated problems and cannot be visualized. Experimental techniques take time to setup and can be costly for people to get measurement tools or setup the real space. Lastly, numerical methods can give visual results and solve complex problems. However, it needs to be validated by analytical or experimental methods. Otherwise, the results cannot be trusted because of the boundary conditions.

1.2 Research Objectives of Thesis

As mentioned above, HVAC elements have an indispensable importance in active systems. These elements may vary according to the system and space usage, but their purpose remains the same—to ensure the comfort of both individuals and space efficiently. This thesis aims to observe the effect of air diffusers, which are accessories commonly found in HVAC systems, on temperature and air velocity distribution in an office. It also aims to assess how these variables impact the thermal comfort of office occupants. The observations will be visualized using CFD (Computational Fluid Dynamics) and validated through experiments.

1.3 Outline of the Thesis

In line with the above-mentioned thesis aims to:

- **In Chapter I:** In the introduction part, the overall problem is highlighted and given the objectives of the thesis.
- **In Chapter II:** Provided a detailed literature review for ventilation systems that are used in the field. Then air diffusers are introduced for air regime and distribution and finally approaches to thermal comfort are reviewed.

- **In Chapter III:** Explained the analytical approaches for investigating air distribution, temperature distribution and thermal comfort. The equations of conservation of energy and fluid flow are discussed in this part. Lastly, thermal comfort equations are discussed.

- **In Chapter IV:** In this chapter of the thesis, the experimental model of the office is thoroughly described. The drawing of this model, specifically prepared for Computational Fluid Dynamics (CFD) simulations, is presented, and the CFD details, including boundary conditions and meshing, are comprehensively explained. Moreover, the chapter delves into the validation process, providing detailed information on how the experimental data is used to validate the accuracy and reliability of the numerical simulations. This thorough examination ensures that the CFD simulations adequately capture the real-world behavior of the office environment, making the study robust and dependable.

- **In Chapter V:** In this chapter of the thesis, a comprehensive discussion is presented regarding the details and comparisons of the numerical analysis study. Various subjects, such as thermal comfort and indoor airflow, are examined in depth, providing insights into behavior of air diffusers and their impact on the topics. Moreover, the chapter sheds light on the validation process, explaining how the numerical analyses were cross-referenced with the experimental data to ensure accuracy and reliability.

- **In Chapter VI:** Finally, in this chapter, a detailed explanation of the comparison of the results and the outputs will be provided. Various aspects and parameters, such as thermal comfort, indoor airflow distribution is thoroughly analyzed and compared among different diffuser scenarios.

CHAPTER II

LITERATURE REVIEW

2.1 Ventilation Systems

The advent of the first electrical air-conditioning unit occurred in the early 20th century, but its popularity surged primarily after the 1950s [15]. Prior to that, passive designs were employed for ventilation and cooling purposes in buildings. Even today, passive designs continue to be utilized to not use any kind of energy. Also, these designs now consider more thermal comfort more than ever before [16]. In passive designs, there are 2 types of ventilation single sided ventilation and cross ventilation, Single-sided ventilation involves the flow of air through a space using a single opening, such as a window or door. It relies on pressure differences between the interior and exterior to facilitate airflow. On the other hand, cross ventilation utilizes pressure difference between the two sides of the building [17]. In recent studies shows that cross ventilation compared to single sided ventilation has much better performance at providing comfortable conditions. While cross ventilation was analyzed indoor conditions were achieved 70% of the time in 24 hours scale. On the other hand, single sided ventilation has been achieved only 1% of the time. Also, similarly, cross ventilation reduced 1.5 °C temperature in the space [18-21].

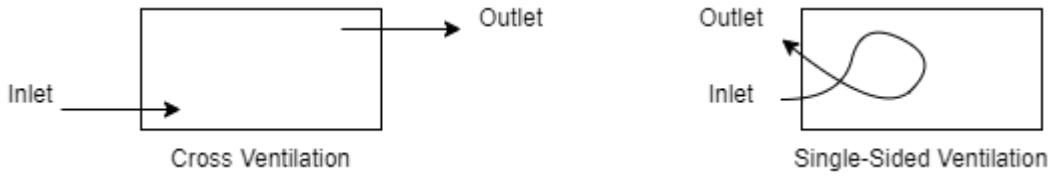

Figure 2: Ventilation types of passive design

There are several ventilation systems mixing, displacement and personalized are

the common ones by used in active systems. These systems vary due to their inlet and outlet placement in a way that they change the air distribution and temperature differently.

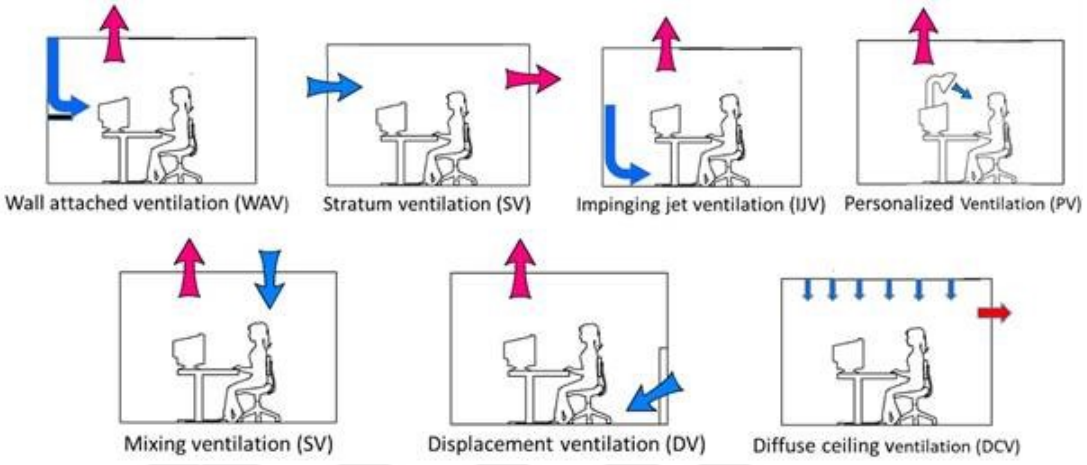

Figure 3: Inlet and Outlet visualization of different ventilation types [22]

Displacement ventilation is a method in which the inlet is positioned at the lower level of a room. Through the utilization of buoyancy forces, the air is directed to move in an upward direction. Along its path, the air encounters heat sources such as computers, occupants, and servers. Furthermore, the outlet enhances this process by drawing the convection plumes that are coming out of the heat sources. The heat source gets fresh air and contaminants that are associated with the heat source removed from the comfort level. It is important to note that the inlet does not need to blow air in high velocity, as it may cause discomfort to occupants by directing air towards their feet, which is the part of the body with the lowest temperature [23,24].

In Mixing ventilation, also the system that is used in this thesis, supply and return air terminals usually planted on the ceiling. The air directly drops from the supply air terminal to the space. Supply air terminal gives an advantage of the Coanda effect of air sticking to a surface to increase the throw of the fresh air. If it meets with the wall, it sticks to the wall and drops down to comfort area [25].

Personalized ventilation has advantages and disadvantages compared to mixing and displacement ventilation. Studies show that personalized ventilation can save up to 60% and 51% of energy compared with mixing ventilation in cold and hot climates, respectively [26,27]. Personalized ventilation meets occupant needs as air flows directly to occupants in a way that it does not bother the occupant. This way, the occupant can adjust as it needs. Personalized ventilation is similar to the temperature stratification with displacement ventilation [28]. It does not have to blow heavily to occupant to draw the convection plumes as it closer to the occupant. As a result, it only deals with occupied zones, and it help to be energy efficient. However, the excessive temperature difference between the head and ankle levels can cause stratification discomfort. Vertical air temperature difference between the ankle level and head level should be less than 3 °C [10,11]. Also, it cannot be moved due to it is connected to HVAC system with the ducts that are fixed to table/chair [29].

2.2 Indoor Airflow

At the end, all ventilation systems serve to achieve indoor environment quality and their subtitles. In this thesis, thermal comfort, and air distribution within the room. These two topics cannot be separated due to their dependence between themselves. Air distribution helps to understand the surroundings of occupants and the room. If one can understand the jets, buoyancy, and the Coanda effect, surely can contribute to thermal comfort analysis.

According to studies, thermal comfort has a direct relationship with productivity. If the space is well conditioned ($-0.5 < \text{PMV} < 0.5$), workers have more productivity during the day [30-33]. In the circumstances, researchers are focused on how to improve workers' productivity with their current layout. Marek Borowski et al [34], studied linear diffusers in an office building in achieving user comfort and productivity in a room. The study conducted on diffuser performance on cooling conditions. There

were to different linear diffuser types that had different openings. The study revealed that even though they are the same type of diffuser one of them offers more consistent airflow distribution and reduces draft risk compared to other. Also, they highlight the significance of airflow fluctuations when assessing thermal comfort of the diffusers [34].

Aziz et al [35], investigated the performance of vortex, round and square ceiling diffusers which are serves in mixing ventilation conditions with experimental and numerical methods. They analyzed the flow pattern and made comments on the air jet zones that we are going to discuss in chapter III. As a result, the vortex diffusers cooled the room more efficiently than the square and round diffusers consuming 50% less energy. The velocity decay coefficient of the vortex diffuser with a 45° swirling angle was 2.6 times lower than the square and round diffusers. That is why, they concluded with the statement of vortex diffusers are more suitable for highrise buildings. Differently from other papers in the field, they used mean age of air (MAA), ventilation effectiveness and effective draft rate to analyze thermal comfort of the room. The mean age of air is related with the temperature distribution and air movement. a lower mean age of air with more frequent air changes tends to promote better temperature distribution and air movement, contributing to improved thermal comfort in indoor spaces [35]:

$$\frac{\partial}{\partial x_i} = \rho u_i MAA - \left(2.88\rho \cdot 10^{-5} + \frac{\mu_{eff}}{0.7}\right) \frac{\partial MAA}{\partial x_i} = S \tag{1}$$

Sami Lestinen et al [36], investigated the air characteristics as the thermal loads of increased. As thermal loads are getting high, the surrounding airflow motion increases and the heat transfer between the occupants and the surrounding also increases. This causes stratification on the ceiling. As a result, they observed that airflow fluctuations are increased with thermal loads. Additionally, turbulent kinetic energy, turbulence dissipation, and the range of length scales increased with thermal load [36].

According to Nielsen [37], his measurements indicate that the velocity at the floor

is influenced not only by the flow rate into the room but also by the temperature difference (Archimedes number). Additionally, the velocity level can vary for different types of diffusers. The flow becomes stratified at larger temperature differences, as evidenced by a constant height of the cold flow independent of the distance from the supply opening. He observed that the radial flow has a virtual origin close to the front of the diffuser, and the velocity level along the floor is inversely proportional to the distance from the diffuser. The velocity decay can be described individually for each type of diffuser using a single equation and a variable dependent on the Archimedes number [37].

The article of Fontaine et al [38], investigated different types of boundary conditions for characterizing the diffusers which are simplified, mixed and complex boundary conditions. Even though the measurements of the diffuser in the manual showed symmetry, the real flow at the experiment showed asymmetry, possibly due to the installation of the diffuser and the airflow around the duct. Three methods were examined: complex, simplified, and mixed boundary conditions. The complex method had convergence issues, while the simplified and mixed methods achieved convergence and grid invariance. The best results were obtained with simplified boundary conditions, but they were symmetrical and unable to model asymmetrical. Mixed boundary conditions faithfully reproduced the asymmetry, yielding good correlation. Simulations with simplified and mixed boundary conditions produced similar flows downstream of the diffuser [38].

Li et al [39], conducted research about swirl diffusers airflow performance. The research conducted on isothermal conditions so that there is no temperature difference between air coming out of the diffuser and the space. Therefore, it shows air characteristics without any buoyancy interruptions. Because of first phase of free jet maximum velocity equals to opening velocity, strong rotation, and vortex formation near the outlet of the diffuser are observed. The swirl diffuser exhibits a lower K value

and higher average entrainment ratio compared to circular ceiling diffusers. These characteristics indicate that the swirl diffuser can induce more air and effectively reduce draught effects for a given flow rate [39].

Andersson et al [40], approached the air jets with new ventilation supply which based on confluent jets. Confluent jets are the jets that merge with multiple air jets into a single jet of air. It occurs when two or more air streams converge and form a unified airflow. By using this phenomenon, Andersson found a new ventilation supply device that can combine air jets to analyze the pattern of air. The device has 95 round nozzles with 28mm diameter that can supply air to space. As a result, they found out that velocity in each nozzle is directly dependent on the airflow rate. In terms of the flow pattern, it does not change between airflow rates. When the airflow rate is high, the velocity profile increases accordingly after colliding with the other airflows [40].

Lastly, a study conducted by Keskin and Mengüç [44] focused on an adaptive vent system designed for localized and customized thermal management in buildings. This system utilizes individually operable flaps, which can asymmetrically open the inlet to control the airflow. Temperature sensors placed throughout space are used to monitor the temperature distribution. By employing this system, the flaps can direct the airflow to specific areas as needed, thereby avoiding unnecessary conditioning of unoccupied regions. Additionally, the system's air terminals contribute to horizontal temperature differentiation by blowing air to condition needed. There are several research about thermal sensation difference on genders. It can be also said that there is difference between human to human [41-43]. Keskin and Mengüç paper also answers this as temperature can be set to different setting horizontally across the room [44].

2.3 Thermal Comfort

In general, thermal comfort occurs when body temperatures are held within narrow ranges, skin moisture is low, and the physiological effort of regulation is minimized [10]. The ability to control the body temperature, moisture and physical effort of the body does itself with hypothalamus (is the central control organ for body temperature) is called thermoregulation. Thermoregulation wants to regulate body temperature at 36 to 38 by sweating when body is too hot or shivering when the body is too cold. Even when there is nothing producing any heat in the room that is currently in, the body produces $58W/m^2$ itself with their organs. Even in optimal conditions, humans need ventilation for fresh air and cooling for their body heat. The heat that human produces is transferred to the surroundings, the transfer occurs by conduction, evaporation, radiation, re-radiation, natural convection.

Especially, the microenvironment around the human body consists of a buoyant convective flow with a thickness of up to 50 mm and a velocity of up to 0.25 m/s. This flow transitions into a thermal plume overhead, and merges with transient flows generated by breathing [10].

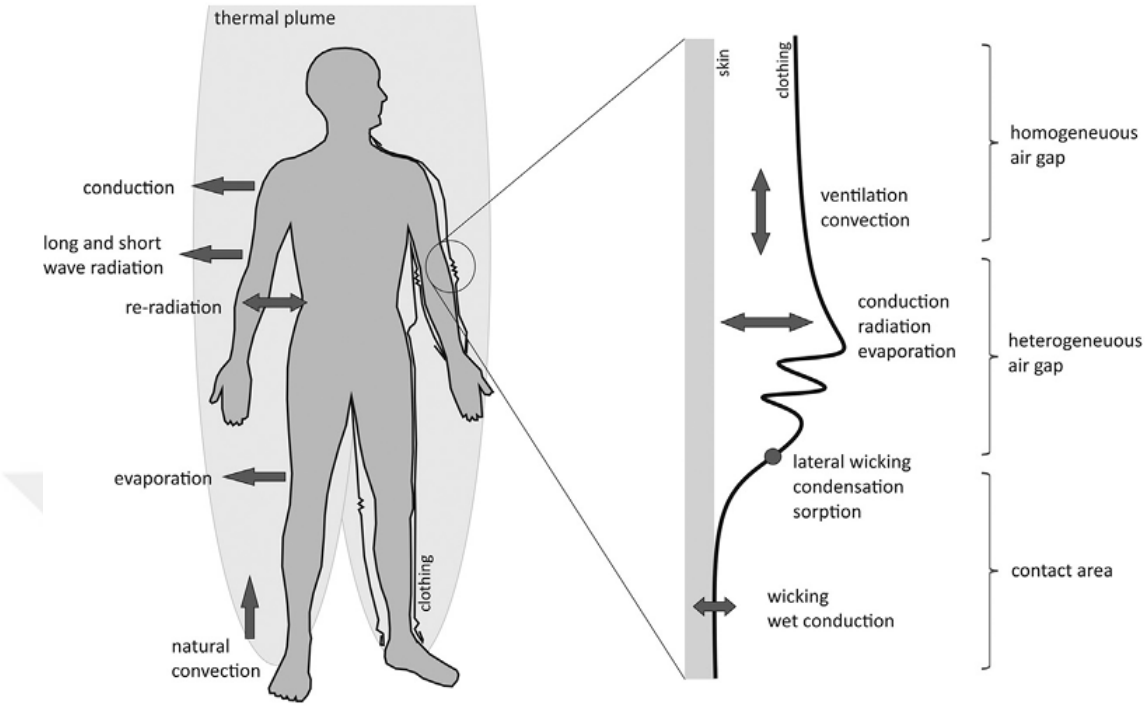

Figure 4: Heat transfer between surroundings and human [45]

For a long time, the thermal reactions of the human body and its interaction with the environment have been among the subjects of human history. In 1911, Lefevre modeled the human body and explained the heat transfer with the environment [46]. Later, in 1934, Burton was the first to describe human anatomy mathematically [47]. Many models have been made since then. These models are part of the thermal comfort and thermal sensation estimation methods. Thermophysiological models are considered as inputs for thermal comfort and thermal sensation predictions.

In this area, the United States National Aeronautics and Space Administration (NASA) has started to develop thermoregulation models for extreme conditions. In recent years, many thermophysiological models have been produced to determine the thermal comfort of people living in buildings [48,49].

One of the most chosen thermal comfort models can be said as Fanger's equation for human body heat exchange. The model requires six variables to solve thermal

comfort in that position. These variables are mean radiant temperature, relative air velocity, water vapor pressure in ambient air, air temperature, activity level and thermal resistance of clothing. The usage of this thermophysiological model is the indoor environment in buildings. The predicted mean votes (PMV) are expressed in 7-point ASHRAE thermal sensation scale [10].

Table 1: Fanger thermal sensation range [10]

No	Definition	Numerical value
1	Cold	-3
2	Cool	-2
3	Slightly cool	-1
4	Neutral	0
5	Slightly warm	+1
6	Warm	+2
7	Hot	+3

As we mentioned earlier in the literature survey, there are several types of ventilation, one of them is the underfloor air distribution system (UFAD). Chung et al, observed the UFAD in terms of thermal comfort. In the thermal comfort, we usually talk about thermal stratification of the room as we usually overhead air distribution systems. In UFAD, thermal stratification is not much of a problem due to it starts heating/cooling from the comfort level. So that, they picked 3 cases which are (1) supply at floor, return at ceiling, (2) return at floor, supply at ceiling, and (3) both at the ceiling. So that they can easily be compared with overhead air distribution systems. They found that the UFAD system shows the benefit of the localized distribution of conditioned air which gives more freedom for the control over the local thermal environment. As for the section average, PMV values came as 0.57, 1.29,

and 0.77, respectively. In conclusion, they picked supply at ceiling and returned at floor level the most comfortable thermal comfort condition [50].

On personal ventilation, there are 2 options, personal control over the ambient space temperature or localized thermal conditioning of occupants' body. Luo et al, aimed to investigate localized thermal conditioning done by personal comfort systems. They proposed heated/cool chair, desk fan, a heated shoe insole and heated/cooled wrist pad. So that they can react quickly as possible. The PCS tried to reach the ambient temperature towards thermal neutrality by as much as 6.5 °K cooling and 3.6 °K heating, overcoming building occupants' typical interpersonal thermal differences and making possible large HVAC energy savings in buildings [51].

At the study in 2004, Calvino introduced an adaptive controller for an office based on PMV values. The controller signals the HVAC unit to open up when the PMV value goes down to -1 until it reaches PMV > -0.5. By this way, thermal comfort has been satisfied. As a result, it was a start for personal ventilation [52]. After almost 20 years later, a game changer thing came up, visual data processing took huge step forward. As a result, it can be combined with thermal comfort. Bo Young Kim and Youngib Ham introduced machine learning algorithms to use on thermal comfort by looking at the facial videos that they collected across the US. The proposed personal thermal comfort modeling had median performance up to accuracy of 78% which is competitive based on other personal thermal comfort models [53].

CHAPTER III

THEORETICAL ANALYSIS

Computational fluid dynamics (CFD) is usually used for different aspects of buildings such as indoor air quality, energy, ventilation by solving Navier Stokes equations to obtain detailed flow field information within the space. In this chapter, mathematical formulations of the problem are given. The model runs by RANS and k-epsilon formulations, each of them explain mathematically and to run thermal comfort wizard of the model, radiation models has been added.

3.1 Conservation Equations

Indoor airflow, convective heat transfer, and species dispersion are controlled by the governing equations for mass, momentum in each flow direction, energy. Below here the governing equations of mass, momentum and energy are:

Conservation of mass (Continuity equation)

$$\frac{\partial \rho}{\partial t} + \frac{\partial \rho u_i}{\partial x_i} = 0 \tag{2}$$

where u is the fluid velocity, ρ is the density of fluid. Where the density ρ is constant for incompressible fluid (here is air), the governing equation becomes:

$$\frac{\partial u_i}{\partial x_i} = 0 \tag{3}$$

Conservation of momentum

$$\frac{\partial(\rho u_i)}{\partial t} + \frac{\partial(\rho u_i)}{\partial x_i} + \frac{\partial(\rho u_j \rho u_i)}{\partial x_j} = -\frac{\partial p u_i}{\partial x_i} + \frac{\partial \tau_{ij}}{\partial x_i} + \rho g_i + F \tag{4}$$

in which p is static pressure, τ is the viscous stress tensor, ρg_i represents gravity forces and F represents external body force.

Conservation of energy

$$\rho\frac{De}{Dt} = [-\nabla(pu)] + \Big[\frac{\partial(u\tau_{xx})}{\partial x} + \frac{\partial(u\tau_{yx})}{\partial y} + \frac{\partial(u\tau_{zx})}{\partial z} + \frac{\partial(v\tau_{xy})}{\partial x} + \frac{\partial(v\tau_{yy})}{\partial y} + \frac{\partial(v\tau_{zy})}{\partial z} + \frac{\partial(w\tau_{xy})}{\partial x} + \frac{\partial(w\tau_{yz})}{\partial y} + \frac{\partial(w\tau_{zz})}{\partial z}\Big] + \nabla(k\nabla T) \tag{5}$$

3.2 k-Epsilon Turbulence Model

Most fluid flows of engineering interest are characterized by irregularly fluctuating flow quantities. These fluctuations at small scale and repeated frequencies can be computationally costly to solve. Direct Numerical Simulation can be time consuming. Therefore, the fluctuations can be filtered or averaged to solve the using the following turbulent flow models:

- k-Epsilon,
- Large Eddy Simulation (LES) and Detached Eddy Simulation (DES)

LES and DES are for simulations that solve large scales of turbulence and model small-scale motions. Also, these simulations take time to create and take time to solve.

On the other hand, Reynolds-Averaged Navier-Stokes (RANS) equations are easy to use and do not take time to run [54].

Reynolds-Averaged Navier-Stokes can be used with k-Epsilon turbulence model is the most commonly used turbulence model in the CFD. Like everything it has pros and cons itself. The k-epsilon does not perform well when there are large adverse pressure gradients [55]. However, it offers a good compromise between robustness, computational cost, and accuracy. That is why k-Epsilon turbulence model is selected to be utilized in this thesis.

As from the name we can understand there are 2 transported variables in this

equation. One of them is turbulent kinetic energy k, the other one is turbulent dissipation ϵ.

For turbulent kinetic energy k,

$$\frac{\partial}{\partial t}(\rho k) + \frac{\partial}{\partial x_i]}(\rho k u_i) = \frac{\partial}{\partial x_j}\left[\left(\mu + \frac{\mu_t}{\sigma_k}\right)\frac{\partial k}{\partial x_j}\right] + p_k + p_b - \rho\epsilon - Y_M + S_k \tag{6}$$

the source terms S_k can be written as;

$$S_k = \tau_{ij}^R \frac{\partial u_i}{\partial x_j} - \rho\epsilon + \mu_t p_b \tag{7}$$

For turbulent dissipation ϵ,

$$\frac{\partial}{\partial t}(\rho\epsilon) + \frac{\partial}{\partial x_i}(\rho\epsilon u_i) = \frac{\partial}{\partial x_j}\left[\left(\mu + \frac{\mu_t}{\sigma_\epsilon}\right)\right] + C_{1\epsilon}\frac{\epsilon}{k}(P_k + C_{3\epsilon} + P_b) - C_{2\epsilon}\rho\frac{\epsilon^2}{k} + S_\epsilon \tag{8}$$

Also, the source term SE can be written as;

$$S_\epsilon = C_\epsilon \frac{\epsilon}{k}\left(f_1 \tau_{ij}^R \frac{\partial u_i}{\partial x_j} + \mu_t C_b P_B\right) - C_{2\epsilon} f_2 \frac{\rho\epsilon^2}{k} \tag{9}$$

where turbulent viscosity is

$$\mu_t = \rho C_\mu \frac{k^2}{\epsilon} \tag{10}$$

And also, the PB is gradient of density term can be defined as,

$$P_b = \beta g_i \frac{u_t}{Pr_t}\frac{\partial T}{\partial x_i} \tag{11}$$

where the eternal expansion β is,

$$\beta = -\frac{1}{\rho}\left(\frac{\partial \rho}{\partial T}\right) \tag{12}$$

where Pr_t is the turbulent Prandtl number for energy and g_i is the component of the gravitational vector in the i^{th} direction. Mostly models take Pr_t number as 0.85.

$$C_{1\epsilon} = 1.44, \quad C_{2\epsilon} = 1.92, \quad C_\mu = 0.09, \quad \sigma_k = 1.0, \quad \sigma_\epsilon = 1.3 \tag{13}$$

3.3 Indoor Air Flow

As mentioned above, there are different types of ventilation systems. The reason why they are so different is due to the forces on the air stream. The air coming out of an air terminal is exposed to many forces such as Coanda effect, air jets, buoyance force. Using these forces for ventilation can be made by changing location of the diffuser, the type of the diffuser or changing the space dimensions.

In rooms that air movement dominated by heat sources which can be directed by natural or displacement ventilation forces, stratification of temperature and contaminant is created vertically. In this type of ventilations air supply and exhaust don't engage with natural forces created by heat sources. Cool air enters from the floor, as occupants' plumes goes up. In the upper zone, plumes stacks along the ceiling.

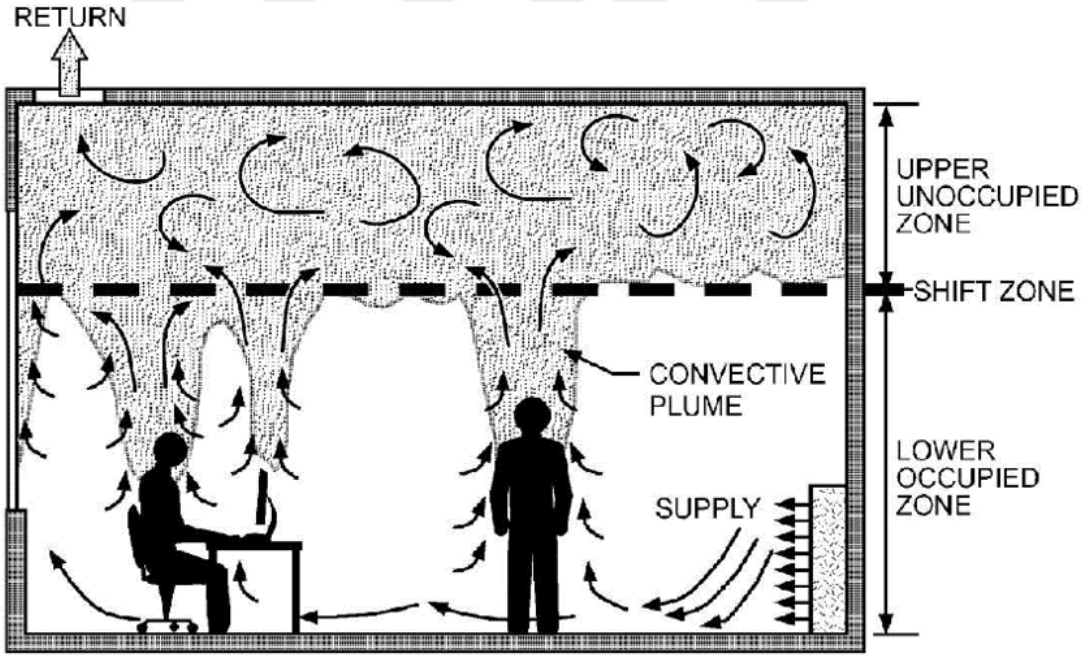

Figure 5: Schematic of airflow within displacement ventilation space [56]

To characterize the airflow in the stratified space, K number is proposed by Elterman, which is a ratio of kinetic energy dissipating in the ventilated space to the

energy used to suppress the buoyancy forces:

$$K = \frac{V^3 C_p \rho L B H}{\beta g W_{conv} l} \tag{14}$$

The K number is similar to Archimedes number which characterizes air jets influenced by buoyancy and also will be discussed in Air Jets part (See Archimedes number given in Eq. 18 below [57]).

In mixing ventilation, air supply with jets projected vertically downward or horizontally going along the ceiling with wall jets. In the second type which is horizontally, the jets reach the wall and if the decay is not started, it follows the room surfaces until it reaches the occupied zone. If the room is too large, it can start vortexes as can be seen in Figure 5. However, while designing a room with mixing ventilation, the airflow needs to prevent warm air to reach upper level that is not inside of the occupied spaces.

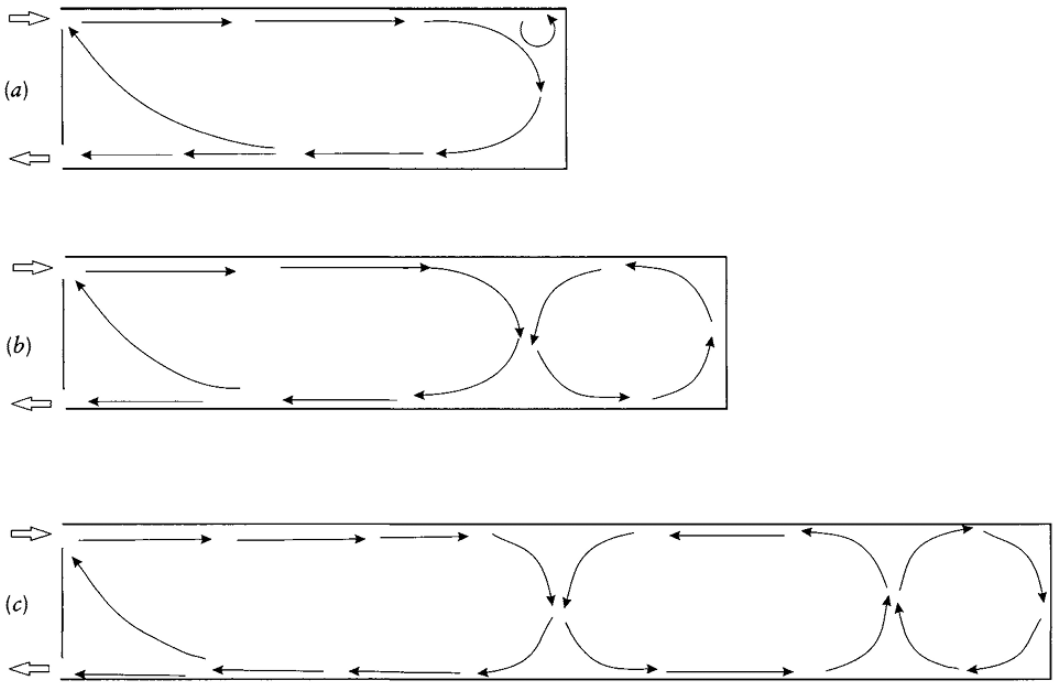

Figure 6: Flow patterns in room with horizontal supply in mixing ventilation (a) primary airflow in short room (b) primary airflow (c) primary and seconday airflows.

3.4 Air Jets

When supply air flows through an air diffuser, a jet is created in front of the opening. If it continues its journey without any interruption, such as wall or surface, it can be called as free jet. Free jet has 4 zones that have different characteristics.

In zone I, the maximum velocity U_m, of the jet is the same as the velocity at the air terminal outlet U_0.

In zone II, maximum velocity decreases with the equation below,

$$U_m \, \alpha \, \frac{1}{x^n} \tag{15}$$

where n is aspect ratio of the opening.

In zone III, is fully developed zone which extends up to $100A_0$ where A_0 is the diameter of the opening.

$$U_m \, \alpha \, \frac{1}{x} \tag{16}$$

Zone IV is the final zone where flow drastically drops with square of the distance it passes.

$$U_m \, \alpha \, \frac{1}{x^2} \tag{17}$$

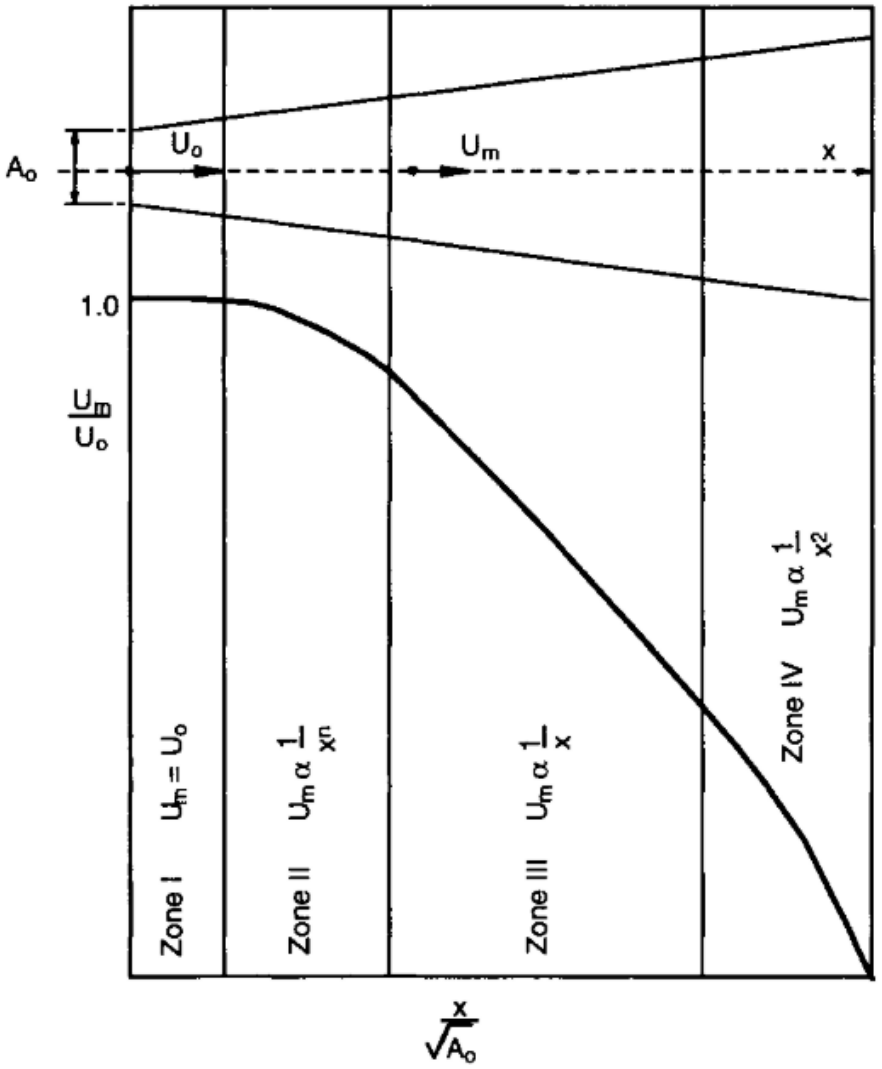

Figure 7: Free Jet zone characteristics [57]

If the temperature of the supplied air is equal to the temperature of the ambient room air, the jet is an isothermal jet. A jet with an initial temperature different from the temperature of the ambient air is called a non-isothermal jet [58]. Representations of the separation distance by buoyancy effect of non-isothermal jet related to Archimedes number:

$$Ar = \frac{\triangle T g l}{T u_0^2} \tag{18}$$

where g is the acceleration of gravity ($9.81 m/s^2$); $\triangle T$ is the temperature difference

between the discharged warm air and the room air (K); T is the absolute temperature in the discharged air (K); and u_0 is the discharge velocity of the warm air (m/s) [59].

As can be seen from the equation, Archimedes number related with buoyancy and viscous forces. If the Archimedes number is higher than 1, it means that buoyancy forces dominate the viscous forces. Therefore, the air jets tend to stick to upper level. This phenomenon occurs when the air jet is colder than the room air. On contrast if the Archimedes number is lower than 1, it means that viscous forces dominate the buoyancy, so that air patterns tend to result in a more downward trajectory.

3.5 Air Terminal Units

There are several air terminal units used in the sector. Depending on their design they have different names such as compact, linear, radial, conical, incomplete radial, swirling. Every diffuser has their own air jet characterization to serve the space (Fig. 7). Some of them such as swirl diffusers are used in high spaces where vortex can be formed to create rotational motion. Compact ones create jets that are three dimensional and axisymmetric at some distance from the diffuser opening. Also, they have their own equations which calculate the velocity.

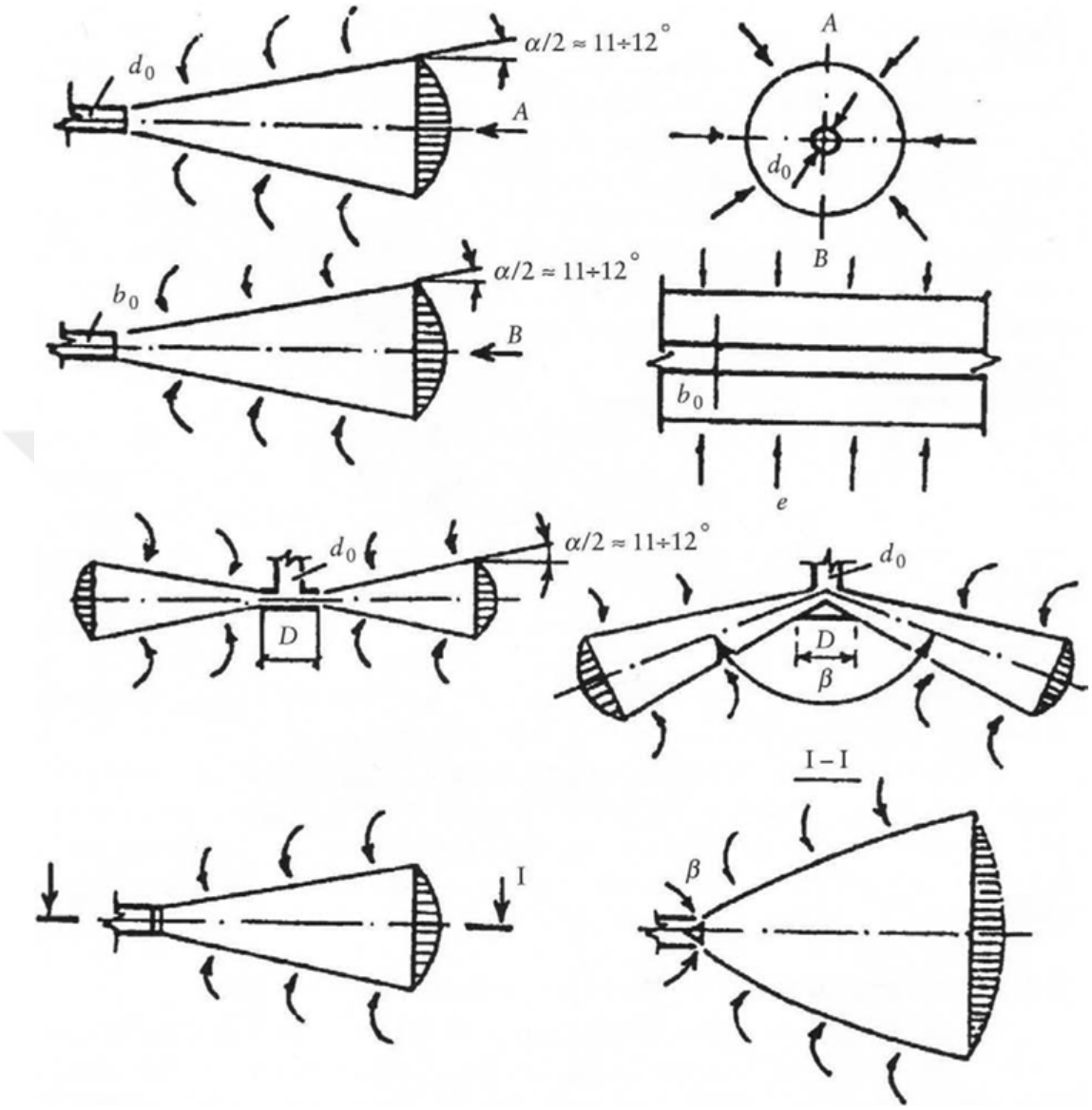

Figure 8: Types of diffusers with their air jet characterizations (a) compact; (b) linear; (c) radial; (d) incomplete radial (e) conical [57]

$$\frac{u_x}{u_0} = \frac{K_\alpha}{\sqrt{2}} \frac{\sqrt{a_0}}{x + x_0} \tag{19}$$

where u/u_o is dimensionless velocity in dimensionless distance $(x + x_0)/\sqrt{a_0}$, where a_0 is the area of the supply opening. K_α is constant in case of high turbulent flow, and it is individual for the different types of diffusers.

3.6 Thermal Comfort

Thermal Comfort can only be maintained when heat produced by metabolism equals the heat lost from body.

$$H - E_d - E_{SW} - E_{res} - L - K = R + C \tag{20}$$

where, H the internal heat production in the human body, E_d is the heat loss by water vapour diffusion through the skin, E_{SW} is the heat loss by evaporation of sweat from the surface of the skin, E_{res} is the latent respiration heat loss, L the dry respiration heat loss, K is the heat transfer by conduction through the clothing, R is the heat loss by radiation from the outer surface of the clothed body and lastly C is the heat loss by convection from the outer surface of the clothed body.

Each of these term are discussed below:

Internal Heat Production: The energy released by the oxidation process in the human body per unit time called metabolic rate M partially converted to external mechanical power W but mainly converted to internal body heat H. It can be written as,

$$M = H + W \tag{21}$$

Also, the mechanical efficiency can be defined as,

$$\eta = \frac{W}{M} \tag{22}$$

If we want to insert the mechanical efficiency to the equation, it turns out as,

$$H = M(1 - \eta) \tag{23}$$

Mechanical efficiency for a person is normally equals to zero since he/she is performing no work from a physical point of view. However, it can take values up to

$0.20 - 0.25$ on special occasions such as walking uphill, lifting sacks to a higher level etc.

The equation (23) can be also expressed per unit body surface area,

$$\frac{H}{A_{Du}} = \frac{M}{A_{Du}}(1 - \eta) \tag{24}$$

The magnitude of M/A_{Du} is a function of the activity of the person. It can vary according to the activity of that person does. As we look at Table 2. It can be seen that there are different metabolic rates for different types of activities.

Table 2: Metabolic rate at different typical activities [60]

Resting	Metabolic Rate	Mechanical Efficiency	Air Velocity
Standing	35	0	0
Reclining	40	0	0
Seated	50	0	0
Standing	60	0	0

Walking	km/h	Metabolic	Mechanical	Air
On the level		Rate	Efficiency	Velocity
	3.2	100	0	0.9
	4.0	120	0	1.1
	4.8	130	0	1.3
	5.6	160	0	1.6
	6.4	190	0	1.8
	8.0	290	0	2.2

Walking Up a grade (%)	km/h	Metabolic Rate	Mechanical Efficiency	Air Velocity
5	1.6	120	0.07	0.6
5	3.2	150	0.10	0.9
5	4.8	200	0.11	1.3
5	6.4	305	0.10	1.8
15	1.6	145	0.15	0.4
15	3.2	230	0.19	0.9
15	4.8	350	0.19	1.3
25	1.6	180	0.20	0.4
25	3.2	335	0.21	0.9

Office work	wpm	Metabolic Rate	Mechanical Efficiency	Air Velocity
Typing (electrical)	30	45	0	0.05
	30	50	0	0.05
Typing (mechanical)	30	55	0	0.05
	40	60	0	0.05
Miscellaneous office work (filling, checking ledgers)	-	50-60	0	0-0.1

Heat Loss by Skin Diffusion: The water vapour diffusion upon the skin is also considered. The magnitude of the diffusion per unit area is assumed to be proportional to the difference between saturated water vapour pressure at the skin temperature (p_s) and the partial pressure of the water vapour (p_a) in the ambient air. So that the

equation becomes,

$$E_d = \lambda m A_{Du}(p_s - p_a) \tag{25}$$

where E_d is heat loss by vapour diffusion through the skin, λ is the heat of vaporization of water, m permeance coefficient of the skin, saturated water vapour pressure at the skin temperature (p_s), the partial pressure of the water vapour (p_a).

The saturated water vapour pressure at the skin temperature can be derived from the function of temperature of the water as,

$$p_s = 1.92t_s - 25.3 \tag{26}$$

If we insert equation (25) to equation (26) and accept that lambda is 575 kcal/kg at 35 degree Celsius, m is $6.1 * 10^{-4}$, we can find the equation for heat loss by skin diffusion.

$$E_d = 0.35A_{Du}(1.92t_s - 25.3 - p_a) \tag{27}$$

Heat Loss by Evaporation of Sweat: In situations where individuals experience moderate sweat secretion and air temperatures, resulting in moderate vapor pressures, typically associated with thermal comfort, it can be reasonably assumed that all the sweat secreted will evaporate. The quantification of sweat secretion involves deducting the heat losses from diffusion and latent respiration. The secretion of sweat is a function that varies based on the interrelation between skin temperature and activity level.

$$E_{SW} = 0.42A_{Du}(H - 50) \tag{28}$$

where E_{SW} Heat loss by evaporation of sweat, A_{Du} Total area of the skin, H Internal heat production.

Heat Loss by Latent Respiration: The exchange of heat and water vapor occurs within the respiratory tract's mucosal lining through convection and evaporation. As the inspired air proceeds to the alveoli, it reaches a temperature matching

the body's core temperature and becomes saturated with water vapor. During its outward journey through the respiratory system, some heat is transferred back to the body, causing water vapor to condense. However, even as the expired air leaving the nose loses heat and water, it still contains more heat and water than the initially inspired air in comfortable environments. Consequently, breathing results in both latent heat loss and dry heat loss from the body.

The magnitude of latent respiration heat loss is influenced by pulmonary ventilation and the disparity in water content between expired and inspired air.

$$E_{re} = V(W_{ex} - W_a)\lambda \tag{29}$$

where E_{re} is Heat loss by respiration, V is Pulmonary ventilation, W_{ex} is Expiration air humidity ratio, W_a is Inspiration air humidity ratio and lambda is heat of vaporization of water.

Pulmonary ventilation is a function of the metabolic rate so that it can be written as,

$$V = 0.0060M \tag{30}$$

The differences of inspired and expired air humidity ratio can be written as a function of ambient air temperature and inspired air humidity ratio by following equation:

$$W_{ex} - W_a = 0.0277 + 0.000065a - 0.80W_a \cong 0.029 - 0.80W_a \tag{31}$$

By substituting Inspiration air humidity ratio as 0.0083 pa in the equation:

$$W_{ex} - W_a = 0.029 - 0.00066p_a \tag{32}$$

Lastly, by substituting the expressions for V and $W_{ex} - W_a$ to equation (29) we get get latent respiration heat loss formula:

$$E_{re} = 0.0023M(44 - p_a) \tag{33}$$

Dry Respiration Heat Loss: The heat loss during respiration, depending on the differences between inspired and expired air temperature can be expressed by

$$L = V c_p (t_{ex} - t_a) \tag{34}$$

Where $c_p = 0.24$ kcal/kg°C the specific heat of dry air at constant pressure.

To calculate exact value of the temperature of the expired air tex as a function of the condition of the inspired air

$$t_{ex} = 32.6 + 0.066 t_a + 32 W_a \tag{35}$$

However, since the dry respiration heat loss is small compared to other terms, it is taken as 34°C. So that equation can be written as

$$L = 0.0014 M (34 - t_a) \tag{36}$$

Heat Conduction Through the Clothing: Due to the complex nature of clothed body heat conduction, the calculations are simplified by Gagge by introducing the term I_{cl} which is a dimensionless expression for the total thermal resistance from the skin to the outer surface of the clothed body:

$$I_{cl} = \frac{R_{cl}}{0.18} \tag{37}$$

where the R_{cl} is the total heat transfer resistance from skin to outer surface of the clothed body.

This dimensionless expression has its own unit as clo-unit. The clo-unit refers to the clothing itself and can be expressed in the dry heat transfer:

$$K = A_{Du} \frac{(t_s - t_{cl})}{R_{cl}} \tag{38}$$

where I_{cl} is Clothing thermal resistance, R_{cl} is Clothing thermal resistance, t_s is Mean skin temperature, t_{cl} is Cloth temperature A_{Du} is total area of the skin.

Heat Loss by Radiation: The radiation occurs between the human body and its surrounding therefore it can be expressed by Stefan-Boltzmann's law:

$$R = A_{eff}\epsilon\sigma[(T_{cl} + 273)^4 - (T_{mrt} + 273)^4] \tag{39}$$

However, the geometry of the human body is irregular caused by appendages, re-entrant angles, the effective radiation area can be formulated as,

$$A_{eff} = f_{eff} f_{cl} A_{Du} \tag{40}$$

where f_{eff} the effective radiation area factor, f_{cl} the ratio of the surface area between clothed body and nude body.

After substituting the parameters, the heat loss from radiation becomes,

$$R = 3.4 \cdot 10^{-8} f_{cl} A_{Du}[(T_{cl} + 273)^4 - (T_{mrt} + 273)^4] \tag{41}$$

Heat Loss by Convection: The heat loss by convection can be expressed as

$$C = A_{Du} f_{cl} h_c (t_{cl} - t_a) \tag{42}$$

where h_c is the convective heat transfer coefficient, f_{cl} the ratio of the surface area between clothed body and nude body.

H_c is determined as the flow is laminar or not in the situation of free and forced convection as follows,

$$h_c = \left\{ \begin{array}{ll} 2.38 \cdot \mid t_{cl} - t_a \mid^{0.5} & \text{for} \quad 2.38 \cdot \mid t_{cl} - t_a \mid^{0.5} > 1.21\sqrt{v_{ar}} \\ 12.1\sqrt{v_{ar}} & \text{for} \quad 2.38 \cdot \mid t_{cl} - t_a \mid^{0.5} < 1.21\sqrt{v_{ar}} \end{array} \right\} \tag{43}$$

All these parameters contains in the equation 20 which is heat balance equation. In the fanger's equation, all parameters are used to find thermal comfort model.

There are few thermal comfort models in the field but the most commonly used it Fanger's thermal comfort model. Fanger's model is based upon an energy analysis that takes into account all the modes of energy loss (L) from the body, including:

the convection and radiant heat loss from the outer surface of the clothing, the heat loss by water vapor diffusion through the skin, the heat loss by evaporation of sweat from the skin surface, the latent and dry respiration heat loss and the heat transfer from the skin to the outer surface of the clothing [60,61]. The model assumes that the person is thermally at a steady state with his environment.

Calculation of PMV as follows:

$$PMV = [0.303 \cdot exp(-0.036 \cdot M) + 0.028] \cdot \left\{ \begin{array}{c} (M-W) - 3.05 \cdot 10^{-3}[5.733 - 6.99 \cdot (M-W) - \rho_a] \\ -0.42 \cdot [(M-W) - 58.15] - 1.7 \cdot 10^{-5} \cdot M \cdot (5.867 - \rho_a) \\ -0.0014 \cdot M \cdot (34 - t_a) - 3.96 \cdot 10^{-8} \cdot f_{cl} \cdot [(t_{cl} + 273)^4 - (\bar{t_r} + 273)^4] \\ -f_{cl} \cdot h_c(t_{cl-t_a}) \end{array} \right\} \quad (44)$$

where metabolic rate is M, effective mechanical power is W, clothing surface area factor is f_{cl}, air temperature is t_a, mean radiant temperature t_r , water vapor partial pressure ρ_a, convective heat transfer coefficient is h_c , clothing surface temperature is t_{cl}.

Clothing surface temperature can be solved by iterations therefore it starts with an initial guess, or it can be predicted without iterations.

$$\begin{array}{l} t_{cl} = 35.7 - 0.028 \cdot (M-W) - I_{cl} \cdot \\ \left\{ 3.96 \cdot 10^{-8} \cdot f_{cl} \cdot [(t_{cl} + 273)^4 - (\bar{t_r} + 273)^4] + f_{cl} \cdot h_c \ \cdot (t_{cl} - t_a) \right\} \end{array} \quad (45)$$

where I_{cl} is clothing insulation.

Also, convective heat transfer coefficient may be solved with iterations, the simulation can be start with the initial condition calculation, but it needs to be change due to temperature differences and relative air velocity.

$$h_c = \left\{ \begin{array}{ll} 2.38 \cdot \mid t_{cl} - t_a \mid^{0.5} & \text{for} \quad 2.38 \cdot \mid t_{cl} - t_a \mid^{0.5} > 1.21\sqrt{v_{ar}} \\ 12.1\sqrt{v_{ar}} & \text{for} \quad 2.38 \cdot \mid t_{cl} - t_a \mid^{0.5} < 1.21\sqrt{v_{ar}} \end{array} \right\} \quad (46)$$

f_{cl} can be calculated as follows,

$$f_{cl} = \left\{ \begin{array}{ll} 1.00 + 1.290\, l_{cl} & \text{for} \quad l_{cl} \leq 0.078 \\ 1.05 + 0.645\, l_{cl} & \text{for} \quad l_{cl} > 0.078 \end{array} \right\} \tag{47}$$

Also, it can be calculated by hand by knowing the clothing insulation. There are few ways to estimate clothing insulation. The first method is to get ASHRAE 55 thermal comfort list that categorizes clothing sets that can be selected. Secondly, the list that has variety of individual garments can be subtracted or added to clothing sets. Finally, someone can use individual garments to cloth the manikin. However, it is recommended to use clothing sets which gives the best option for predicting clothing insulation [62].

Metabolic rate is the energy transformation from chemical energy to mechanical work by the activities that organisms do. It is expressed by met units within range.

$$46\frac{W}{m^2} \leq M \leq 232\frac{W}{m^2} \qquad 0.8\, met \leq M \leq 4\, met \tag{48}$$

PPD is an index that establishes prediction of the percentage of thermally dissatisfied people which a function of PMV. PPD is based on the assumption that people voting far from the neutral -1 to 1.

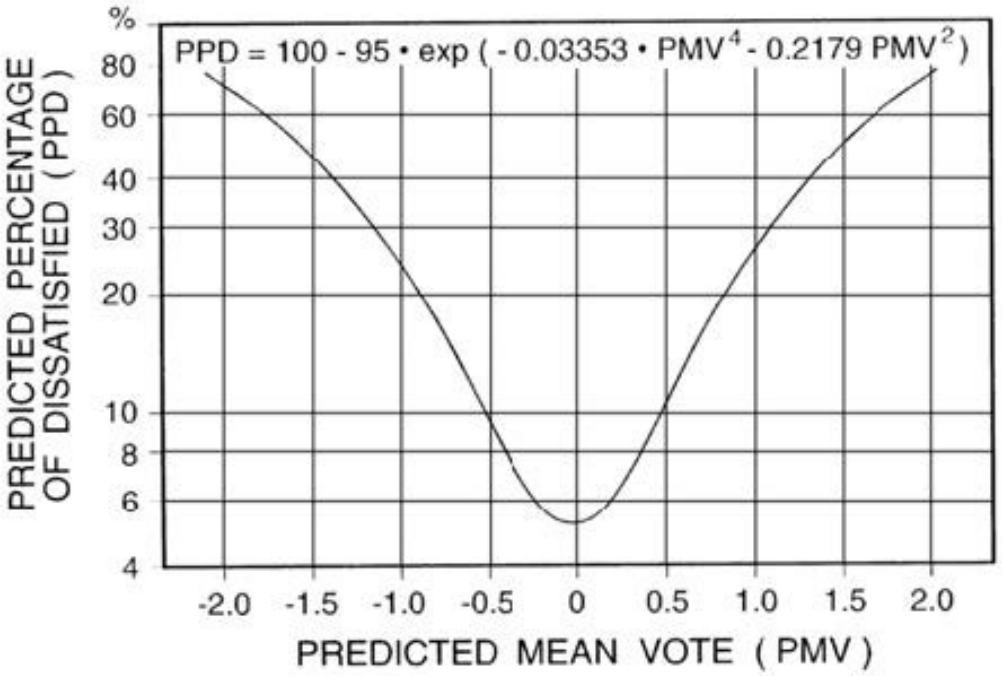

Figure 9: Predicted percentage dissatisfied based on PMV [10]

And can be written as,

$$PPD = 100 - 95 \cdot \exp(-0.03353 \cdot PMV^4 - 0.2179 \cdot PMV^2) \tag{49}$$

PMV-PPD values give an average result of whole human body. In real life, thermal dissatisfaction can be caused by unwanted cooling/heating to single body part. This sensation is called local discomfort. Local discomfort can be caused by draught, high temperature difference between head and ankle, high radiant asymmetry and too hot or too cold floor [11].

The most commonly encountered local discomfort issue is often attributed to a high draught rate. The calculation of draught can be performed using the following method:

$$DR = (34 - t_{\alpha,l})(\bar{v}_{\alpha,l} - 0.05)^{0.62}(0.37 \cdot \bar{v}_{\alpha,l} \cdot T_u + 3.14) \tag{50}$$

where:

$\bar{v}_{\alpha,l} = 0.05m/s$ for $\bar{v}_{\alpha,l} < 0.05m/s$

$DR = 100\%$ for $DR > 100\%$

$t_{\alpha,l}$: local air temperature between 20 °C to 26 °C.

$\bar{v}_{\alpha,l}$: local mean air veocity $< 0.5m/s$

T_u : local turbulance intensity, between 10% to 60%

As mentioned above, other discomfort is the high vertical air temperature difference between ankle and the head.

$$PD - \frac{100}{1 + \exp(5.76 - 0.856 \cdot \triangle t_{\alpha,v})} \tag{51}$$

Each physical body emits a specific amount of radiative energy depending on the temperature levels. This energy is either emitted, absorbed, transmitted, or reflected in a specific amount by interacting with the unique properties of selected material. Considering that each material has its own unique properties, the radiative properties vary significantly; hence, correct radiative values must be entered while conducting numerical studies to obtain accurate results. However, it must be noted that obtaining accurate results is not only limited to selecting the materials correct radiative properties, but also calculating the heat exchange between the interacting surfaces using surface patches and view factors. These three parameters are crucial for accurate modelling of heat transfer.

To model this behavior, the Surface-to-Surface Radiation (S2S Radiation) model was chosen as the majority of the geometry models contain flat surfaces with minimum number of complex shapes. It is known that for simple systems with dominant surface to surface energy exchanges, S2S model performs particularly well (insert a reference here). The S2S model can further be simplified for faster results by assuming the surface to be 'gray', or wavelength-independent, which neglects the independence of

properties such as emissivity, or reflectivity on radiative wavelength. Wavelength-independency results in a constant radiative property throughout all wavelengths. This assumption may result in either elevated, or reduced energy transfer, causing temperature variations compared to real life scenarios. This phenomenon is observed throughout all numerical analysis conducted.

$$\begin{aligned}
&\left(1-\tau_{i,\lambda}-\rho_{s,i,\lambda}\right)\left(1-F_{i-i,\lambda}\right)J_{i,\lambda}^{eff}-\rho_{d,i,\lambda}\sum_{j=1,j\neq i}^{N_p}F_{i-j,\lambda}J_{j,\lambda}^{eff}\\
&\quad=\epsilon_{i,\lambda}\triangle_{(\lambda_1\to\lambda_2,T_i)}\sigma T_i^4+E_{d,i,\lambda}\\
&\qquad+\rho_{d,i,\lambda}\left\{F_{i-e,\lambda}\left[\triangle_{(\lambda_1\to\lambda_2,T_e)}\sigma T_e^4+\triangle_{(\lambda_1\to\lambda_2,T_{sun})}J_{d,solar,e}\right]+J_{dir,solar,i,\lambda}\right\}
\end{aligned}\tag{52}$$

where

$\triangle_{(\lambda_1\to\lambda_2,T_i)}$ is the fraction of total blackbody emission for the spectrum or band

λ_1 and λ_2 represent the lower and upper wavelength bounds of the spectrum or band

$\epsilon_{i,\lambda}$ is the emmissivity

σ is the Stefan-Boltzmann constant $\frac{W}{m^2K^4}$

$J_{d,source,e}$ is a specified external diffuse radiative flux source, in this case its solar radiation

$J_{dir,source,i,\lambda}$ is a specified external collimated flux source in this case its solar

CHAPTER IV

METHODOLOGY

4.1 Layout of the Experiment Office

The model developed in this thesis was centered around an office space situated on the first floor of Özyeğin University. Presently, this office is utilized by researchers from the CEEE team, led by Cem Keskin and M. Pınar Mengüç.

The office is equipped with windows on the west side only, and there is a single door on the east side. The walls are asymmetrical, with columns that have indentations into the walls. The dimensions of the office are 4.4 meters in width, 6.2 meters in length, and 2.45 meters in height, with an additional 60 centimeters for the suspended ceiling. The architectural design of the office was provided by Cem Keskin [23] in his doctoral dissertation. Furthermore, a 3D model was initially created by Cem and later modified by me to reflect the changes made in the office layout. The 3D model was developed using STAR CCM+, which is the software program we utilized for our computational fluid dynamics (CFD) simulations. The decision to use STAR CCM+ for the sketches was to ensure that there would be no misinterpretation of the sketches when transferring them between different software programs.

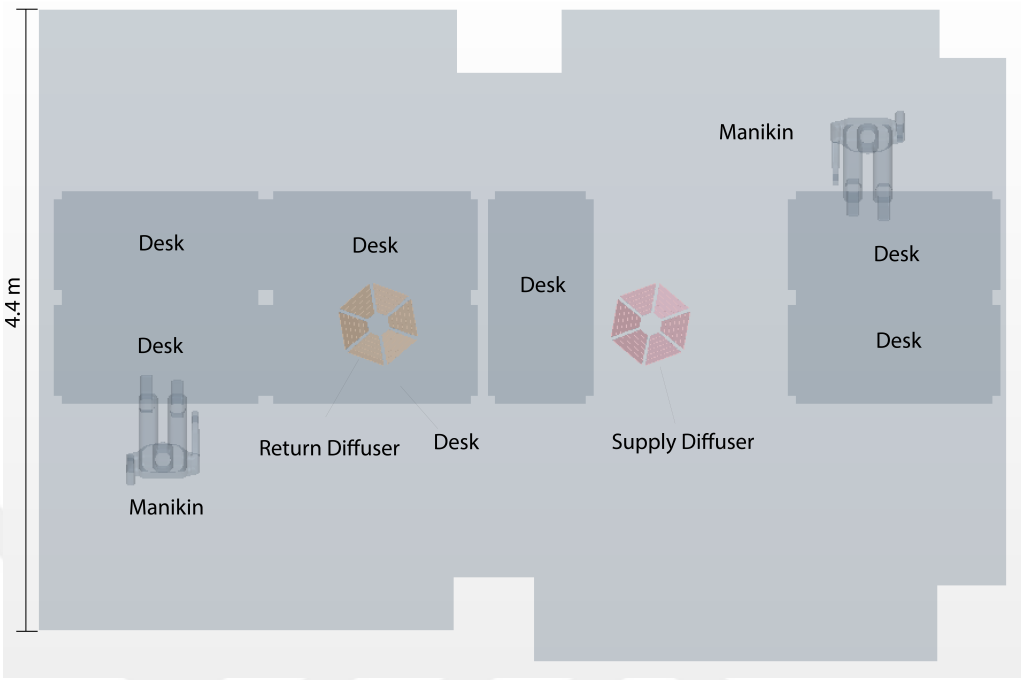

Figure 10: Top view of the office model

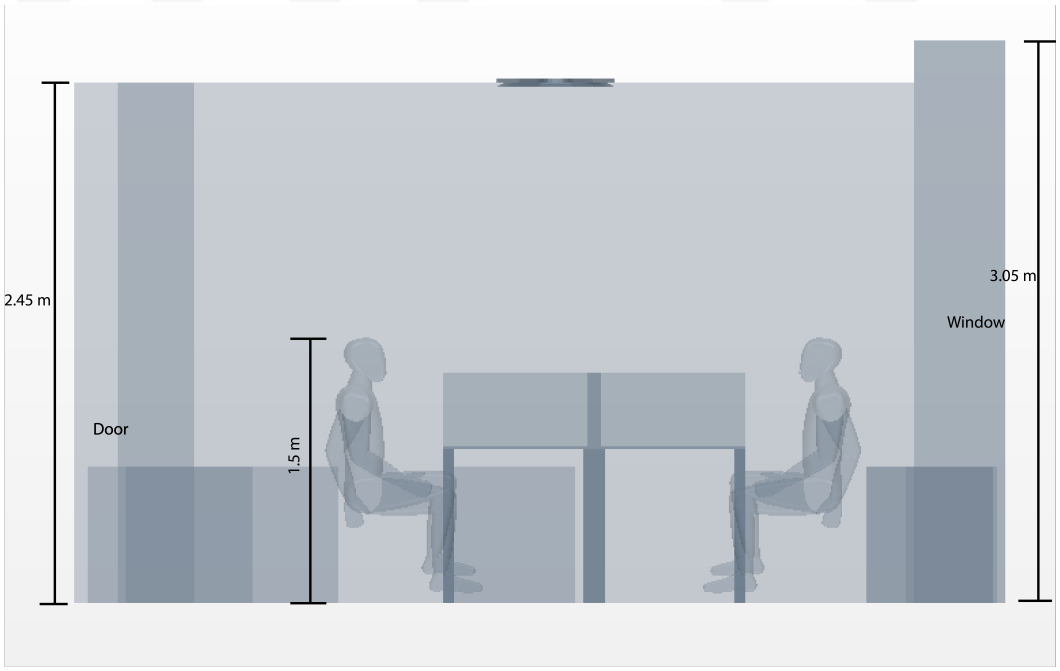

Figure 11: Side view of the office model

The model was created in previous research, the modification is made due to it is

still in use for researchers so that layout changes in the office regularly. Here is the 3D model of the office, all walls are inside wall therefore, they conditioned from both ways. There is not much heat loss/gain from conduction on the wall.

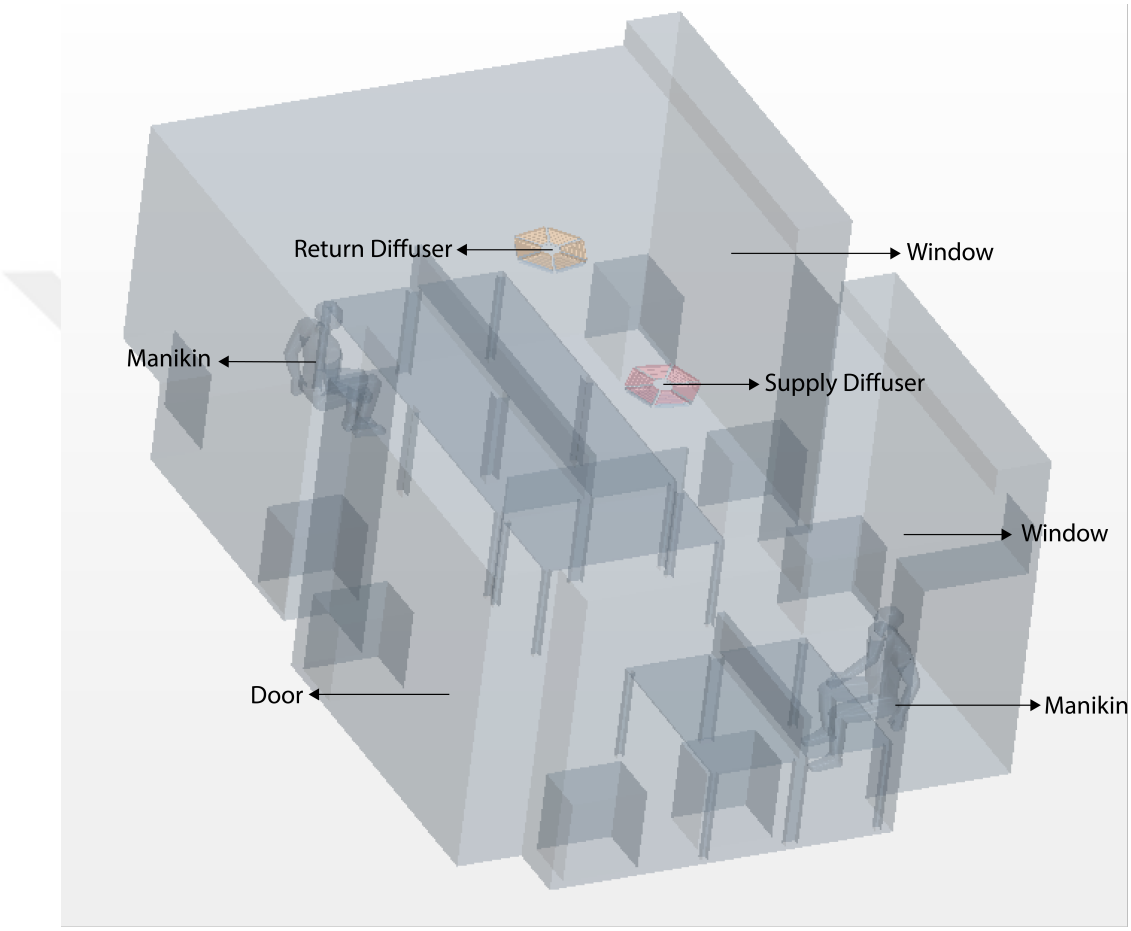

Figure 12: 3D model of the office space

As depicted in the figure, there are two diffusers installed in the room. These diffusers are connected to the fancoil unit responsible for providing heating and cooling within the room. However, to meet the office's fresh air requirements, it is necessary to supply fresh air. This can be achieved by opening a window (natural ventilation) or using the centralized Air Handling Unit that is designed to supply and exhaust the dirty air. To supply air from AHU unit, normally there is a need for second supply/return diffuser unit to be installed, or it can be connected to the plenum

box positioned above the diffusers of the heating and cooling unit in more confined spaces. Due to the cramped nature of the suspended ceiling in this office design, only one supply and one return diffuser are placed. Naturally, fresh air connected to the plenum box of these diffusers. In this specific office, the FCU unit couldn't do enough to heat up the place due to poor estimation of heat losses. So that, a heater is added to the system.

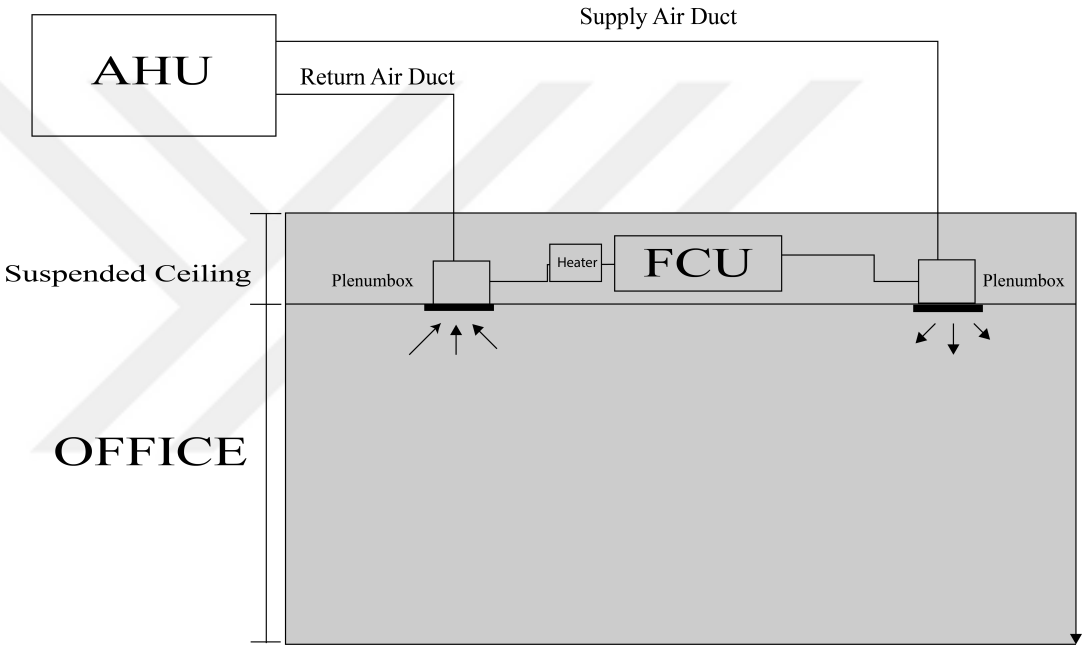

Figure 13: HVAC system schematic of the office space

As previously mentioned, air diffusers play a crucial role within the HVAC system. Their appearance can vary based on factors such as the chosen ventilation strategy, the size and height of the space, and their specific placement. The industry offers a wide array of air diffusers tailored to various needs, with thousands of different types available. Among the most commonly used ones are linear, square, and swirl diffusers.

In addition to the widely-used diffusers, academic studies have also led to the development of specialized diffusers that deviate from conventional designs. These

unique diffusers contribute to advancements in the sector and push it in new directions, promoting innovation and progress.

In this thesis, our investigation focused on three distinct air diffusers, each carefully chosen to suit the design of the grid-based ceiling. Unfortunately, linear diffusers were excluded from the selection as they are not compatible with the grid-based ceiling. Among them, two are widely employed in the industry, while the third one stands out as a unique diffuser developed by Cem Keskin and M.P. Mengüç for their project. This exceptional diffuser is an outcome of their ongoing efforts to enhance thermal comfort for all users. Their continuous development aims to achieve superior performance and deliver better thermal comfort to a broader audience.

The square diffuser (Fig. 14) is commonly used in commercial and residential buildings to distribute conditioned air evenly throughout a space. It is typically mounted on the ceiling or wall and works by directing air in multiple directions through a series of adjustable blades or vanes. The air exits between the blades of square diffuser goes parallel to the wall and ceiling due to the Coanda effect. This results in the air stream hugging the surface. By this way, thermal stratification is ended and air goes down by going parallel to the walls.

The diffuser design in the model was obtained from the manufacturer's technical design datasheet. This particular diffuser was equipped with a damper to control the airflow. As the other diffusers in the model did not have a damper, it was extracted from the diffuser that possessed one, enabling proper comparison between the diffusers.

Figure 14: Inside of the square diffuser

The swirl diffuser (Fig. 15) is specifically employed for supplying hot or cold air to conference halls, sports halls, or spaces with high ceilings where conventional diffusers may not effectively reach the ground. It features adjustable blades that can be directed in four different directions. Additionally, the flaps can be closed in any of these directions. The typical configuration of the swirl diffuser positions its flaps at a 45-degree angle to the ceiling. During the modeling process, we experimented with various scenarios, including closing some of the flaps, to observe the effect on the

airflow. By reducing the number of open flaps, we hoped to observe an increase in the airflow in certain directions. This may allows for better control of the air distribution within the space, optimizing thermal comfort for the occupants.

Figure 15: Four-way Swirl Diffuser

Lastly, the unique solution designed by Cem was integrated into the simulations. This distinct diffuser maintains the dimensions of 60x60cm, similar to the others, but stands out with its hexagonal shape. It possesses six operable flaps, where each section can be individually opened or closed. Additionally, the diffuser is equipped with a motorized system that allows for angle optimization, offering further flexibility in directing the airflow.

As depicted in Figure 16, this unique diffuser is not parallel to the false ceiling. This intentional design decision aims to maximize the openings of the diffuser, granting it the ability to blow air in different directions. By incorporating this innovative feature, the diffuser can efficiently distribute air in the desired patterns, enhancing

thermal comfort and improving air circulation within space.

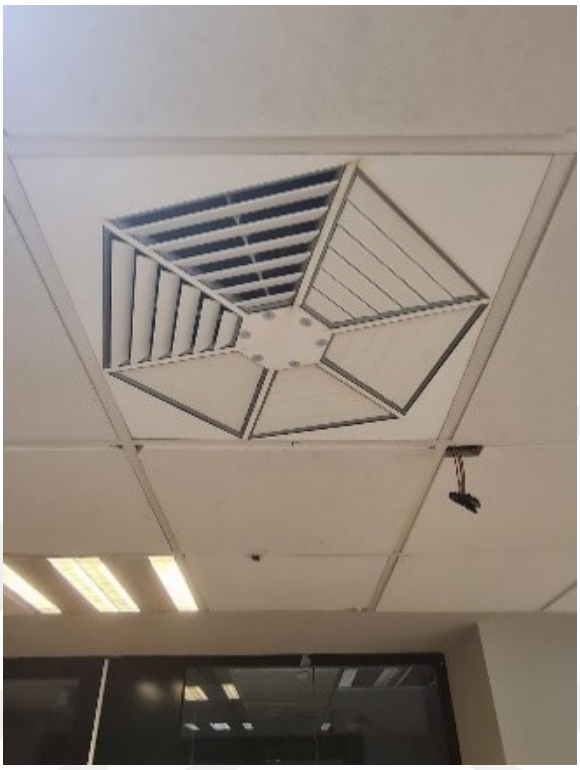

Figure 16: Hexagonal air diffuser with operable flaps

Measuring air parameters from air diffusers is a crucial aspect of this research, but it requires specific tools. The experimental data obtained from these measurements will serve as essential inputs for both the validation and numerical analysis stages of the study. As the main focus of this thesis is thermal comfort in office rooms, the selected variables for validation were carefully determined to align with this objective.

Air velocity is directly associated with the thermal comfort variables that we mentioned in chapter 3. Also, the temperature is another crucial factor for the thesis. After mentioning PMV values, we mentioned that PMV values might be missing the local discomfort due to taking variables as average. The thesis also measures draft risk and the variable that is used to find draft risk Turbulence intensity to use in validation.

For this thesis, two Testo 440 devices were utilized. The Testo 440 is a versatile

tool capable of measuring air velocity and air quality within space. It has the capability to connect up to three probes simultaneously. These probes include a Bluetooth probe, a wired probe, and a temperature probe with a type K thermocouple connector. Such tools are indispensable for gathering accurate data and validating the findings of numerical simulations.

Figure 17: Measurement tools, Testo 440, and its probes

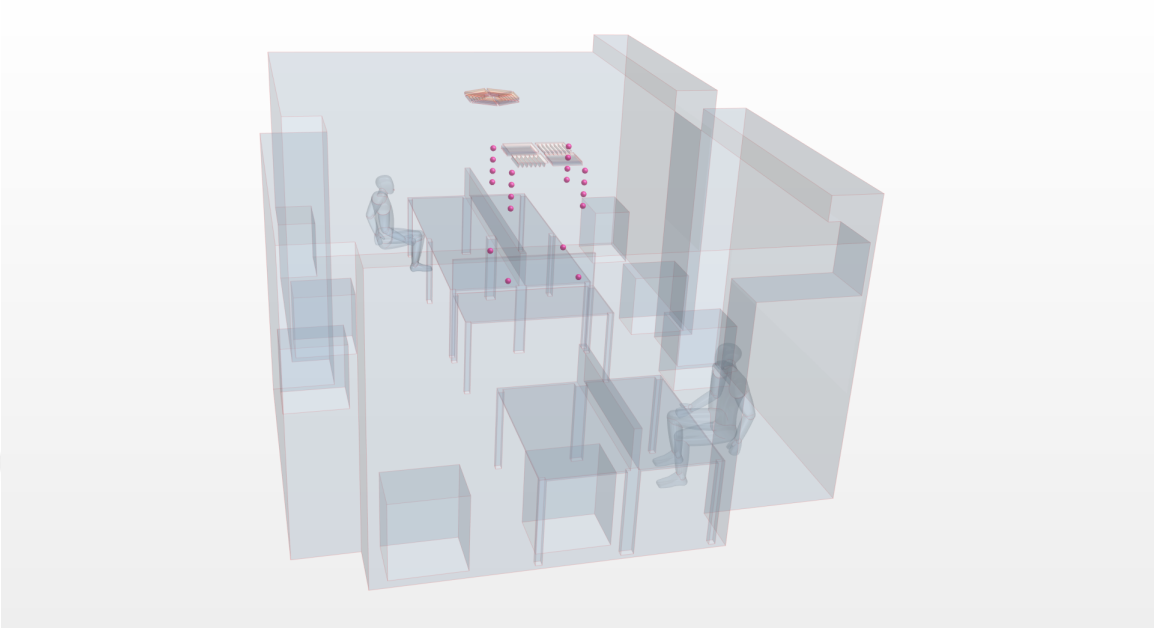

Figure 18: The probe placement in the simulation model

Testo 400 can measure temperature without any probe that is connected to it. It measures -40 to 150 °C with an accuracy of table below.

Table 3: Testo 440 accuracy within specific ranges

Range	Accuracy
-40 to -25 °C	±0.4 °C
-40 to 74.9 °C	±0.3 °C
75 to 99.9 °C	±0.4 °C
100 to 150 °C	±0.5 °C

As mentioned above, 3 probes can be connected to testo 440, we connected 2 probes on to it. One of them Testo Turbulence probe (digital) – wired 0628 0152 for turbulence intensity and draught risk according to ASHRAE 55 and EN ISO 7730. It measures temperature with ±0.5°C accuracy with 0 – 50 °C measuring range. Also,

can measure velocity with hot wire 0 to 5 m/s with ±0.3 accuracy so that it can find turbulence intensity. The other probe is High-precision humidity/temperature probe (digital) – wired 0636 9772. It measures temperature with an accuracy of 0.3°C within the -20 to +70 °C range. Even though turbulence probe was recommended to use in workplace measurements of temperature and velocity. Humidity probe had better accuracy than the turbulence probe, that is why we chose to use it in temperature measurements. And also, it can measure relative humidity (RH), which was 55% in this room when the experiments occurred, from 0 to 100% with ±0.6 %RH + 0.7 % of mv at 0 to 90 %RH and ±1.0 %RH + 0.7 % of mv at 90 to 100 %RH.

Experimental measurements were conducted on November 26, 2022, on a cloudy day, with the initial room relative humidity set at 55%. To ensure accurate validation of each simulation, each experiment was accompanied by its corresponding measurement. Testo calculates the variables in every 3 seconds then after 3 minutes it takes an average of them automatically. The test points were chosen vertically at a distance of 30 cm from the diffusers and in 4 different directions. Data from selected test points 5 cm, 15 cm, 25 cm, 35 cm and 98 cm below the ceiling were combined to form a chart and compared with data from CFD simulations. Additionally, a break was introduced between two experiments to allow the experiment room to be ventilated with outside air and reach a steady state before commencing the next measurement. This careful approach ensures that the experimental data aligns with the conditions and variables considered in the numerical simulations, enabling a comprehensive validation process.

Table 4: The experimental air temperature result of experiment 1

Distance between ceiling and probe	Probe 1	Probe 2	Probe 3	Probe 4
5 cm	35°C	40.5°C	35.8°C	37.1°C
15 cm	34.9°C	38.9°C	32°C	32.6°C
25 cm	34°C	35.5°C	31.4°C	31.7°C
35 cm	33.5°C	34.1°C	31.4°C	31.7°C
98 cm	32.5°C	36.2°C	31.4°C	31.2°C

Table 5: The experimental air temperature result of experiment 1

Distance between ceiling and probe	Probe 1	Probe 2	Probe 3	Probe 4
5 cm	0.22 m/s	0.44 m/s	0.41 m/s	0.38 m/s
15 cm	0.17 m/s	0.29 m/s	0.14 m/s	0.23 m/s
25 cm	0.14 m/s	0.19 m/s	0.05 m/s	0.14 m/s
35 cm	0.12 m/s	0.12 m/s	0.03 m/s	0.12 m/s
98 cm	0.05 m/s	0.05 m/s	0.03 m/s	0.04 m/s

Table 6: The experimental turbulence intensity of experiment 1

Distance between ceiling and probe	Probe 1	Probe 2	Probe 3	Probe 4
5 cm	29.9	11.9	17.9	10.5
15 cm	16.8	23.7	36.9	22.6
25 cm	16.5	21.7	53.8	15.4
35 cm	20.9	20.4	75.1	13.1
98 cm	16.9	24.5	29.9	25.7

Table 7: The experimental draft rate of experiment 1

Distance between ceiling and probe	Probe 1	Probe 2	Probe 3	Probe 4
5 cm	-2.2%	-18.5%	-11.6%	-12%
15 cm	-0.6%	-8.4%	1.4%	-0.5%
25 cm	0.2%	-1.1%	0%	1%
35 cm	0.4%	0.2%	0%	1.4%
98 cm	0.1%	0.2%	0%	0%

4.2 Simulation Setup

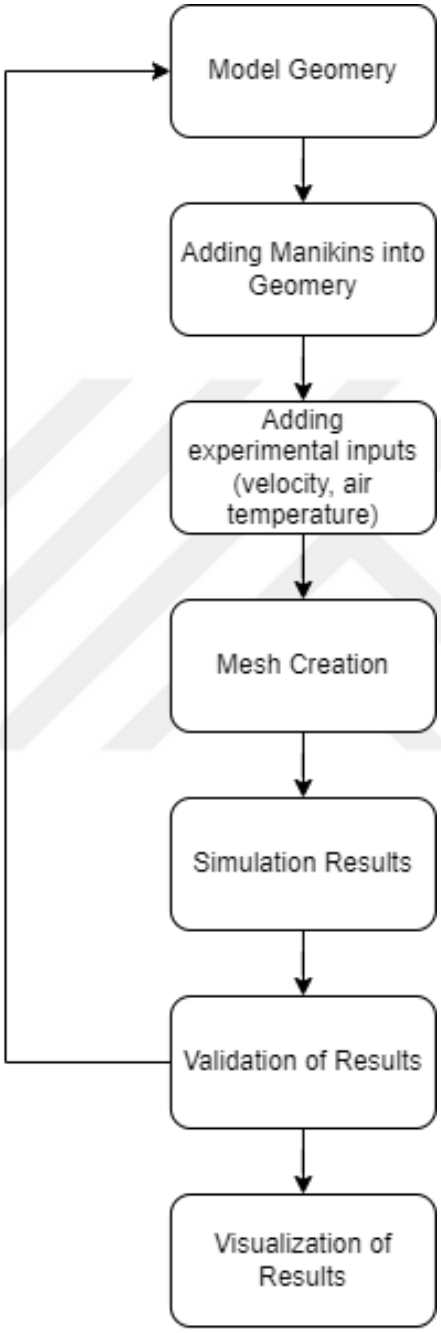

Figure 19: Flowchart of simulation process

One of the significant components of the thesis is the CFD modeling, which was conducted using the STAR CCM+ software. The decision to choose this particular software was primarily influenced by the presence of a thermal comfort wizard, which greatly facilitates the analysis of thermal comfort. Moreover, the user-friendly interface for drawing geometry further supported the selection of STAR CCM+.

4.2.1 Geometry of model

The initial step in the CFD modeling process involves realistically incorporating the architectural geometry into the software. While this addition could potentially be imported from a different software, transitioning between software platforms may sometimes lead to errors or discrepancies. To ensure accuracy and avoid such issues, the geometry was drawn directly within the STAR CCM+ software for this thesis. By doing so, a seamless and error-free integration of the geometry was achieved, allowing for more reliable and precise CFD simulations.

The manikin, which will be incorporated into the room geometry, plays a crucial role in illustrating the interaction between thermoregulation and the environment. In previous work by Choudhary, B., & Udayraj, the chest was divided into 9 regions to study thermal comfort [64]. However, for the thermal comfort wizard provided by STAR CCM+, manikins need to be divided into 14 separate pieces. This level of detail may vary depending on the specific requirements of the study.

Since STAR CCM+ is used in this thesis, the manikin is divided into 14 parts to meet the software's specifications. These parts include: head, torso, upper left arm, upper right arm, lower left arm, lower right arm, left hand, right hand, upper right leg, upper left leg, lower right leg, lower left leg, left foot, and right foot.

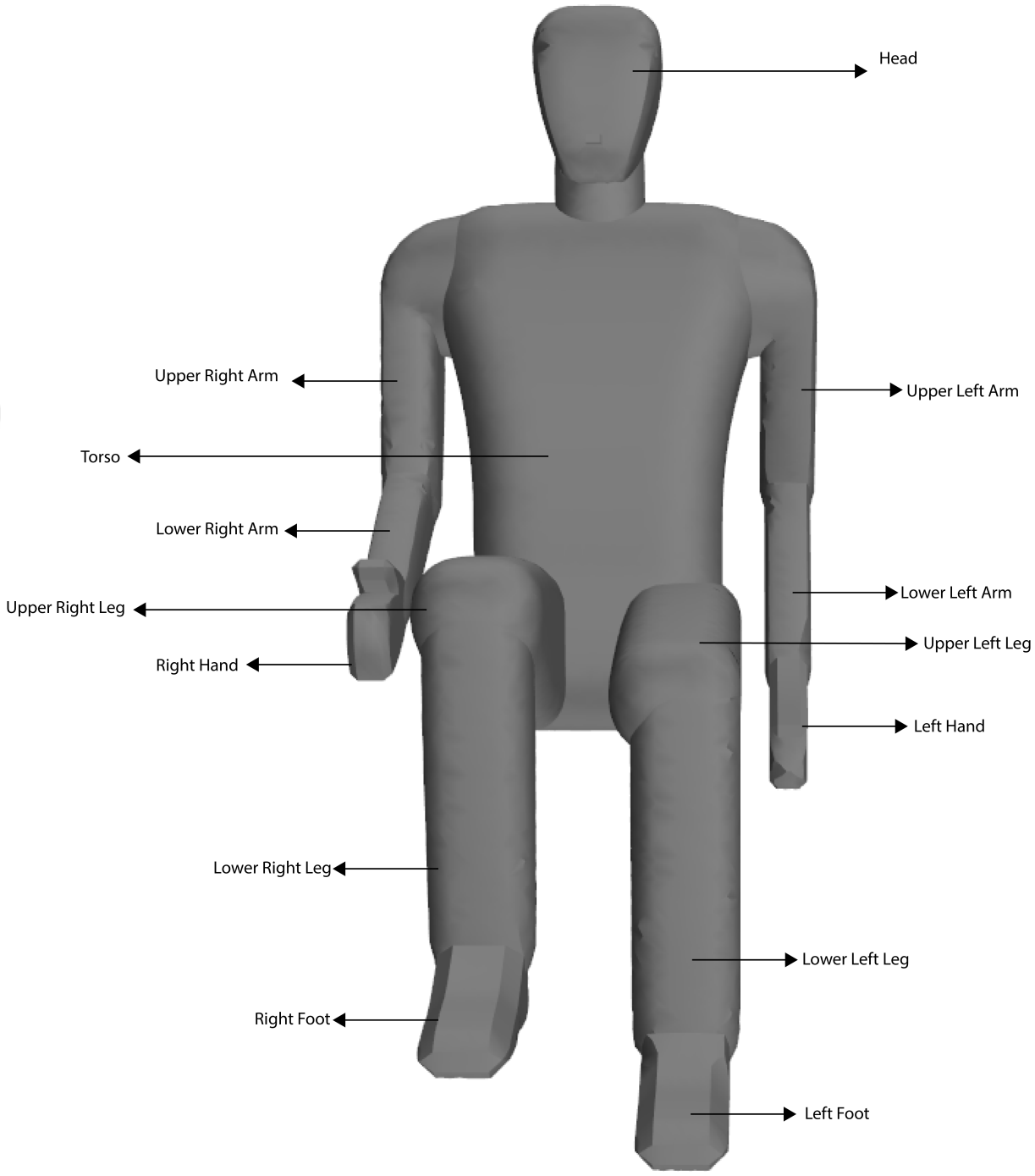

Figure 20: The utilized manikin geometry in the model

After placing the manikins in the geometry, the only remaining task is to model the geometries of the diffusers that will be compared. Given that each diffuser is produced differently by the manufacturer, the geometries were precisely modeled using the

manufacturer's documentation as a reference (See Appendix B and Appendix C). The use of manufacturer-provided documentation ensures that the modeled geometries align with the real-world characteristics of the diffusers.

4.2.2 Initial and boundary conditions

The initial conditions of air velocity and temperature of air that is coming out of diffusers are experimentally acquired (See Appendix D). Also, the temperature of the office room is measured experimentally for each case. The outside temperature and humidity is measured as well. To place initial condition of air velocity and temperature to inlet of the diffusers, due to the thermal comfort wizard does not allowing us to use air velocity inlet condition, mass flow inlet is chosen. The initial experiment data transformed from air velocity to mass flow inlet. Also, the return diffuser is selected as a pressure outlet which is commonly used in indoor air flow simulations.

Setting the walls to a constant temperature of 12 °C is a practical approach for buildings with significant thermal mass, as they take longer to heat up or cool down. By assuming a constant temperature for the walls, computational resources can be conserved, as it would not be computationally feasible to consider them as variable surfaces. Regarding the windows, they are assigned a specific thermal conductivity value of 0.65 W/mK. This value represents the window's ability to conduct heat and is crucial for accurately modeling the heat transfer through the windows.

Regarding the manikin body, it is set to have a wall condition with temperature thermal specification. This setup creates an interface between the surrounding air and the manikin body, allowing thermal calculations to be performed on wall-type surfaces. The inclusion of radiation models becomes necessary when using the thermal comfort wizard to calculate the Mean Radiant Temperature (MRT), which plays a critical role in assessing thermal comfort.

4.2.3 Model physics

As mentioned earlier, the CFD model employs the segregated flow model to solve the governing equations detailed in Chapter III. Additionally, the segregated fluid temperature is included to solve the total energy equations with temperature as the solved variable. The enthalpy is then computed based on the solved temperature, utilizing the equation of state.

For the simulation, a steady-state condition is selected as the time concern. This means that the model assumes that the flow and temperature distribution within the office space remain constant over time. Regarding turbulence modeling, the RANS (Reynolds-Averaged Navier-Stokes) model is chosen due to its computational efficiency compared to more time-consuming models like LES (Large Eddy Simulation) and DES (Detached Eddy Simulation). Among the available turbulence models, the k-epsilon model is deemed the most suitable, as discussed in Chapter III. It is preferred over the Omega and Epsilon models based on its performance. The specific choices for wall distance, realizable k-epsilon two-layer, and two-layer all y+ wall treatment are made in line with the decision to use the k-Epsilon turbulence model in STAR CCM+.

In order to activate thermal comfort wizard, radiation was necessary. That is why, surface to surface model is added to physic model. The surface-to-surface radiation model is an effective method for considering radiation exchange within an enclosure comprising gray-diffuse surfaces. The energy exchange between two surfaces is influenced by factors such as their size, separation distance, and orientation, which are all incorporated through a geometric function known as the "view factor." The primary assumption of the S2S model is that any absorption, emission, or scattering of radiation can be disregarded, simplifying the analysis. Consequently, the model solely focuses on "surface-to-surface" radiation interactions, making it a suitable approach for studying heat transfer in systems where the radiative properties of surfaces are

considered uniform.

4.2.4 Mesh Selection

A well-structured and appropriate mesh helps the CFD solver converge to a solution efficiently. On the other hand, an inadequate mesh may cause convergence issues, prolong computation times, or even prevent the solver from reaching a solution. Polyhedral meshes are a well-suited solution for intricate mesh generation challenges. They are relatively simple and efficient to construct, requiring no additional surface preparation compared to tetrahedral meshes [54]. Turbulent flows, like in this thesis, require smaller mesh sizes to accurately capture the rapid changes in velocity and pressure. Additionally, polyhedral meshes contain about five times fewer cells than tetrahedral meshes for a given surface. So computing costs drop significantly.

Prism layers play a crucial role in accurately resolving near-wall flow, which is vital for determining forces and heat transfer on walls. These layers not only provide mesh density near the wall but also allow the use of high-aspect-ratio cells, improving cross-stream resolution without compromising stream-wise resolution excessively. Furthermore, prism layers reduce numerical diffusion near the wall, resulting in minimized discretization errors that can smear discontinuities and steep gradients in finite volume advection schemes. The utilization of prism layers significantly enhances simulation accuracy.

As depicted in Figure 21, the manikin is enveloped by polyhedral meshes, while the surrounding area is covered with prism layers. This strategic meshing approach allows for efficient and accurate resolution of airflow close to the manikin's surface.

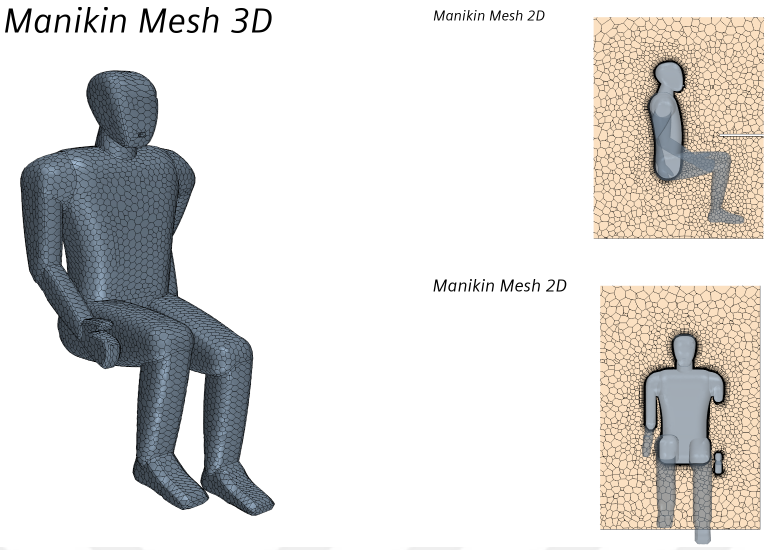

Figure 21: Manikin polyhedral and prism layer meshes

As this thesis works on both thermal comfort and diffusers, diffusers also needed to be considered specially. If we can improve cell quality in those areas it will give more accurate solutions. Therefore, the diffusers and manikins are covered with a zone that has more cells from the other areas of the has. Because we don't need to solve everywhere in detail due to it would take too much time to run. However, we can solve critical areas in detail by assigning increased prism layer quantity or increasing the cell ratio at those areas. In this thesis, both thermal comfort and diffusers are significant areas of focus. Ensuring accurate solutions is essential, and for that reason, special attention is given to the diffuser and manikin regions. By enhancing cell quality in these areas, the CFD model yields more reliable results.

To achieve this, specific zones with higher cell density are assigned to cover the diffusers and manikins. This approach allows for detailed resolution in critical areas, where precise flow patterns and thermal behavior are crucial. By selectively increasing the quantity of prism layers or adjusting the cell ratio in these zones, the model can focus on areas requiring in-depth analysis without incurring excessive computational time. This adaptive approach strikes a balance between computational efficiency and

accuracy, enabling the CFD simulations to provide valuable insights.

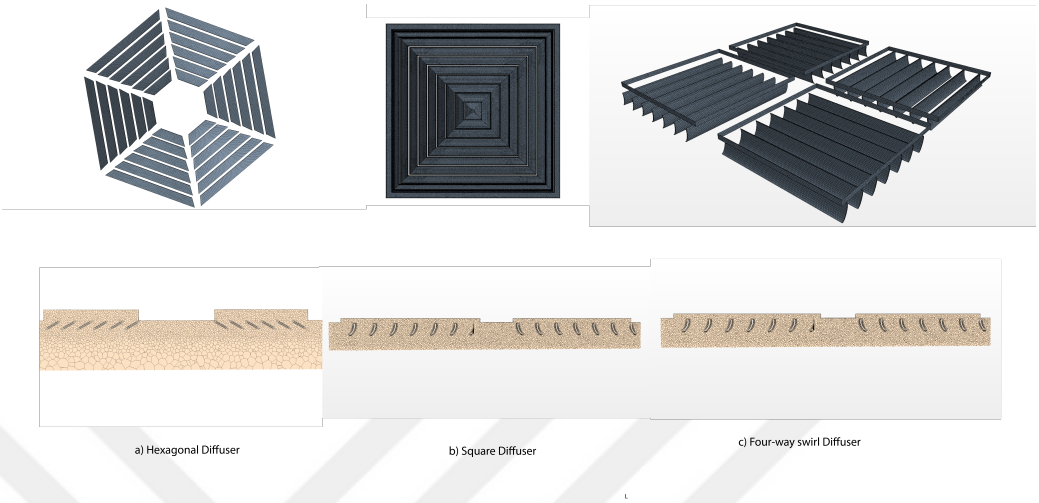

Figure 22: Mesh visualization of diffusers

Using a fine mesh in CFD simulations is crucial for achieving accurate results, especially when dealing with gradients, small-scale details, and boundary layer behavior. This approach ensures a precise representation of flow patterns and contributes to quicker convergence towards stable solutions. Moreover, a fine mesh enhances the accuracy of gradient calculations, which is essential for estimating forces and heat transfer. It also improves the validation process against experimental or analytical data, leading to more dependable comparisons.

However, employing a fine mesh has its drawbacks, including higher computational demands that lead to increased resource usage and longer simulation durations. Due to these trade-offs, we focus on using a refined mesh selectively, prioritizing areas with the most significance, such as the manikin and diffusers.

The cross-sectional view of the mesh and surface mesh distribution on diffuser. Between coarse mesh and fine mesh, we can see the number of cells were increased between the diffuser blades. In validation study, when the coarse mesh is used, the velocity consistency could be achieved between the experimental and simulation results.

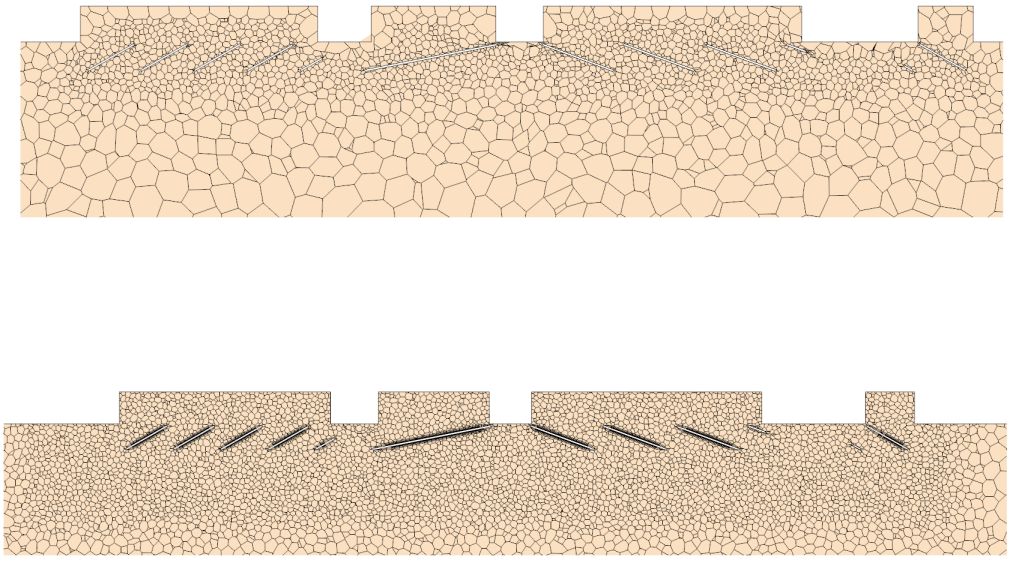

Figure 23: Comparisons for different mesh selections

4.2.5 Validation of results

Validation of results is a critical aspect of this research. Each case required separate models, and in-house validation was conducted for each of them. For validation purposes, the probes mentioned in Chapter 2 were deployed. These probes measured data from four different points and five different heights. However, a limitation of these measurements was that only two measurements could be taken simultaneously. As depicted in Figure 17, the Testo 440 was connected to reciprocal probes to perform the measurements. The measurements were taken every three seconds for a duration of three minutes, and the average result was used. Following each set of two measurements, the process was repeated for the next points. Although there may have been fluctuations due to the lack of simultaneous measurements, STAR CCM+ provided results for all selected probes at the same time.

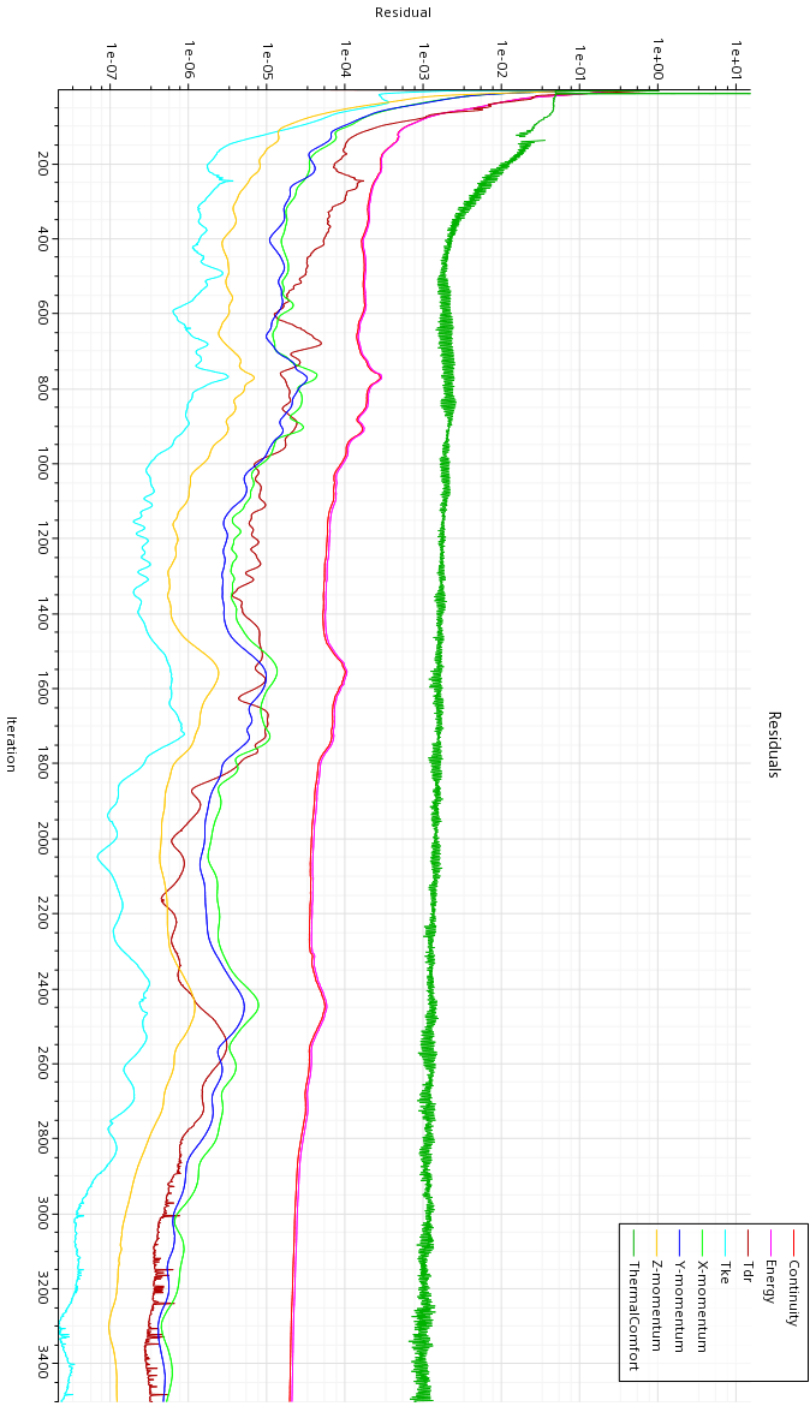

Figure 24: Residual of an experiment

The Mean Absolute Percentage Error (MAPE) was employed to compare the experimental results with the numerical results. This formula is commonly used to

assess the accuracy of predictions and provides the percentage of deviation between the two sets of data. By calculating the MAPE, researchers can quantify the level of agreement between the experimental measurements and the numerical simulations.

$$MAPE = \frac{100}{n} \sum_{t=1}^{n} \left| \frac{A_t - F_t}{A_t} \right| \tag{53}$$

Table 8: MAPE results of the cases at 0.98 m

Case	MAPE of Temperature at 0.98 m (%)	MAPE of Velocity at 0.98 m (%)
1	3.3	3.5
2	1.8	2.1
3	7.3	6.0
4	4.1	5.1
5	1.2	1.1
6	6.6	5.9
7	8.5	12.1
8	3.2	2.3
9	3.5	5.0

CHAPTER V

RESULTS AND DISCUSSION

In this chapter, the results of the case studies described above are presented and discussed. The CFD simulations were conducted in a steady-state environment, using RANS (Reynolds-Averaged Navier-Stokes) and k-epsilon turbulence models. To validate these simulations, experiments were performed on 26th November. The experiments were carried out at the same flow rate. However, it was anticipated that each flap of the diffusers might experience different flow rates due to the mixing of air from the FCU (Fan Coil Unit) and AHU (Air Handling Unit) in the plenum box. As a result, the air velocity from the diffusers for each case was experimentally obtained and assigned to the respective flaps. To facilitate the thermal comfort analysis, a surface-to-surface model was incorporated.

This thesis consists of nine different cases, with five of them featuring hexagonal diffusers, three with four-way swirl diffusers, and one completed with a square diffuser. The distinguishing factor among these cases is the different flap configurations for each. The reason for having only one square diffuser case is that there are no variations in flap configuration for this type. The following table presents the configurations for each case, outlining the specific differences among them.

Table 9: Diffuser flap configuration

Case	Diffuser Type	Flap 1	Flap 2	Flap 3	Flap 4	Flap 5	Flap 6
1	Hexagonal	Open	Open	Open	Open	Open	Open
2	Hexagonal	Open	Closed	Closed	Closed	Closed	Open
3	Hexagonal	Closed	Closed	Closed	Open	Open	Closed
4	Hexagonal	Open	Open	Closed	Closed	Closed	Open
5	Hexagonal	Closed	Closed	Open	Open	Open	Closed
6	Fourway	Open	Open	Open	Open	-	-
7	Fourway	Open	Closed	Closed	Closed	-	-
8	Fourway	Closed	Closed	Open	Closed	-	-
9	Square	Open	Open	Open	Open	-	-

In this study, various groupings were made to facilitate comparisons among the cases. First, a comparison was conducted between cases where each flap is open on all diffusers. These cases include case 1, case 6, and case 9. Additionally, comparisons were made within each diffuser type. These groupings are as follows:

Comparison of Cases with All Flaps Open on All Diffusers:

- Case 1
- Case 6
- Case 9

Comparison of Cases with Flaps Directed Toward the Manikins Only:

- Case 4
- Case 7
- Case 8

Energy Analysis:

- Case 3 Revised (reduced airflow)
- Case 9 Revised (reduced airflow)

These comparisons were carried out for both indoor airflow and thermal comfort analyses. The results obtained from these groupings provide valuable insights into the impact of different flap configurations on indoor airflow patterns and thermal comfort distribution within the office space.

In the 9 case studies, although the total airflow rate remains constant, the airflow rate at the diffuser openings differs due to the different entry points of the FCU and AHU unit plenum box. Additionally, the number of opened flaps on the diffusers also contributes to the variation in airflow rates at the diffuser openings. Due to the main topic is the comfort on people and their surroundings, the results are visualized in the direction of supply air and manikins.

Comparison of Cases with All Flaps Open on All Diffusers:

The design of four-way swirl diffusers makes them particularly suitable for applications in cinema and conference halls. One of the key reasons they are preferred in these spaces is due to their longer velocity decay compared to other diffusers. As observed in Case 6 (See Fig. 24), the longer velocity decay of four-way swirl diffusers results in air jets exhibiting a downward descent due to the buoyancy effect. In the context of cinema, this downward descent is beneficial as it helps in delivering the conditioned air to the occupied area at a level that ensures comfort for watchers. However, in office environments, this downward descent of air over the occupants can lead to undesirable consequences. It can create discomfort and disrupt the thermal comfort of the individuals working in the office. In offices, it is more important to have a diffuser design that ensures a gentle and even distribution of air without causing direct drafts over the occupants.

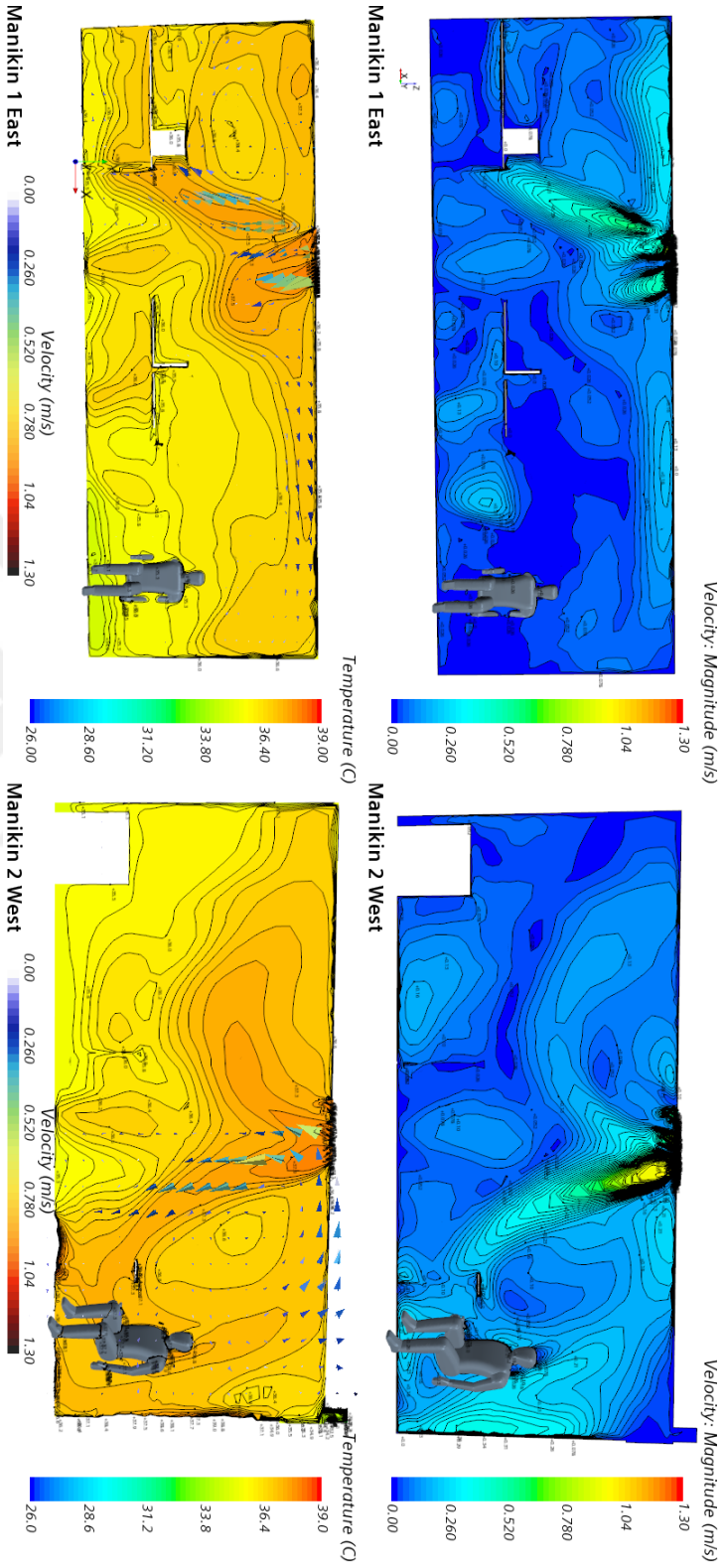

Figure 25: Case 6: Velocity and temperature distribution

Square diffusers provide a different approach to airflow distribution compared to other diffuser types. The flaps of square diffusers are always open, and the flow rate can be adjusted solely with the use of a damper. As the flow rate through the opening decreases, the velocity and temperature decay decrease rapidly. Moreover, the design of square diffusers promotes a wall jet effect, where the flaps direct the air sideways, causing the air jets to run parallel to the ceiling and then descend along the opposite wall. creates a circulating vortex around the right part of the room which is caused by the stream of the upward moving thermal plum, ensuring a more uniform distribution of air. In Case 9, as observed, the air released from the square diffuser moves down the wall, generating gentle circulation. Additionally, the velocity of the air reaching the manikins from the square diffuser is within the range of 0.2 to 0.05 m/s, which aligns with the guidelines set by ASHRAE 55 standards for thermal comfort.

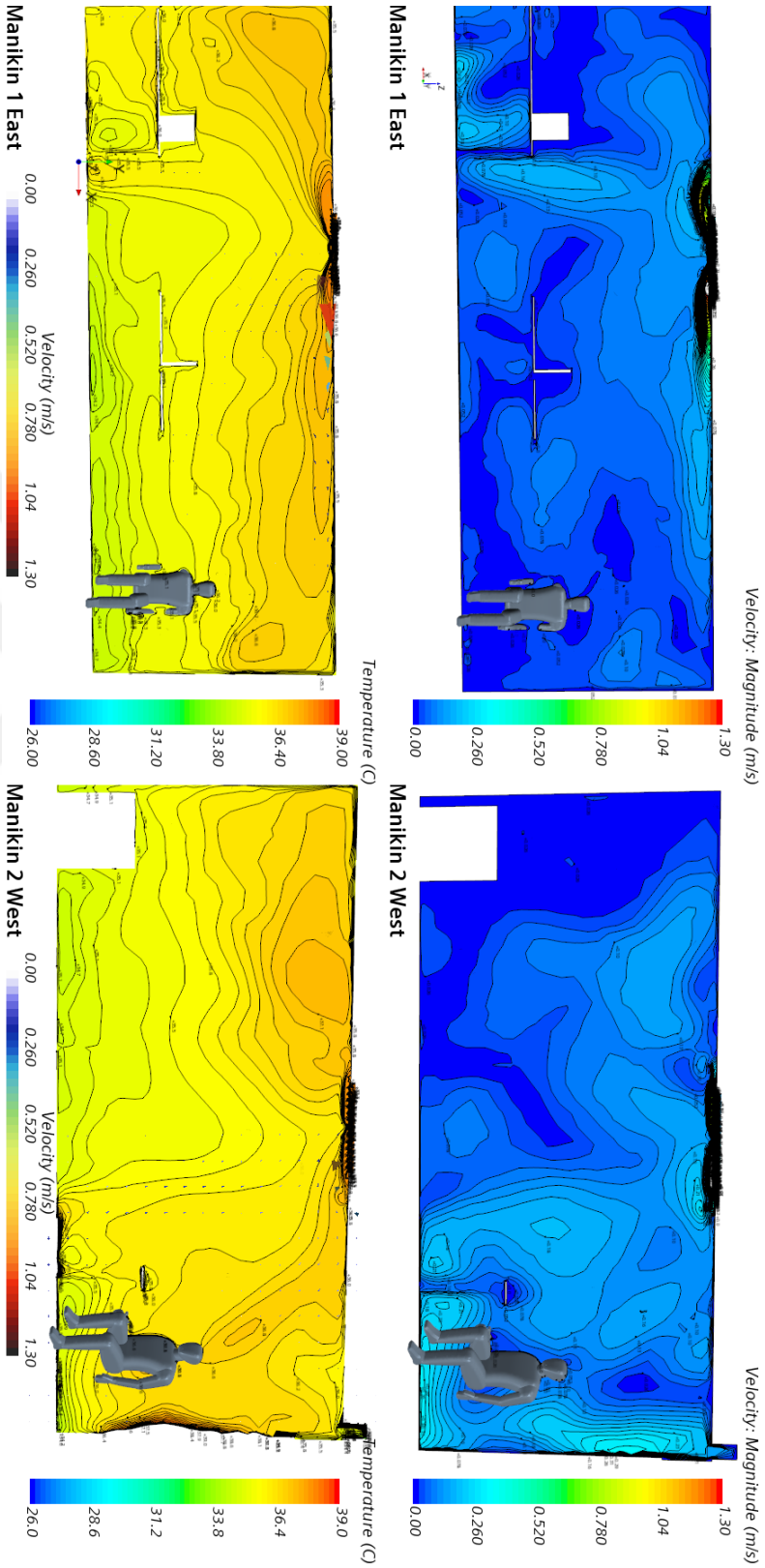

Figure 26: Case 9: Velocity and temperature distribution

The hexagonal diffuser is a versatile type of diffuser that can be utilized in office buildings, similar to the square diffuser. Its unique feature lies in its adjustable flaps, which allow it to function either as a wall jet or a free jet, depending on their orientation.

As demonstrated in Case 1, when all of the flaps of the hexagonal diffuser are open and parallel to the surface, it serves as a wall jet, akin to the square diffuser. The interaction between these forces causes velocity and temperature peaks to occur closer to the ceiling. This phenomenon is typical in wall jet flows, where the air velocity increases near the ceiling due to entrainment of ambient air. This configuration generates a flow pattern where the air moves parallel to the wall and then descends along it. Consequently, this arrangement results in a combination of inlet buoyancy forces and prevailing momentum forces.

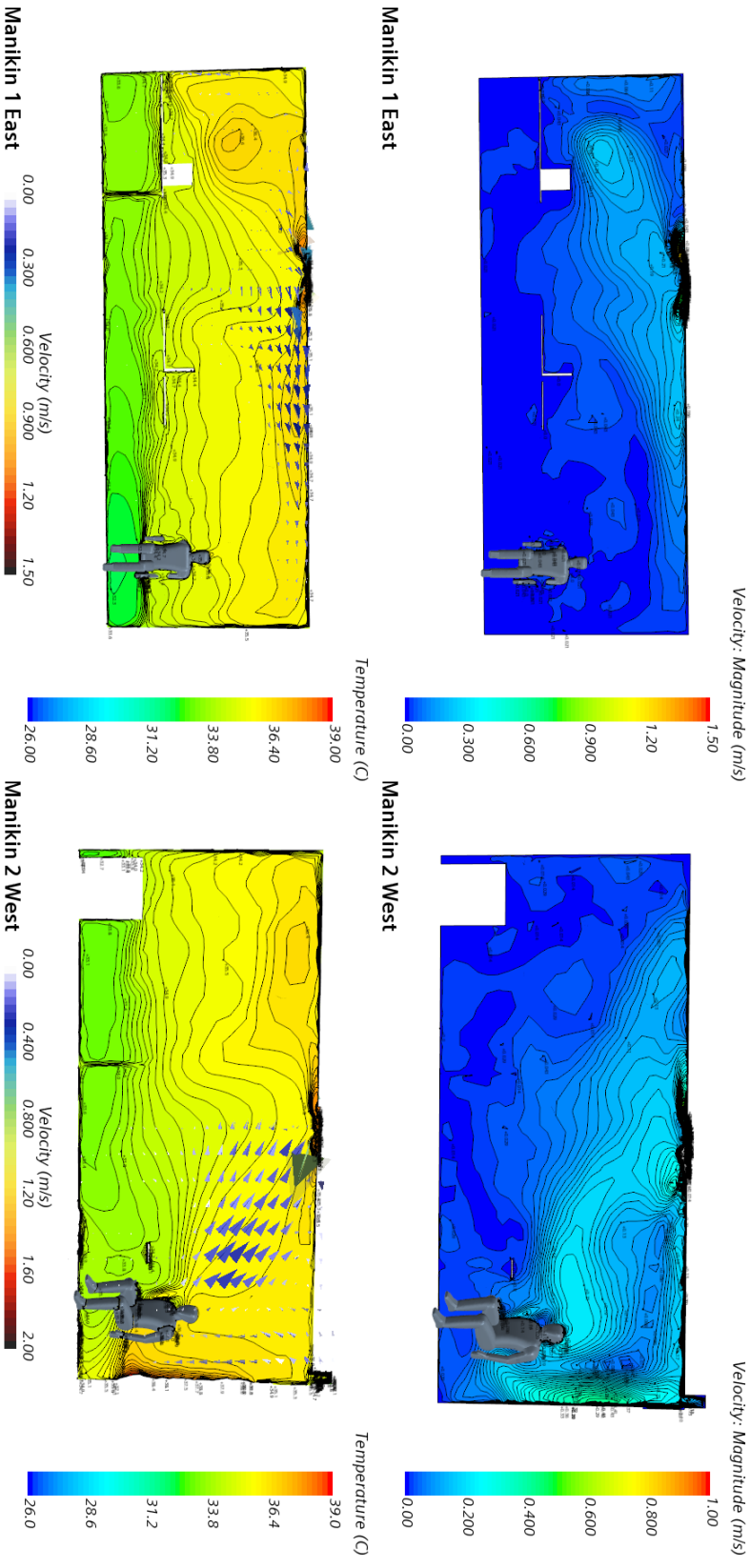

Figure 27: Case 1: Velocity and temperature distribution

Temperature distribution is indeed a crucial factor to consider in indoor air conditioning and thermal comfort analysis. Even when air is blown from the same fan coil unit (FCU), differences in outlet temperatures can be observed, which may be attributed to various factors, including the air remaining in the plenum box and not being effectively discharged.

In Case 1, while the exit temperature may not be significantly different from the other cases, the presence of thermal stratification can still be observed. This stratification can be linked to the buoyancy effect and the parallel movement of air jets. The wall jets, as seen in the image of Manikin 2 West, can create significant heating along the wall, which can lead to variations in temperature across different heights in the occupied space. The thermal stratification becomes more apparent when considering the lower levels of the occupied zone. As indicated in Figure 25, Case 9, the horizontal advancement of the air jets contributes to the formation of thermal stratification, resulting in cooler temperatures at lower levels compared to the upper levels. as depicted in the lines of Case 1 and Case 9 (Figure 27), the outcome can be similar, even when using different diffuser shapes (square diffuser in one case and hexagonal diffuser in the other). This similarity in outcome can be attributed to the fact that both diffusers exhibit similar jet characteristics. In certain situations, different diffuser types may produce comparable airflow patterns and temperature distributions if their fundamental jet characteristics are similar. In this case, both the square diffuser and the hexagonal diffuser have been configured to generate wall jets, resulting in comparable thermal stratification and airflow patterns.

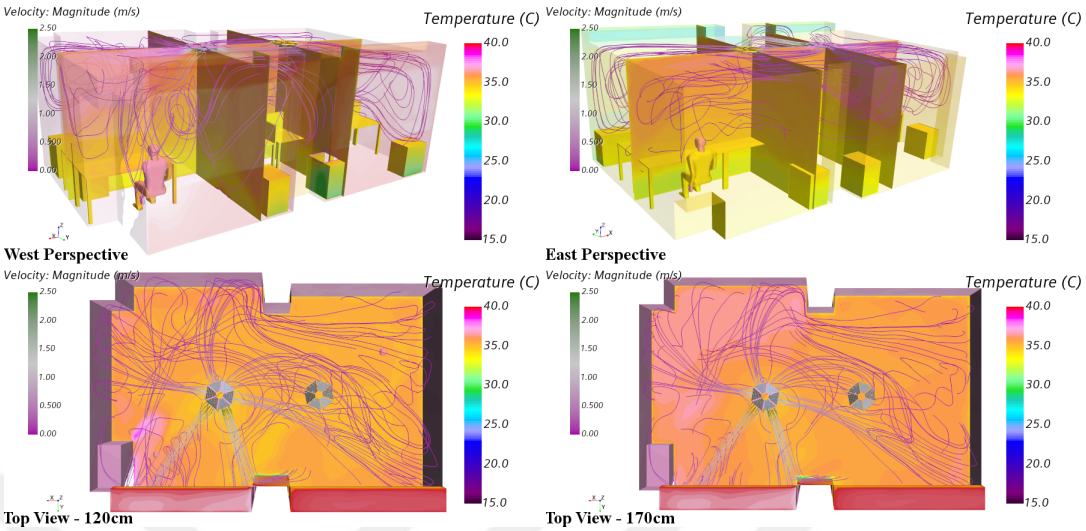

Figure 28: Velocity lines of Case 1

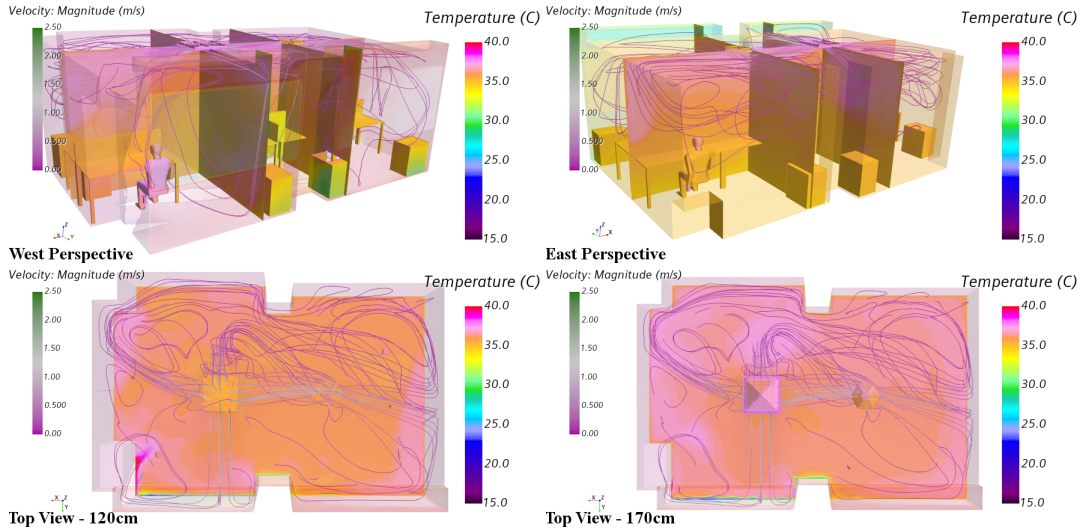

Figure 29: Velocity lines of Case 9

These two phenomena affect thermal comfort since it's a variation of air temperature and air velocity. In each of the cases presented in this study, the air velocity on the virtual manikin surfaces was closely monitored using the "Cell Relative Velocity" function provided by Star-CCM+. This built-in field function is specifically designed to track the "near" wall velocity of fluids, making it highly useful for observing air velocity patterns in close proximity to manikin surfaces. Additionally, the heat flux

distributions on the virtual manikin surfaces are also presented for each case. Furthermore, the Predicted Mean Vote (PMV) value, which quantifies thermal comfort, was calculated using a Python script for each case for the scenes at 100 cm away from the floor.

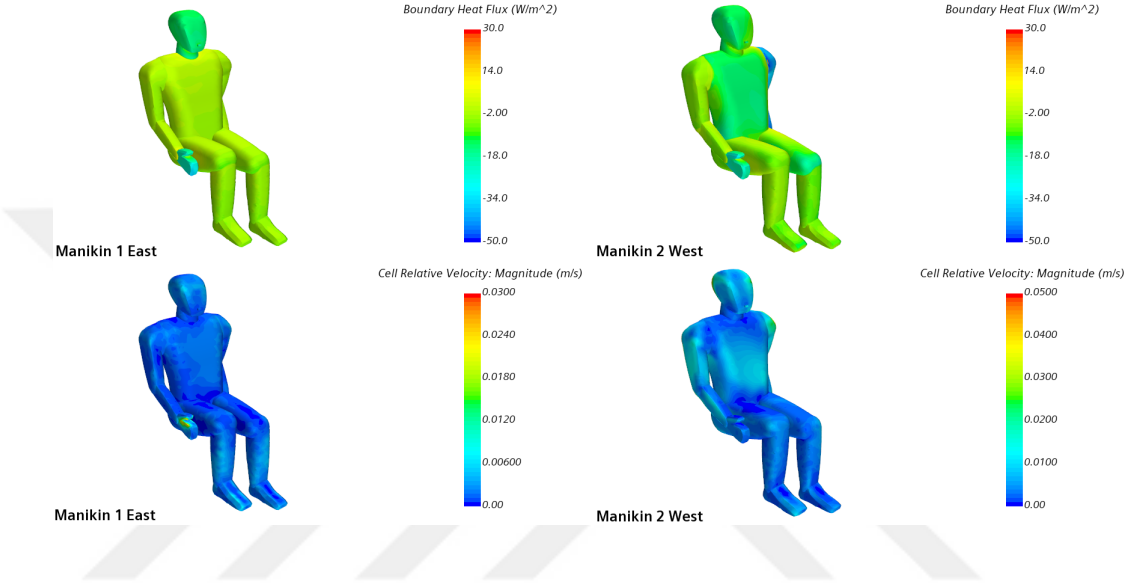

Figure 30: Case 1: Heat flux and cell relative velocity

As observed in Figure 29, Manikin 2 experiences high air velocity on the upper left arm and low boundary heat flux. This phenomenon can be attributed to the airflow coming from the opening of the hexagonal diffuser in Case 1 and Case 9. In Case 1, the airflow from the hexagonal diffuser behaves like a wall jet, moving downward in a direction parallel to the walls. Consequently, it encounters the left arm of the manikin (as depicted in Figure 26). The high air velocity impinging on the manikin's left arm results in the observed high air velocity ingredient on the upper left arm. Similarly, in Case 9, the air descending from the square diffuser also moves along the wall, reaching the manikin's left arm, which results in the same effect of high air velocity on the upper left arm and low boundary heat flux.

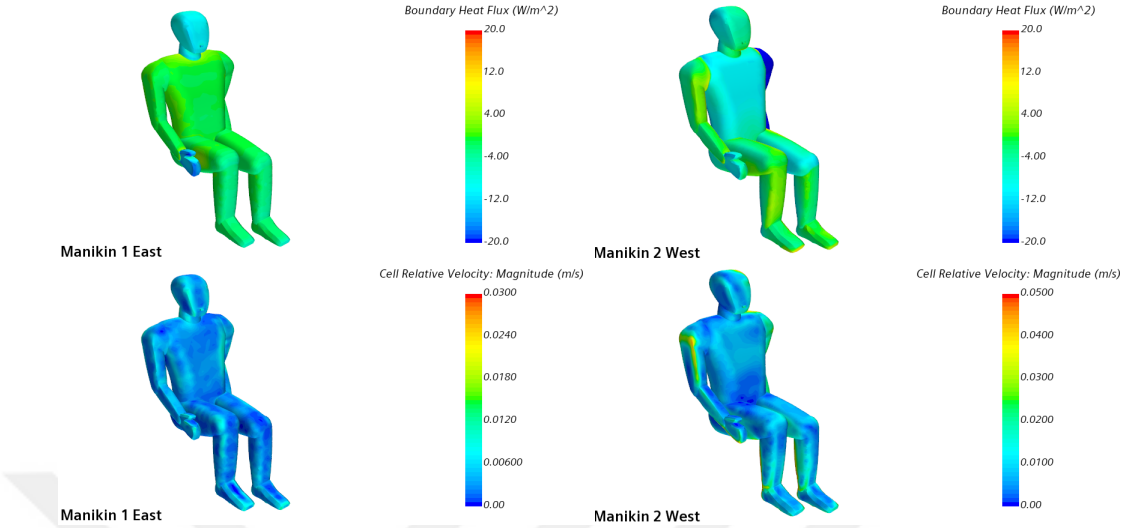

Figure 31: Case 9: Heat flux and cell relative velocity

The difference between the four-way swirl diffuser and the other two continues in the thermal comfort also. Due to free jets in the four-way swirl, it pierce through the buoyancy effect to reach bottom of the room. Therefore, we couldn't see thermal stratification as it reaches below the desks. However, if we look at the figure 31, we can see the cell relative velocity of manikins at upper and lower legs are higher compared to case 1 and case 9 where they were close to 0.00 – 0.006. So, four-way diffuser might reach the bottom of the room to condition but it also made manikins discomfort because of the high velocity.

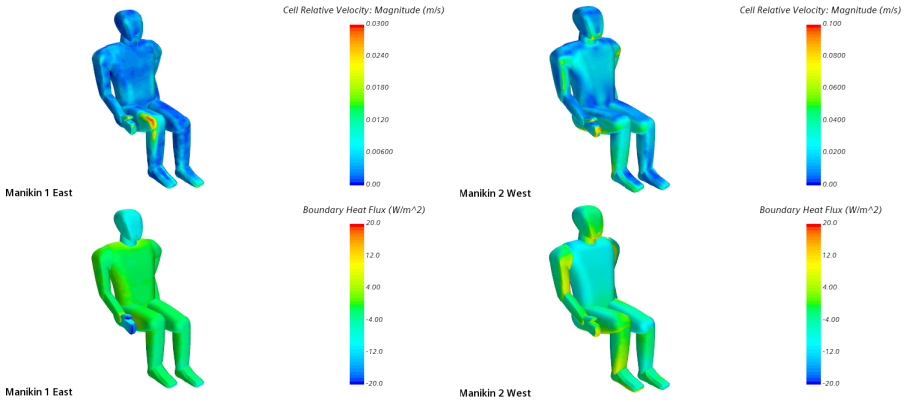

Figure 32: Case 9: Heat flux and cell relative velocity

Comparison of Cases with Flaps Directed Toward the Manikins Only:

After comparing the different diffusers, we can further analyze the behavior of the hexagonal and four-way diffusers with respect to their airflow direction towards the manikins. Normally, direct air blowing towards the manikins is not intended. In these cases, all flaps of the diffusers, except the ones directed towards the manikins, are closed. Although it may appear that the air is blowing directly towards the manikins, it is important to note that these diffusers are not designed to operate with only one flap open. Typically, in practical applications, if only one flap is needed to be open, it would be connected to the Building Management System (BMS) to regulate the airflow in the room. However, in this thesis, the primary focus is on studying the behavior of the air and assessing thermal comfort under constant airflow conditions for all the different cases.

In Case 4, two of the six flaps of the hexagonal diffuser are in the open position. Notably, one of the open flaps is almost aligned with Manikin 2. As previously explained, typically, all six open flaps should have sufficient airflow to pass when they are open (as depicted in Figure 32). However, in this specific case, we can observe that the air jets, behaving like wall jets, reach very high velocities, resulting in a primary airflow towards the return diffuser, which is located in the room.

Figure 32 also shows the presence of a secondary airflow to the left of the primary airflow in this case. Consequently, horizontal thermal stratification occurs. This means that the right side of the room experiences a temperature of 36 degrees, while the left side is at 34 degrees, indicating that two regions of the room are being air-conditioned differently.

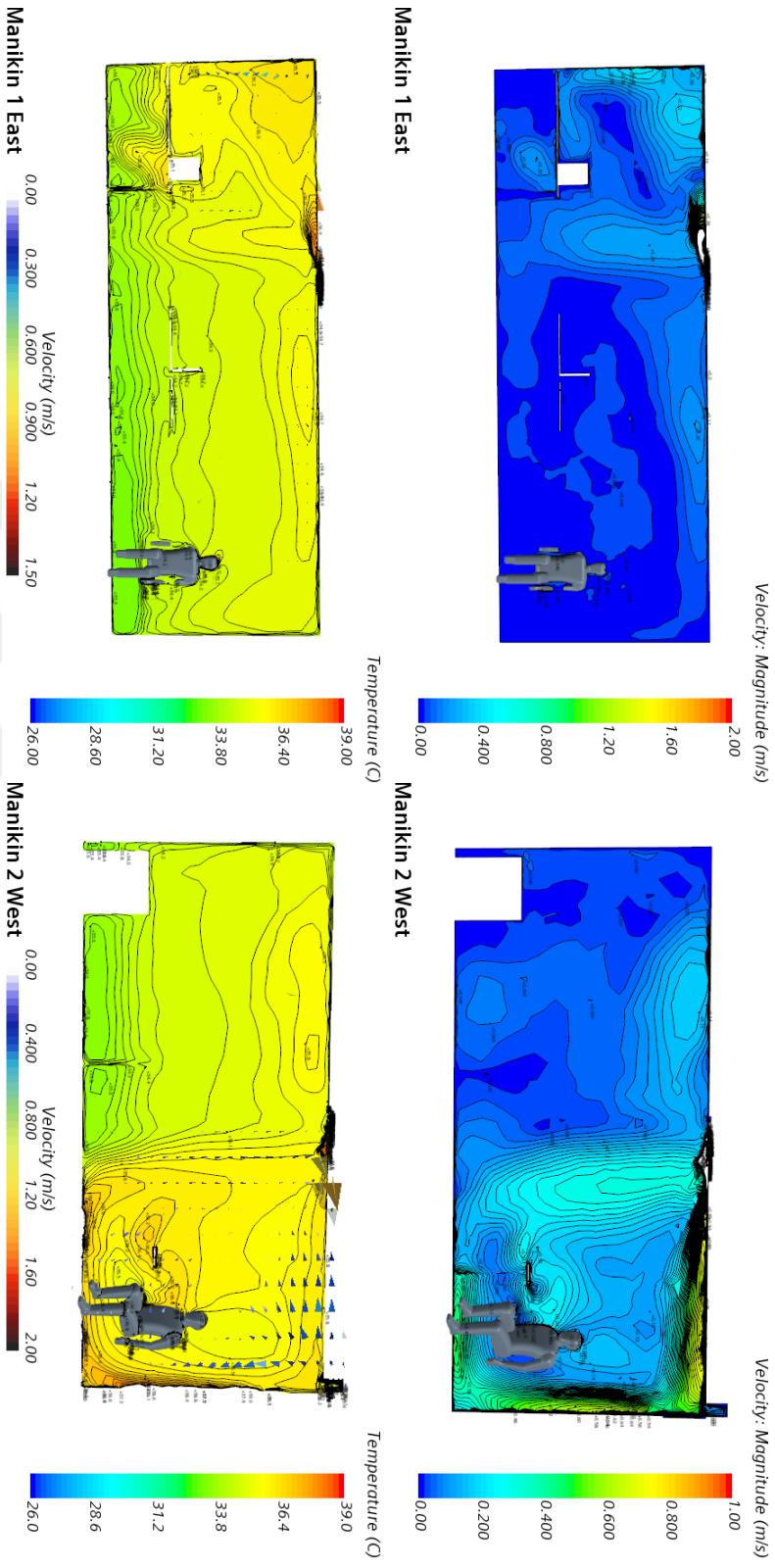

Figure 33: Velocity and temperature distribution of Case 4

Case 4 demonstrates how personal ventilation systems, such as the use of specific diffuser configurations, can lead to different air-conditioning of distinct areas within a room. However, while implementing such customized air-conditioning solutions, it is crucial to prioritize the thermal comfort of the individuals occupying those spaces.

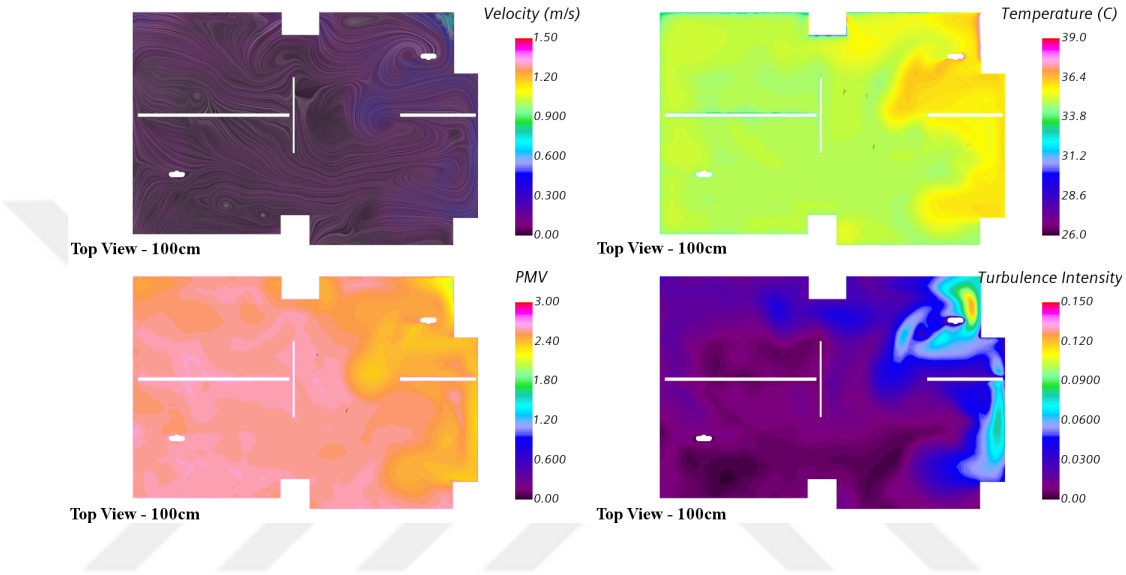

Figure 34: PMV, Turbulence intensity, velocity and temperature visual at 100 cm from floor of case 4

In Figure 33, we can observe that the Predicted Mean Vote (PMV) values are significantly higher than the optimum value of 0, indicating that the thermal comfort conditions in the room are not ideal. Several factors contribute to these higher PMV values, including the velocity component caused by the air flow and the temperature of the air being blown into the space.

The high air velocity resulting from the diffuser configuration can create locally undesirable draft rates, leading to discomfort for the occupants. Additionally, the significant temperature difference caused by the air blowing into the room can result in a higher PMV value, as it impacts the overall thermal sensation experienced by individuals. Furthermore, the turbulence intensity in the space is also affected by the high velocity and temperature difference, contributing to the overall thermal

discomfort experienced by the occupants. Turbulent air movement can lead to uneven temperature distribution and may exacerbate the discomfort caused by drafts.

To improve thermal comfort, it is essential to carefully balance the airflow velocity and temperature to create a more uniform and comfortable indoor environment. Lowering the air velocity and ensuring a more gradual temperature distribution can help reduce the locally undesirable draft rates and turbulence intensity, leading to improved thermal comfort for occupants.

In Case 7, a discomfort has occurred due to the high air velocity. The air jets, initially moving as free jets, descended on the table surface and ran parallel to the feet of the table upon impact. As a result, the table surface was heated, and the air flow reached the manikin from the table surface. Consequently, a fast cell relative velocity is observed in the chest region of the manikin.

This case exhibits a different airflow pattern compared to Case 4. In Case 4, the air flow descends down the wall, while in Case 7, it exhibits a reverse flow. Here, the air flow, influenced by the buoyancy effect, moves upward near the wall and heads towards the return diffuser.

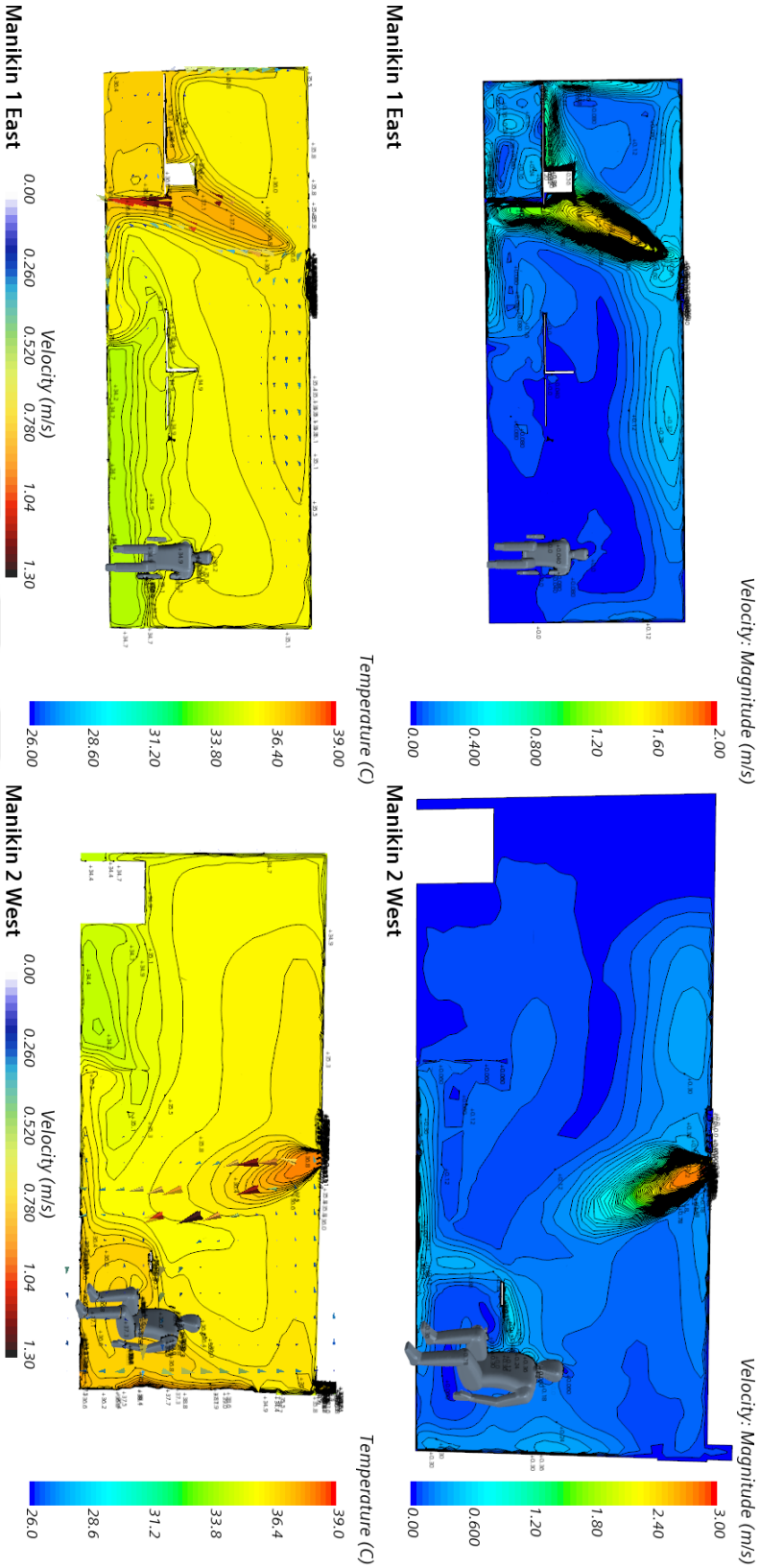

Figure 35: Case 7 velocity and temperature distribution

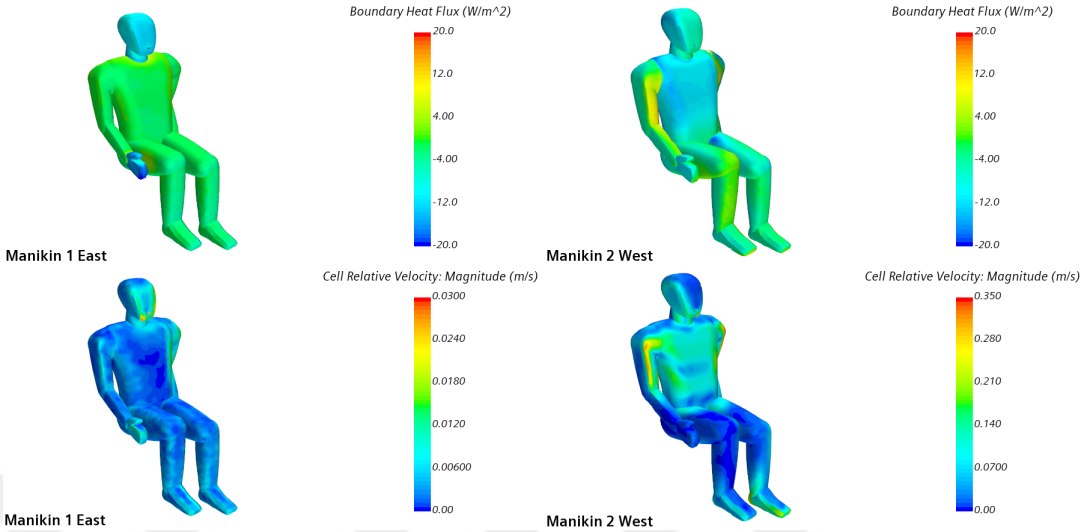

Figure 36: Heat flux and cell relative velocity of case 7

In Case 8, where the air is blown towards the table, the air does not descend to the foot level, resulting in temperature stratification between the air on the table surface and the bottom of the table. This condition has led to a significant temperature difference between the feet and the head level, exceeding the recommended limit of 3 degrees according to the standards. As a result, the feet were measured at 26 degrees, while the head level was at 32 degrees, causing local discomfort due to the temperature disparity.

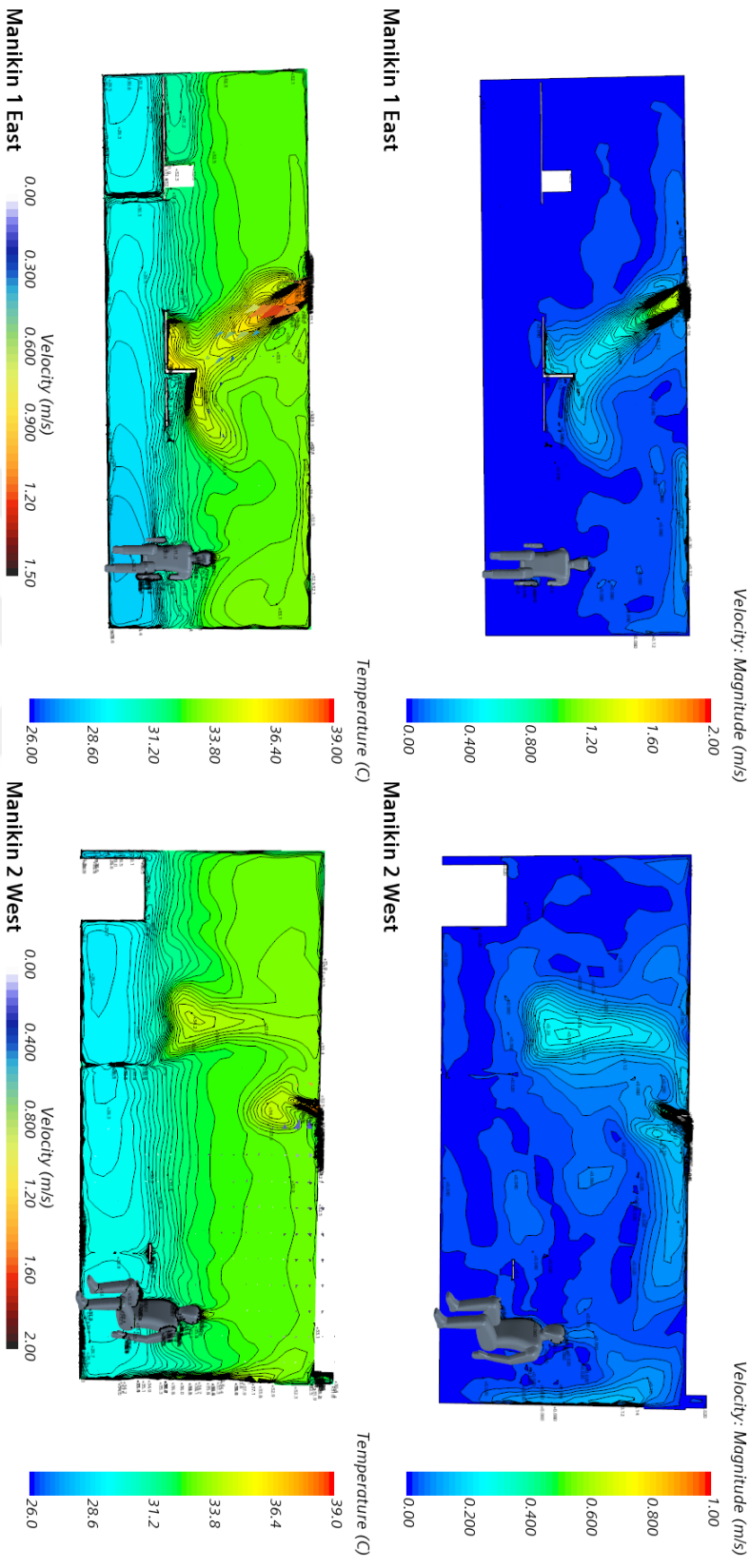

Figure 37: Case 8 velocity and temperature distribution

Energy Analysis

The progression of the economy and the continuously increasing emphasis on achieving optimal indoor thermal comfort have led to a surge in energy consumption within both residential and commercial buildings. The incorporation of air diffusers into building envelopes has garnered significant attention as an efficient method to enhance thermal comfort. This is achieved by minimizing indoor temperature fluctuations and optimizing energy conservation through the reduction of HVAC system operational periods.

Energy efficiency can be achieved in office spaces through two distinct avenues. The first involves diminishing the airflow into the room by reducing fan speeds, while the second focuses on curbing the necessity for heating coils by lowering the temperature of the incoming air. In this thesis, airflow reduction is used to find out the energy analysis between hexagonal and square diffusers. To make it more realistic, PMV value set to 1 where manikins can be slightly warm in winter conditions.

In the case of the hexagonal diffuser, the air blowing towards manikin 2 was simulated under the same conditions as in case 3 which can be seen in figure 37. Square diffuser had only one experiment which is all open mode and it's used in this simulation also.

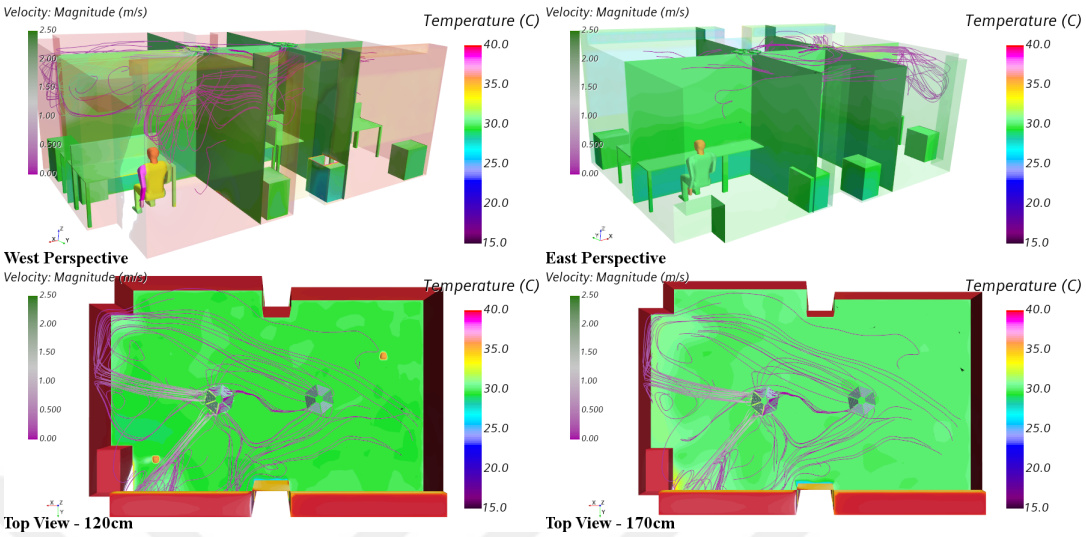

Figure 38: Case 3 with reduced airflow

However, to meet PMV value +1 expectations, the airflow rate of the hexagonal diffuser was reduced by 50%. For the square diffuser case, the airflow condition was also reduced by 25% due to the PMV values obtained from the experiments, which were relatively high, around +3.

Since the heaters total capacity was 6 kw, they also decreased to relatively 4.1 kW and 5 Kw while they met the PMV = 1 condition.

Hexagonal diffuser can save 0.9kW compared to conventional square diffusers in just blowing air to single manikin which is stands in one side of the room.

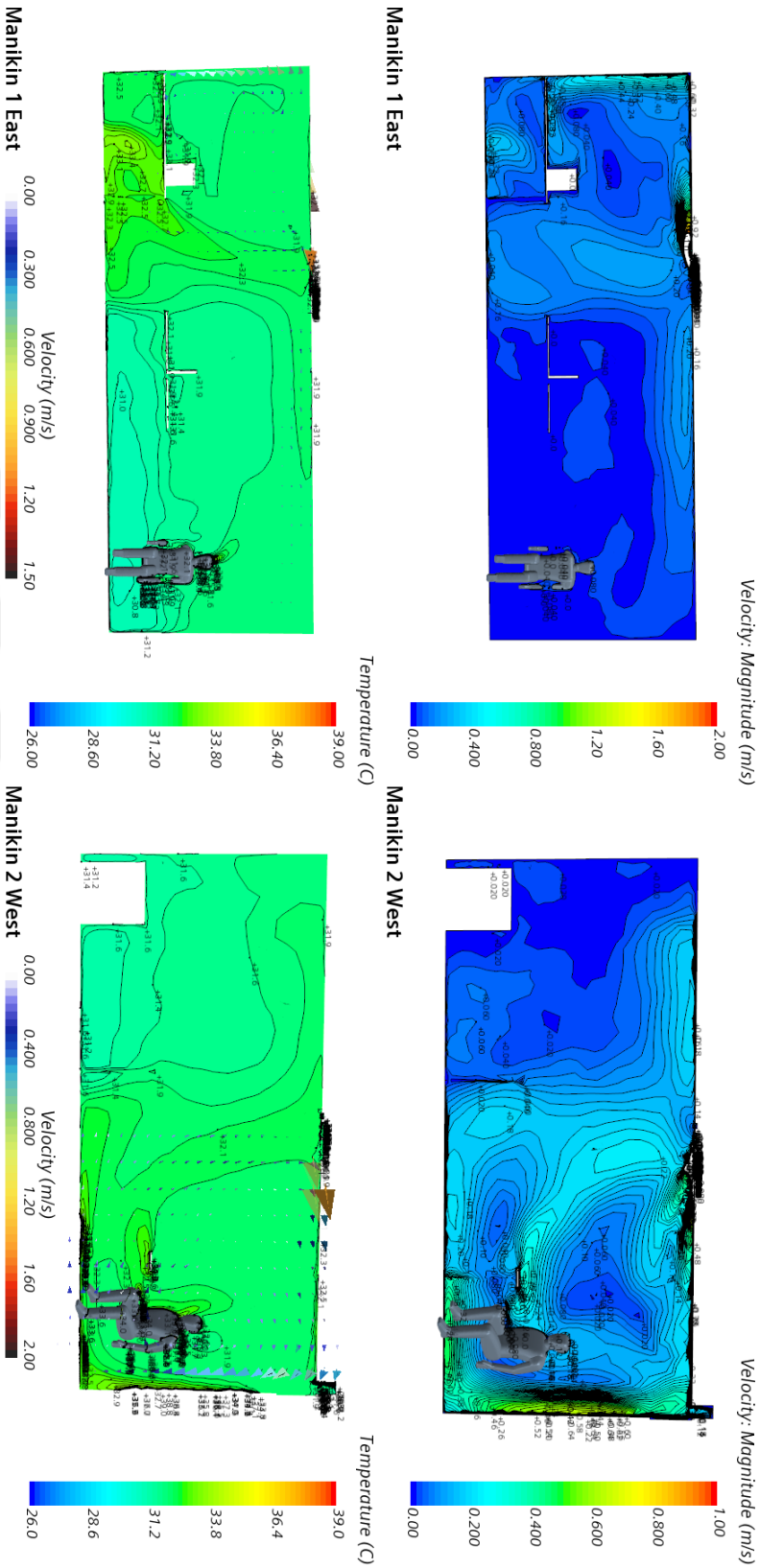

Figure 39: Hexagonal diffuser with reduced airflow

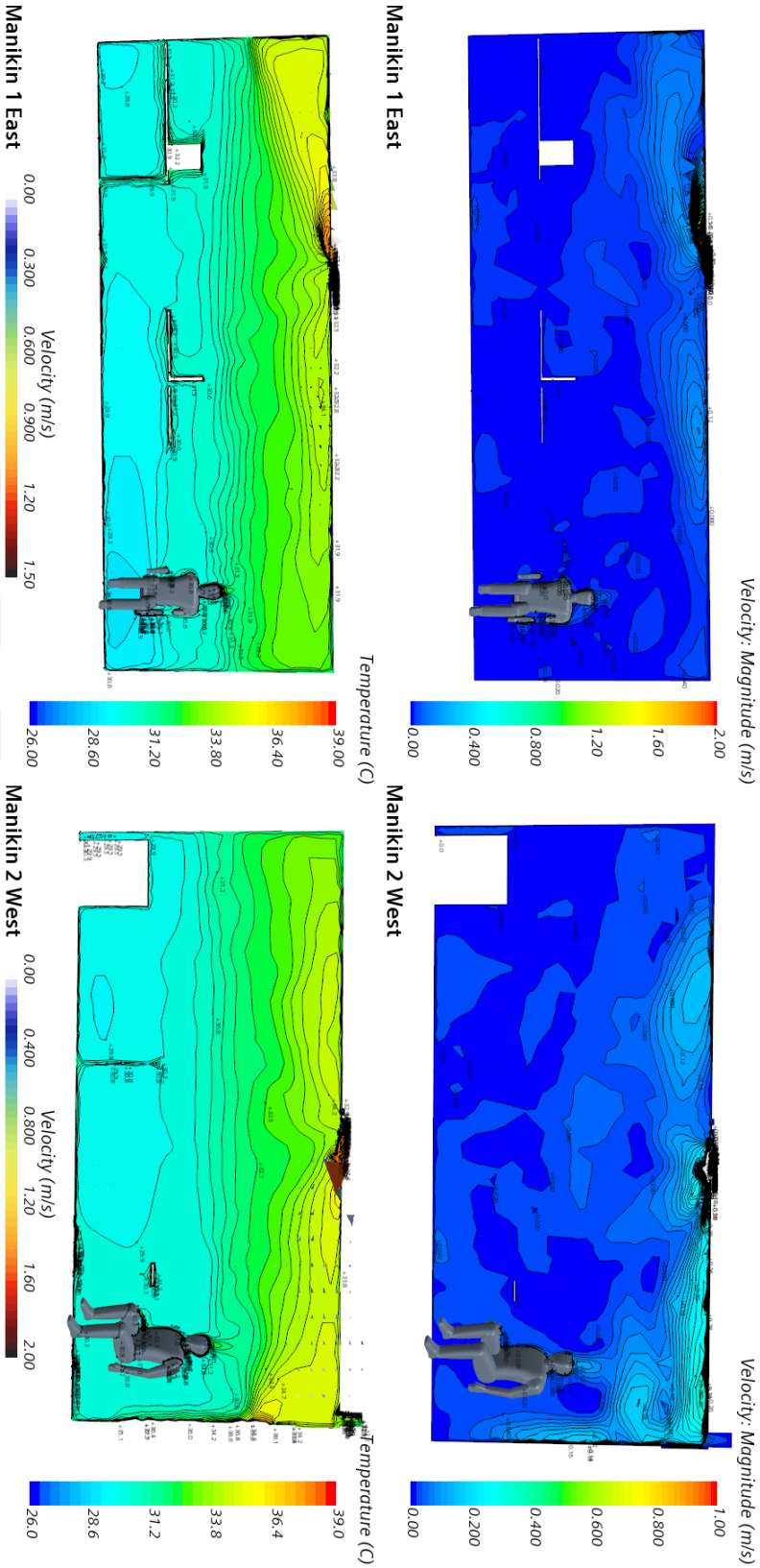

Figure 40: Square diffuser with reduced airflow

These scenarios allowed for energy-related assessments of the impact of hexagonal and other diffusers. However, in the situation of all the flaps were open on the hexagonal diffuser, it only met the conditions when the airflow is same with other diffusers. Because, as we mentioned while we comparing the all flap opened experiments, hexagonal diffuser act like square diffuser in both airflow characteristics and thermal comfort perspective. Therefore, if there is an homogeneous layout in the room where hexagonal need to open all the flaps and condition all the space like square diffuser does, then it will not save any energy more than other diffusers.

CHAPTER VI

CONCLUSION AND FUTURE WORK

In conclusion, this thesis focused on the importance of thermal comfort in indoor environmental quality (IEQ) and the role of HVAC systems in achieving optimal thermal comfort. The advancements in technology have allowed HVAC systems to become more energy-efficient and accessories like air diffusers to improve their performance.

The literature review highlighted the significant contributions of researchers like M. Pınar Mengüç and Cem Keskin, who continue to work on improving air diffusers and thermal comfort. Various articles explored different ventilation systems and their impact on thermal comfort and airflow patterns within a room. The mathematical aspect of the thesis was equally crucial, as it explained the principles and equations behind Computational Fluid Dynamics (CFD) simulations. Understanding these equations and solution methods formed the basis for the CFD simulations carried out in the study.

In Chapter 4, the office room's details and HVAC system were thoroughly explained, including the challenges posed by the room's asymmetrical structure and the presence of a heater. The room was modeled using STAR CCM+ due to its thermal comfort wizard and user-friendly interface.

The results section presented the outcomes of numerical experiments and validated simulations for different diffusers under varying conditions. It was observed that the hexagonal diffuser behaves similarly to the square diffuser when all flaps are open and can create horizontal thermal stratification with closed flaps. Meanwhile, the four-way swirl diffuser was found to be less suitable for office rooms.

Overall, the thesis aimed to investigate thermal comfort in an office room by

analyzing various air diffusers. By understanding the impact of different diffusers and ventilation systems on thermal comfort, the study contributes valuable insights to the field of indoor environmental quality and HVAC design.

For the future work, there are several potential works can be found below,

- As mentioned, conducting Large Eddy Simulation (LES) in addition to RANS could provide valuable insights into the differences between these two CFD modeling approaches. LES is known for capturing finer turbulent structures and unsteady flow phenomena, which might have an impact on thermal comfort and airflow patterns within the room.

- Currently, the study assumed a constant airflow rate. However, in real-world scenarios, Variable Air Volume (VAV) systems are often used, where the airflow rate can be adjusted based on the need for heating or cooling. Investigating the behavior of different air diffusers under VAV conditions could reveal more nuanced results and help optimize diffuser configurations for energy efficiency and thermal comfort.

- The current study focused on a specific office configuration. Future work could investigate different occupancy scenarios, such as full occupancy or partial occupancy, to assess how thermal comfort and airflow patterns change with varying number of occupants.

APPENDIX A

JAVASCRIPT CODE FOR PMV

```
// Data Entry
const CLO = getSimulation().issueQuery('Enter value for
   Clothing (clo): ');
const MET = getSimulation().issueQuery('Enter value for
   Metabolic rate (met): ');
const WME = getSimulation().issueQuery('Enter value for
   External work, normally around 0 (met): ');
const TA = getSimulation().issueQuery('Enter value for Air
   Temperature (\textdegree C): ');
const TR = getSimulation().issueQuery('Enter value for Mean
   radiant temperature (\textdegree C): ');
const VEL = getSimulation().issueQuery('Enter value for
   Relative air velocity (m/s): ');
const RH = getSimulation().issueQuery('Enter value for
   Relative humidity (%): ');
const PA = getSimulation().issueQuery('Enter value for Water
   vapor pressure (Pa): ');

// Saturated vapor pressure in kPa
const FNPS = (T) => Math.exp(16.6536 - 4030.183 / (T + 235));

if (PA == 0) {
  // Calculate water vapor pressure if not provided
```

```
16    const saturatedVaporPressure = FNPS(TA);
17    PA = RH * 10 * saturatedVaporPressure;
18  }
19
20  const ICL = 0.155 * CLO; // Thermal insulation of the clothing
        in m2K/W
21  const M = MET * 58.15; // Metabolic rate in W/m2
22  const W = WME * 58.15; // External work in W/m2
23  const MW = M - W; // Internal heat production in the human
        body
24
25  let FCL;
26  if (ICL < 0.078) {
27    FCL = 1 + 1.29 * ICL;
28  } else {
29    FCL = 1.05 + 645 * ICL;
30  }
31
32  const HCF = 12.1 * Math.sqrt(VEL); // Heat transfer
        coefficient by forced convection
33  const TAA = TA + 273; // Air temperature in Kelvin
34  const TRA = TR + 273; // Mean radiant temperature in Kelvin
35
36  // Calculate surface temperature of clothing by iteration
37  let TCLA = TAA + (35.5 - TA) / (3.5 * (6.45 * ICL + 0.1));
38  let P1 = ICL * FCL;
39  let P2 = P1 * 3.96;
40  let P3 = P1 * 100;
41  let P4 = P1 * TAA;
```

```
let P5 = 308.7 - 0.028 * MW + P2 * Math.pow(TRA / 100, 4);
let XN = TCLA / 100;
let XF = XN;
let N = 0;
const EPS = 0.00015;

while (true) {
  XF = (XF + XN) / 2;
  const HCN = 2.38 * Math.pow(Math.abs(100 * XF - TAA), 0.25);
  const HC = (HCF < HCN) ? HCF : HCN;
  XN = (P5 + P4 * HC - P2 * Math.pow(XF, 4)) / (100 + P3 * HC)
     ;
  N++;

  if (N > 150 || Math.abs(XN - XF) <= EPS) {
    break;
  }
}

const TCL = 100 * XN - 273; // Surface temperature of the
   clothing

// Heat loss components
const HL1 = 3.05 * 0.001 * (5733 - 6.99 * MW - PA); // Heat
   loss diff. through skin

let HL2;
if (MW > 58.15) {
```

```
  HL2 = 0.42 * (MW - 58.15); // Heat loss by sweating (comfort
     )
} else {
  HL2 = 0;
}

const HL3 = 1.7 * 0.00001 * M * (5867 - PA); // Latent
   respiration heat loss
const HL4 = 0.0014 * M * (34 - TA); // Dry respiration heat
   loss
const HL5 = 3.96 * FCL * (Math.pow(XN, 4) - Math.pow(TRA /
   100, 4)); // Heat loss by radiation
const HL6 = FCL * HC * (TCL - TA); // Heat loss by convection

// Calculate PMV and PPD
const TS = 0.303 * Math.exp(-0.036 * M) + 0.28; // Thermal
   sensation trans. Coeff.
const PMV = TS * (MW - HL1 - HL2 - HL3 - HL4 - HL5 - HL6); //
   Predicted mean vote
const PPD = 100 - 95 * Math.exp(-0.03353 * Math.pow(PMV, 4) -
   0.2179 * Math.pow(PMV, 2)); // Predicted percentage dissat.

// Output
println('Predicted Mean Vote (PMV): ' + PMV.toFixed(3));
println('Predicted Percentage of Dissatisfied (PPD): ' + PPD.
   toFixed(3));
```

APPENDIX B

SQUARE DIFFUSER DIMENSIONS

KARE TAVAN DİFÜZÖRÜ / CEILING DIFFUSERS

STANDART ÖLÇÜLER
STANDARD DIMENSIONS

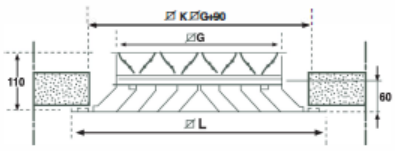

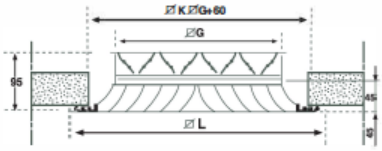

G (mm)	K (mm)	L (mm)
150 * 150	240	295
225 * 225	315	370
300 * 300	390	445
375 * 375	465	520
450 * 450	540	(Clip-in) * 600 595
525 * 525	615	670
600 * 600	690	745

* İşaretliler T profil veya özel taşımalı tip asma tavan sistemi için özel çerçevelidir.

Has a special type frame for T profile or special type ceiling system.

Ø G (mm)	Ø K (mm)	Ø L (mm)
100 * 100	160	218
150 * 150	210	268
200 * 200	260	318
250 * 250	310	368
300 * 300	360	418
350 * 350	410	468
400 * 400	460	518
450 * 450	510	568
500 * 500	560	618
477 * 477	537	* 595 * 600
550 * 550	610	668
600 * 600	660	700

* İşaretliler T profil veya özel taşımalı tip asma tavan sistemi için özel çerçevelidir.

Has a special type frame for T profile or special type ceiling system.

AKSESUARLAR
ACCESSORIES

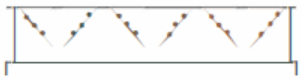

Anemostat Damperi
Diffuser Damper

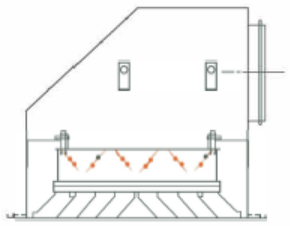

Bağlantı Kutusu
Plenum Box
Daha fazla detay için sayfa 25-26'ya bakınız.
For more details see page 25-26.

APPENDIX C

FOURWAY DIFFUSER DIMENSIONS

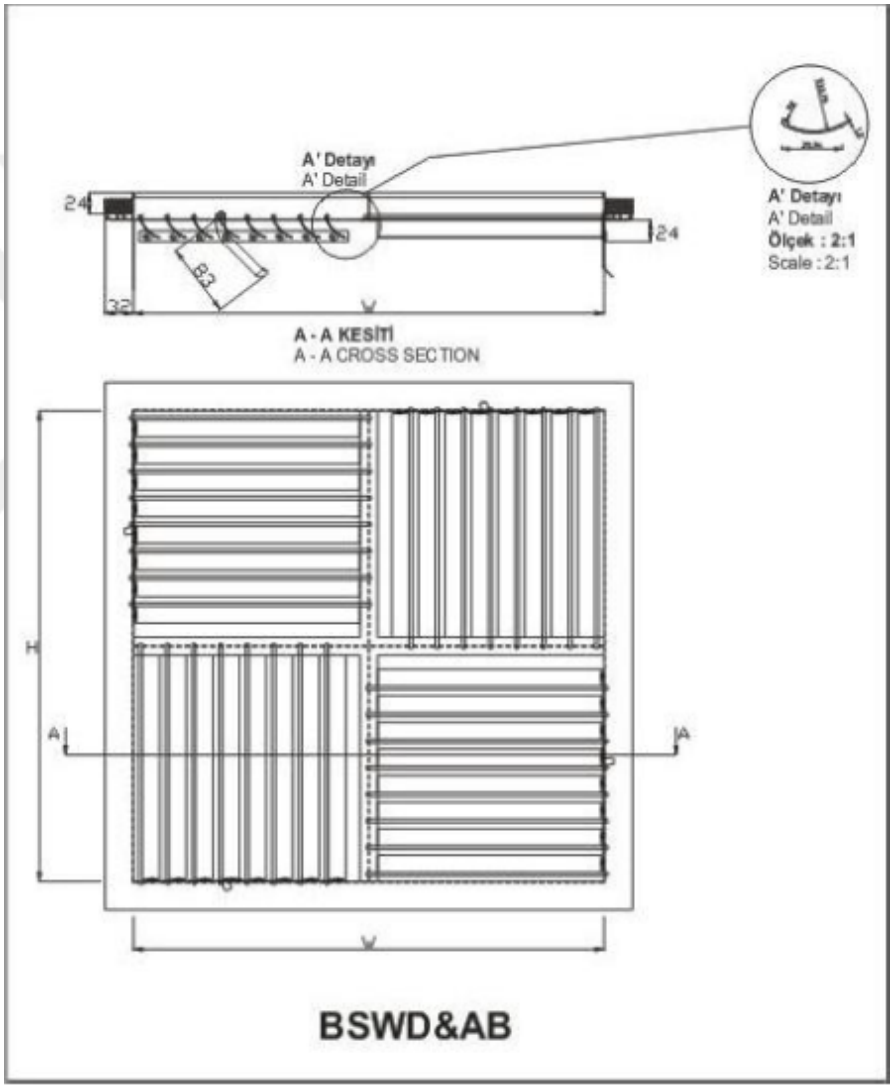

APPENDIX D

EXPERIMENT MEASUREMENTS FOR INLET AIR VELOCITY

	EXP1				Initial Temperature:	35 celsius
	Group 1	Group 2	Group 3	Group 4	Group 5	Group 6
Flap 1	0.12	0.16	0.18	0.21	0.57	0.38
Flap 2	0.17	0.18	0.21	0.47	0.81	0.63
Flap 3	0.28	0.3	0.2	0.62	1.32	1.23
Flap 4	0.48	0.39	0.24	0.86	1.75	1.75
Flap 5	0.95	0.5	0.49	0.97	2.05	2.35
Flap 6	1.5	1.05	0.89	1.36	2.38	3.4
	EXP2				Initial Temperature:	38 celsius
	Group 1	Group 2	Group 3	Group 4	Group 5	Group 6
Flap 1	0.56	Closed	Closed	Closed	Closed	0.69
Flap 2	1.18	Closed	Closed	Closed	Closed	0.97
Flap 3	1.44	Closed	Closed	Closed	Closed	1.72
Flap 4	2.18	Closed	Closed	Closed	Closed	2.64
Flap 5	2.49	Closed	Closed	Closed	Closed	3.58
Flap 6	3.3	Closed	Closed	Closed	Closed	3.86
	EXP3				Initial Temperature:	38 celsius
EXP3	Group 1	Group 2	Group 3	Group 4	Group 5	Group 6
Flap 1	Closed	Closed	Closed	0.74	1.04	Closed
Flap 2	Closed	Closed	Closed	1.38	1.11	Closed
Flap 3	Closed	Closed	Closed	1.62	1.94	Closed
Flap 4	Closed	Closed	Closed	1.96	2.38	Closed
Flap 5	Closed	Closed	Closed	2.43	2.46	Closed
Flap 6	Closed	Closed	Closed	2.65	2.62	Closed
	EXP4				Initial Temperature:	37 Celsius
	Group 1	Group 2	Group 3	Group 4	Group 5	Group 6
Flap 1	0.24	0.3	Closed	Closed	Closed	0.4
Flap 2	0.46	0.35	Closed	Closed	Closed	1.08
Flap 3	0.75	0.5	Closed	Closed	Closed	2.2
Flap 4	1.2	0.6	Closed	Closed	Closed	2.5
Flap 5	1.7	0.4	Closed	Closed	Closed	3.2
Flap 6	2.3	0.6	Closed	Closed	Closed	3.4
	EXP5				Initial Temperature:	39 Celsius
	Group 1	Group 2	Group 3	Group 4	Group 5	Group 6
Flap 1	Closed	Closed	0.34	0.76	0.72	Closed
Flap 2	Closed	Closed	0.84	1.38	0.84	Closed
Flap 3	Closed	Closed	1.14	1.44	1.36	Closed
Flap 4	Closed	Closed	1.46	1.57	1.57	Closed
Flap 5	Closed	Closed	1.88	1.78	1.7	Closed
Flap 6	Closed	Closed	1.96	2.08	2.12	Closed
	EXP6				Initial Temperature:	35.5 Celsius
	Group 1	Group 2	Group 3	Group 4	-	-
Flap 1	0.15	0.14	0.2	0.21	-	-
Flap 2	0.18	0.16	0.25	0.56	-	-
Flap 3	0.18	0.15	0.5	1.44	-	-
Flap 4	0.24	0.14	1	1.45	-	-
Flap 5	0.34	0.18	1.06	1.71	-	-
Flap 6	0.89	0.34	1.4	1.94	-	-
	EXP7				Initial Temperature:	35 Celsius
	Group 1	Group 2	Group 3	Group 4	-	-
Flap 1	0.3	0.1	0.15	0.66	-	-
Flap 2	0.44	0.14	0.15	1.1	-	-
Flap 3	0.57	0.2	0.25	1.38	-	-
Flap 4	0.6	0.56	0.3	1.47	-	-
Flap 5	0.72	0.7	0.48	1.62	-	-
Flap 6	0.94	0.88	0.6	1.78	-	-
Flap 7	1.3	1.2	0.77	1.92	-	-
Flap 8	2.05	1.55	0.94	2.18	-	-
	EXP8				Initial Temperature:	41 celcius
	Group 1	Group 2	Group 3	Group 4	-	-
Flap 1	0.8	0	0	0	-	-
Flap 2	1.6	0	0	0	-	-
Flap 3	2.3	0	0	0	-	-
Flap 4	2.6	0	0	0	-	-
Flap 5	2.6	0	0	0	-	-
Flap 6	2.9	0	0	0	-	-
Flap 7	2.9	0	0	0	-	-
Flap 8	3.6	0	0	0	-	-
	EXP9				Initial Temperature:	44 Celcius
	Group 1	Group 2	Group 3	Group 4	-	-
Flap 1	0	0	0.2	0	-	-
Flap 2	0	0	0.7	0	-	-
Flap 3	0	0	0.95	0	-	-
Flap 4	0	0	1.2	0	-	-
Flap 5	0	0	1.3	0	-	-
Flap 6	0	0	1.3	0	-	-
Flap 7	0	0	1.4	0	-	-
Flap 8	0	0	1.6	0	-	-

REFERENCES

[1] C. Spandagos and T.-L. Ng, "Equivalent full-load hours for assessing climate change impact on building cooling and heating energy consumption in large asian cities," *Applied Energy*, vol. 189, pp. 352–368, 2017.

[2] A. A. A. Gassar, C. Koo, T.-W. Kim, and S.-H. Cha, "Performance optimization studies on heating, cooling and lighting energy systems of buildings during the design stage: a review," *Sustainability*, vol. 13, no. 17, pp. 1–47, Paper No. 9815, 2021.

[3] S. Roumi, R. A. Stewart, F. Zhang, and M. Santamouris, "Unravelling the relationship between energy and indoor environmental quality in australian office buildings," *Solar Energy*, vol. 227, pp. 190–202, 2021.

[4] M. Frontczak and P. Wargocki, "Literature survey on how different factors influence human comfort in indoor environments," *Build. Environ.*, vol. 46, pp. 922–937, 2011.

[5] M. Mihajlović, M. Jovanović, R. Pešić, J. Jovanović, and Z. Milanović, "Volatile organic compounds (voc) policy innovation in petrochemicals river barge transportation," *Journal of Cleaner Production*, vol. 112, no. 2, pp. 1559–1567, 2016.

[6] P. Xue, C. M. Mak, and Z. Ai, "A structured approach to overall environmental satisfaction in high-rise residential buildings," *Energy and Buildings*, vol. 116, pp. 181–189, 2016.

[7] W. Yang and H.-J. Moon, "Combined effects of acoustic, thermal, and illumination conditions on the comfort of discrete senses and overall indoor environment," *Building and Environment*, vol. 148, pp. 623–633, 2019.

[8] H. Choi, H. Kim, T. Hong, and J. An, "An individual weightage for indoor environmental quality component to enhance work performance in office buildings," *Building and Environment*, vol. 236, pp. 1–11, Paper No. 110278, 2023.

[9] bfa, "Indoor air quality (iaq) vs indoor environmental quality (ieq)," 2021, November 11.

[10] ASHRAE, *Standard 55, Thermal Environmental Conditions for Human Occupancy*. 2004.

[11] ISO, *ISO 7730:2005, Ergonomics of the Thermal Environment - Analytical Determination and Interpretation of Thermal Comfort using Calculation of the PMV and PPD Indices and Local Thermal Comfort Criteria*. 2005.

[12] U. Amin, M. J. Hossain, and E. Fernandez, "Optimal price based control of hvac systems in multizone office buildings for demand response," *Journal of Cleaner Production*, vol. 270, pp. 1–20, Paper No. 122059, 2020.

[13] S. Wen, R. Gao, H. Guan, H. Li, M. Wang, S. Zhang, and A. Li, "Air damper with controlling capacity unrelated to duct system resistance," *Journal of Building Engineering*, vol. 43, pp. 1–13, Paper No. 102388, 2021.

[14] P. Bragança, K. Sodjavi, A. Meslem, and L. Serres, "Airflow characteristics and thermal comfort generated by a multi-cone ceiling diffuser with and without inserted lobes," *Building and Environment*, vol. 108, pp. 143–158, 2016.

[15] EIA, "Recs survey data." `https://www.eia.gov/consumption/residential/data/2015/index.php?view=characteristics`, 2015.

[16] M. N. Assimakopoulos, A. Tsangrassoulis, G. Mihalakakou, M. Santamouris, and S. Jauré, "Development of a control algorithm to optimize airflow rates through variable size windows," *Energy Build*, vol. 34, no. 4, p. 363–8, 2002.

[17] V. Bradshaw, *The Building Environment: Active and Passive Control Systems*. John Wiley Sons, 2010.

[18] S. Omrani, V. Garcia-Hansen, B. R. Capra, and R. Drogemuller, "Effect of natural ventilation mode on thermal comfort and ventilation performance: full-scale measurement," *Energy Build*, vol. 146, p. 1–16, 2017.

[19] A. A. Jamaludin, H. Hussein, A. R. Mohd Ariffin, and N. Keumala, "A study on different natural ventilation approaches at a residential college building with the internal courtyard arrangement," *Energy Build*, vol. 72, p. 340–52, 2014.

[20] N. Nasrollahi and P. Ghobadi, "Field measurement and numerical investigation of natural cross-ventilation in high-rise buildings; thermal comfort analysis," *Applied Thermal Engineering*, vol. 211, pp. 1–25, Paper No. 118500, 2022.

[21] E. Spentzou, M. J. Cook, and S. Emmitt, "Modelling natural ventilation for summer thermal comfort in mediterranean dwellings," *Int J Vent*, vol. 18, no. 1, p. 28–45, 2019.

[22] A. K. Melikov, A. Li, R. Kosonen, X. Li, Z. Lin, G. Cao, and B. Yang, "Occupant targeted ventilation brings clean air to occupants," *REHVA Journal*, vol. 59, no. 2, pp. 30–34, 2022.

[23] C. Keskin, *Augmenting occupant thermal experience with cyber-physical-social systems: A case study on adaptive vents*. PhD thesis, Department of Mechanical Engineering, Özyeğin University, İstanbul, Türkiye, 2020.

[24] X. Yuan, Q. Chen, and L. R. Glicksman, "A critical review of displacement ventilation," *ASHRAE Trans.-Am. Soc. Heat. Refrig. Airconditioning Engin.*, vol. 104, p. 78–90, 1998.

[25] L. Zhang, T. T. Chow, K. F. Fong, Q. Wang, and Y. Li, "Comparison of performances of displacement and mixing ventilations. part i: thermal comfort," *International Journal of Refrigeration*, vol. 28, no. 2, pp. 276–287, 2005.

[26] S. Schiavon and A. K. Melikov, "Energy-saving strategies with personalized ventilation in cold climates," *Energy Build*, vol. 41, pp. 543–550, 2009.

[27] S. Schiavon, A. K. Melikov, and S. Chandra, "Energy analysis of the personalized ventilation system in hot and humid climates," *Energy Build*, vol. 42, pp. 699–707, 2010.

[28] B. Yang, P. Liu, Y. Liu, and F. Wang, "Performance evaluation of ductless personalized ventilation combined with impinging jet ventilation," *Applied Thermal Engineering*, vol. 222, pp. 1–15, Paper No. 119915, 2023.

[29] M. Dalewski, A. K. Melikov, and M. Vesely, "Performance of ductless personalized ventilation in conjunction with displacement ventilation: Physical environment and human response," *Build. Environ.*, vol. 81, pp. 354–364, 2014.

[30] S. Kawakubo, M. Sugiuchi, and S. Arata, "Office thermal environment that maximizes workers' thermal comfort and productivity," *Building and Environment*, vol. 233, pp. 1–13, Paper No. 110092, 2023.

[31] E. Kükrer and N. Eskin, "Effect of design and operational strategies on thermal comfort and productivity in a multipurpose school building," *Journal of Building Engineering*, vol. 44, pp. 1–14, Paper No. 102697, 2021.

[32] A. Kaushik, M. Arif, P. Tumula, and O. J. Ebohon, "Effect of thermal comfort on occupant productivity in office buildings: Response surface analysis," *Building and Environment*, vol. 180, pp. 1–9, Paper No. 107021, 2020.

[33] T. Akimoto, S. Tanabe, T. Yanai, and M. Sasaki, "Thermal comfort and productivity - evaluation of workplace environment in a task conditioned office," *Building and Environment*, vol. 45, no. 1, pp. 45–50, 2010.

[34] M. Borowski, R. Łuczak, J. Halibart, K. Zwolińska, and M. Karch, "Airflow fluctuation from linear diffusers in an office building: The thermal comfort analysis," *Energies*, vol. 14, no. 16, 2021.

[35] M. A. Aziz, I. A. M. Gad, E. S. F. A. Mohammed, and R. H. Mohammed, "Experimental and numerical study of the influence of air ceiling diffusers on room air flow characteristics," *Energy and Buildings*, vol. 55, pp. 738–746, 2012.

[36] S. Lestinen, S. Kilpeläinen, R. Kosonen, J. Jokisalo, H. Koskela, and A. Melikov, "Flow characteristics in occupied zone – an experimental study with symmetrically located thermal plumes and low-momentum diffuse ceiling air distribution," *Building and Environment*, vol. 128, pp. 77–88, 2018.

[37] P. V. Nielsen, "Velocity distribution in a room ventilated by displacement ventilation and wall-mounted air terminal devices," *Energy and Buildings*, vol. 31, no. 3, pp. 179–187, 2000.

[38] J. R. Fontaine, R. Rapp, H. Koskela, and R. Niemelä, "Evaluation of air diffuser flow modelling methods experiments and computational fluid dynamics simulations," *Building and Environment*, vol. 40, no. 3, pp. 377–389, 2005.

[39] A. Li, C. Yang, T. Ren, X. Bao, and E. Qin, "Piv experiment and evaluation of airflow performance of swirl diffuser mounted on the floor," *Energy and Buildings*, vol. 156, pp. 58–69, 2017.

[40] H. Andersson, M. Cehlin, and B. Moshfegh, "Experimental and numerical investigations of a new ventilation supply device based on confluent jets," *Building and Environment*, vol. 137, pp. 18–33, 2018.

[41] A. Asif, M. Zeeshan, S. R. Khan, and N. F. Sohail, "Investigating the gender differences in indoor thermal comfort perception for summer and winter seasons and comparison of comfort temperature prediction methods," *Journal of Thermal Biology*, vol. 110, pp. 1–16, Paper No. 103357, 2022.

[42] L. Yang, S. Zhao, S. Gao, H. Zhang, and E. Arens, "Gender differences in metabolic rates and thermal comfort in sedentary young males and females at various temperatures," *Energy and Buildings*, vol. 251, pp. 1–12, Paper No. 111360, 2021.

[43] Q. Zhao, J. Lyu, H. Du, Z. Zhao, and Z. Zhao, "Gender differences in thermal sensation and skin temperature sensitivity under local cooling," *Journal of Thermal Biology*, vol. 111, pp. 1–12, Paper No. 103401, 2023.

[44] C. Keskin and M. P. Mengüç, "An adaptive vent system for localized and customized thermal management in buildings," *ASME. J. Heat Transfer*, vol. 142, no. 5, pp. 1–11, Paper No. 052903, 2020.

[45] A. Psikuta, J. Allegrini, B. Koelblen, A. Bogdan, S. Annaheim, N. Martínez, D. Derome, J. Jan Carmeliet, and R. M. Rossi, "Thermal manikins controlled by human thermoregulation models for energy efficiency and thermal comfort research – a review," *Renewable and Sustainable Energy Reviews*, vol. 78, pp. 1315–1330, 2017.

[46] L. Yi, L. Fengzhi, L. Yingxi, and L. Zhongxuan, "An integrated model for simulating interactive thermal processes in human-clothing system," *Journal of Thermal Biology*, vol. 29, pp. 567–575, 2004.

[47] R. Holopainen, *A Human Thermal Model for Improved Thermal Comfort*. PhD thesis, Department of Technology, Aalto University, Espoo, Finland, 2012.

[48] D. Fiala, K. J. Lomas, and M. Stohrer, "Computer prediction of human thermoregulatory and temperature responses to a wide range of environmental conditions," *International Journal of Biometeorology*, vol. 45, pp. 143–159, 2001.

[49] H. Zhang, C. Huizenga, E. Arens, and T. Yu, "Considering individual physiological differences in a human thermal model," *Journal of Thermal Biology*, vol. 26, pp. 401–408, 2001.

[50] J. D. Chung, H. Hong, and H. Yoo, "Analysis on the impact of mean radiant temperature for the thermal comfort of underfloor air distribution systems," *Energy and Buildings*, vol. 42, no. 12, pp. 2353–2359, 2010.

[51] M. Luo, E. Arens, H. Zhang, A. Ghahramani, and Z. Wang, "Thermal comfort evaluated for combinations of energy-efficient personal heating and cooling devices," *Building and Environment*, vol. 143, pp. 206–216, 2018.

[52] F. Calvino, M. La Gennusa, G. Rizzo, and G. Scaccianoce, "The control of indoor thermal comfort conditions: introducing a fuzzy adaptive controller," *Energy and Buildings*, vol. 36, no. 2, pp. 97–102, 2004.

[53] B. Y. Kim and Y. Ham, "Personal thermal comfort modeling based on facial expression," *Journal of Building Engineering*, vol. 75, pp. 1–15, Paper No. 106956, 2023.

[54] *STARCCM+. Users Guide (Version 12).* 2017.

[55] D. C. Wilcox, *Turbulence Modeling for CFD. Second edition.* Anaheim: DCW Industries, 1998.

[56] K. Li and W. Xue, "Exploring the environment/energy pareto optimal front of an office room using computational fluid dynamics-based interactive optimization method," *Energies*, vol. 10, no. 2, pp. 1–15, Paper No. 231, 2017.

[57] H. B. Awbi, *Architecture: Comfort and Energy.* Elsevier, 1998.

[58] A. Zhivov, H. Skistad, E. Mundt, V. Posokhin, M. Ratcliff, E. Shilkrot, and A. Strongin, *Principles of Air and Contaminant Movement Inside and Around Buildings.* Academic Press, 2001.

[59] H. Yu, C. M. Liao, H. M. Liang, and K. C. Chiang, "Scale model study of airflow performance in a ceiling slot-ventilated enclosure: Non-isothermal condition," *Building and Environment*, vol. 42, pp. 1142–1150, 2007.

[60] P. O. Fanger, *Thermal Comfort: Analysis and Applications in Environmental Engineering.* Danish Technical Press, 1970.

[61] ISO, *Moderate Thermal Environments Determination of the PMV and PPD Indices and Specification of the Conditions for Thermal Comfort.* International Organization for Standardization, iso 7730:2005 ed., 2005.

[62] ASHRAE, *2009 ASHRAE Handbook—Fundamentals, Chapter 9: Thermal comfort.* The American Society of Heating, Refrigerating and Air-Conditioning Engineers, 2009.

[63] J. R. Howell, M. P. Mengüc, K. Daun, and R. Siegel, *Thermal Radiation Heat Transfer*. CRC Press, 7th ed., 2021.

[64] B. Choudhary and Udayraj, "A coupled cfd-thermoregulation model for air ventilation clothing," *Energy and Buildings*, vol. 268, pp. 1–18, Paper No. 112206, 2022.

VITA

Tolga Arda Eraslan obtained her B.Sc. in Mechanical Engineering from Özyeğin University in 2019. Currently, he is pursuing the M.Sc. degree at Özyeğin University, focusing on thermal comfort and indoor airflow.

During her studies, he used experimental, theoretical, and computational research methods actively in Center for Energy, Environment and Economy (CEEE).